On the processing of second-order information in normal and amblyopic vision

Yi Gao

2017/10/25

A thesis submitted to McGill University in partial fulfillment of the requirements of the degree of doctor of philosophy.

Table of Contents

Abstract

Natural scenes are composed of first-order and second-order information. First-order information is defined by variations in luminance or chromaticity, while second-order information is defined by variations in properties other than luminance or color, such as contrast, texture or motion. This thesis investigates the processing of second-order information in normal and amblyopic visual systems.

Amblyopia is a neuro-developmental disorder of human vision. Processing nonlinearities are relevant to both first- and second-order visual mechanisms and are an important feature for any sensory system. In the current thesis, second-order processing nonlinearities were investigated using a pedestal masking paradigm and were modeled with a divisive gain control model. Second-order nonlinearities are involved in processing three kinds of second-order information; these are contrast-modulation (CM), orientation-modulation (OM) and motion-modulation (MM). In normal vision, CM and OM go through the same second-order nonlinearity while MM undergoes a second-order nonlinearity of a different form. This result suggests that second-order modulations are not always processed by a common mechanism in a "cue-invariant" manner.

In an orientation discrimination sensitivity task, amblyopic subjects demonstrated general deficits in all three second-order modulation conditions during amblyopic eye stimulation, and also demonstrate reduced sensitivity in MM stimuli during fellow eye stimulation. Likewise, second-order nonlinearities in amblyopic vision involved in processing CM and MM reveal that only MM stimuli are processed differently. The altered second-order

nonlinearity for MM exists during individual stimulation of both the amblyopic and fellow eye. The different deficit patterns for MM compared to other types of second-order modulation are consistent with the earlier conclusion that MM and CM are processed by separate mechanisms. While the dorsal and ventral visual pathways are both affected in amblyopia, these results suggest that they are affected to different degrees.

French version

Dans les scènes naturelles, il y a des informations de premier-ordre, définies par des variations de luminance ou de chrominance, et des informations de second-ordre, définies par d'autres types de variations telles que des modulations de contraste, texture ou mouvement. Cette thèse a étudié le traitement de ce second type d'information dans les systèmes visuels normaux et amblyopiques. L'amblyopie est un désordre développemental de la vision humaine. La non-linéarité du traitement, qui concerne à la fois les mécanismes de premier- et second-ordre, est une propriété importante des systèmes sensoriels. Dans cette thèse, la non-linéarité de second-ordre impliquée dans le traitement de trois types d'information de second-ordre que sont la modulation de contraste (MC), la modulation d'orientation (MO) et la modulation de mouvement (MM) a été étudiée en utilisant un paradigme de masquage par piédestal et modélisée par un modèle de contrôle de gain divisif. Il a été observé, en vision normale, que les MC et MO passent par la même non-linéarité de second-ordre alors que la MM subit une non-linéarité de second-ordre de forme différente. Ce résultat suggère que tous les types de modulations de second-ordre ne sont pas traités par un mécanisme commun d'une manière "invariante aux indices". La mesure de la sensibilité à la discrimination d'orientation pour ces trois types de stimuli de second-ordre chez les amblyopes a montré des déficits généralisés dans les trois

conditions pour la stimulation de l'œil amblyope (OA) et une sensibilité réduite uniquement dans la condition MM pour la stimulation de l'œil dominant (OD). Aussi, pour la vision amblyopique, l'étude de la non-linéarité de second-ordre impliquée dans le traitement des MM et MC révèle qu'elle est uniquement affectée pour la MM. L'altération de la non-linéarité de second-ordre de la MM est présente pour la stimulation de chaque œil des amblyopes. Les patterns de déficit différents pour la MM en comparaison des autres types de modulation de second-ordre sont consistants avec la conclusion précédente que les MM et MC sont traitées par des mécanismes distincts. Ils suggèrent également que les voies dorsale et ventrale dans le cortex extrastrié sont toutes deux affectées par l'amblyopie, mais à des degrés différents.

Acknowledgements

This thesis is under supervision of Prof. and Dr. Robert Hess who has been a supportive, helpful, resourceful, caring and considerate PhD supervisor. He provided guidance to me on the experimental design, data collection, analysis and interpretation. He also edited all four manuscripts when they were ready, as well as this thesis. I would like to express my appreciation for his guidance in academia and in life which have been essential for my academic and person growth.

Besides my supervisor, Dr. Alexandre Reynaud is a co-author of Manuscript 3; Dr. Alexander Baldwin has been a co-author of Manuscript 1, 2, and 4. Both of them guided me through out the projects for designing, analyzing and writing. They also edited the respective manuscripts more than once. Dr. Reynaud helped me with translating the Abstract of this thesis into French. Without their help, this thesis would not be the same quality or taking as little time.

Professor Frederick Kingdom and Reza Farivar have been providing constructive feedback for each of my projects and answering my questions about the projects as the thesis committee members. Professor Curtis Baker has also been very helpful at answering my questions and telling the stories about the developments of certain research topics. I would also like to thank Dr. Jiawei Zhou, who has never been officially working with me on a same project but has always been accessible for my questions about literature review, methodology, career choices etc.

At the end, I would like to thank Cuauhtémoc Reale Hernandez, for being supportive, positive and tolerant when I went through a car accident, emotional trough and confusion about life. Without him, I would not be the same me today. And I give special thanks to my parents Guanglu Gao and Yufen Sun for giving me life, passing me healthy lifestyles, providing the best education they could have and always being on my side.

Preface

For Manuscript 1, 2 and 4, Yi Gao took part in designing the experiments and writing the MATLAB codes. Yi Gao collected the data, analyzed the data, generated the figures and wrote the manuscripts. For Manuscript 3, Yi Gao collected half of the data in Canada, analyzed the data, generated the figures and wrote the manuscripts.

For Manuscript 1, 2, and 4, Dr. Alexander Baldwin took part in designing the experiments and writing the MATLAB codes, and edited the manuscripts. For Manuscript 3, Dr. Alexandre Reynaud led designing the experiments and writing the MATLAB, and edited the manuscripts. For Manuscript 3, Dr. Yong Kang collected half of the data in China.

For all manuscripts, Dr. Robert Hess took part in the whole discussion about designing, analyzing and writing. He also edited all four manuscripts.

Introduction

There are various kinds of information in the visual world, including first-order information, which is defined by luminance or chromaticity variations, and second-order information, which is defined by variations other than luminance or color, such as contrast, texture or motion. The mechanism of first-order processing has been modeled as a set of linear filters (Hubel & Wiesel, 1959, 1962) followed by a nonlinear transducer in the form of divisive normalization (David J. Heeger, 1992). Second-order mechanisms, on the other hand, have been modeled by a linear-nonlinear-linear (LNL) model and are studied less extensively. First-order processing is thought to happen mainly in the primary visual cortex (Hubel and Wiesel 1959, 1962) whereas second-order processing involves extrastriate cortex (Albright, 1992; Larsson, Heeger, & Landy, 2010; Larsson, Landy, & Heeger, 2006; Zhou & Baker, 1993, 1994). A nonlinearity after the second set of linear filters is also found in processing several kinds of second-order stimuli, for example contrast-modulation (CM) (Huang & Chen, 2014; Schofield & Georgeson, 1999) and orientation-modulation (OM) (F. A. Kingdom, Prins, & Hayes, 2003; Schofield & Yates, 2005). Nonlinearity in both first- and second-order processing is often times studied with the pedestal masking function – a pattern which shows a "dipper" shape if the underlying transducer function is nonlinear. The shape of the nonlinearity is an important resultant feature of neural responses and can provide clues to the types of underlying computations involved. Modeled as divisive normalization (David J. Heeger, 1992), the

nonlinearity reflects the active and inhibitory lateral connections among cortical neurons. Studying the second-order nonlinearity contributes not only to understanding second-order processing generally, but also to determining whether different types of modulations are processed by the identical mechanism. The first purpose of this thesis is to investigate the second-order nonlinearities involved in three kinds of second-order stimuli – CM, OM and motion-modulation (MM). I investigated, assuming each type of second-order stimulus had its own nonlinear transducer function, whether and how these functions differ across the three different second-order modulations.

In Manuscript 1, the second-order nonlinearities involved in CM and OM processing are studied by a pedestal masking paradigm and modeled with divisive normalization. The pedestal masking functions both showed the typical dipper shape. Likewise, the nonlinear transducer functions are found to be the same for CM and OM. In Manuscript 2, the same method was employed to study nonlinearities for CM and MM. A "dipper" function was also found in this dataset. Surprisingly, however, the nonlinear transducer function for MM has a different shape than for CM.

The second and third aims of this thesis concern second-order processing in human amblyopia. Amblyopia is a neuro-developmental disorder of the visual system. It affects various visual functions on different levels due to disrupted visual input from the amblyopic eye in early childhood. A better understanding of amblyopia is important for developing new treatment methods. Investigating amblyopia also contributes to a deeper understanding of neural plasticity – specifically, how early disruption in neural input can affect the structure and function of adult brains and how plasticity can be utilized for novel treatments. My investigation concerned the prevalence of second-order deficits in amblyopia. In Manuscript 3, orientation discrimination

sensitivities to three kinds of second-order modulations, CM, OM and MM, are measured over a large range of spatial frequencies. Second-order deficits were found to be general in the AE. Sensitivities to all three modulations are impaired, compared to normal observers, especially at high spatial frequencies. Reduced sensitivity was also found in the FE but only for MM processing.

This was not the first time that amblyopic deficits were found in both the amblyopic and fellow eyes. FE deficits in amblyopes usually involve higher-level motion-related functions including second-order motion (Zhou & Baker, 1993, 1994). Different nonlinear transducer functions were found for MM and CM in Manuscript 2; and different second-order modulations were found to be affected differently in Manuscript 3. Because of these findings, I wanted to know if any change in the second-order nonlinearity can account for the different deficit patterns for CM and MM in amblyopia. Does amblyopia affect the form of the second-order response nonlinearity? If so, is it affected to the same degree for CM and MM, as well as for the amblyopic eye and the fellow eye? I investigated this question in Manuscript 4, using the same pedestal masking method to study the second-order nonlinearities involved in monocular processing of CM and MM stimuli. Only the MM nonlinearity was affected and we found no difference between the two eyes. This result is consistent with those of the previous manuscripts. Jointly, they suggest that: (1) MM is processed by a separate mechanism to that of CM and OM, (2) the second-order MM deficit is binocular in amblyopia, and (3) the dorsal and ventral pathways in the extrastriate cortex are likely to be both affected by amblyopia but to different degrees.

Literature review

Classification of visual information

There are various forms of visual information in the world that the human visual system is adapted to process, such as color, shape, motion, texture and depth. In the perspective of evolutionary theory, the ability to process each of these different forms of information is necessary for our ability to perceive the world. Understanding how the human visual system perceives the world is the goal of vision scientists. In studying the mechanisms of visual perception, an important job of vision scientists is the classification of visual information. A clear structure of categorization enables us to focus on one or more specific kinds of visual information so that we can design experiments in a logical way to understand the complex mechanisms of visual perception and their relationships piece by piece.

One of the classical ways of categorizing visual stimuli is to differentiate between first-order and second-order information. The definition of first-order information is, " a change in luminance level or color". First-order information refers to a spatiotemporal modulation of luminance or color. On the other hand, second-order information is spatiotemporal modulation of first-order information (Huang & Chen, 2014). In their review about motion perception, Cavanagh and Mather (1989) first proposed the terms "first-order" and "second-order" motion to replace the conventional dichotomy of "short-range" and "long-range" motion. They generalized the terms to stationary information as well. Before the terms were proposed, in their foundation-laying work for second-order processing, Chubb and Sperling (1988) proposed a kind of second-order motion stimulus that they termed a "drift-balanced" random stimulus. This kind of stimulus

is distinguished from first-order information that has energy or power in the Fourier domain at corresponding spatiotemporal frequency. First-order information has energy in the Fourier domain whereas second-order information does not (Chubb & Sperling, 1988). Therefore, first-order motion is also called Fourier-motion and second-order motion is often called non-Fourier motion.

This classification was also proposed (Cavanagh & Mather, 1989) based on the response that they characterized from low-level retinal ganglion cells, lateral geniculate nucleus and standard direction- and orientation-selective neurons in early visual cortex. First-order information is effective at generating strong responses in these low-level visual cells. The physiological mechanism and the location in which first-order information is processed have been investigated long before the notion of first-order was proposed. Studying receptive fields is informative in understanding how neurons in sensory systems transform sensory information into perceptually meaningful states. The receptive field of a neuron in the visual system is the region in visual field or the retina in which visual stimuli influence its firing activities (Hartline, 1938). In their Nobel prize-winning work, Hubel and Wiesel (1959, 1962) mapped the receptive fields of neurons in various areas of cat visual cortex by varying the shape, size, location, orientation and motion direction etc. of spots of light shone onto one or both retinas and analyzing the response of individual neurons using micro-electrodes. In primary visual cortex, most neurons have “simple receptive field” composed of adjacent excitatory and inhibitory regions that are usually elongated along their boundaries. An individual receptive field can have a center region of either excitatory or inhibitory nature and two flanks, one on each side, of opposite sign. It can also have only two regions of opposite signs. Neurons with this kind of receptive field respond strongest to a light slit or a dark bar of specific size, shape, orientation, location and velocity.

The stimulus can be stationary or moving across the receptive field. This kind of slit or bar is defined by luminance change corresponding to first-order stimuli.

There are also cells with "complex receptive field", especially in higher-level visual areas, which also responds to first-order stimuli. They show selectivity for orientation, spatial frequency and velocity as well. One difference is that the requirement for the location of the stimulus does not hold. That is to say that the excitatory and inhibitory regions are not spatially separated. The structure and responsive properties of neurons in the primary visual cortex suggest that it is more sensitive to perceiving luminance (or color) changes, i.e. contrast, than absolute luminance level. Since luminance and color changes usually signify the edges of object, it is important for object recognition and motion perception.

First-order processing

Neurons with simple receptive fields correspond to the linear filter model for first-order processing. One receptive field with excitatory and inhibitory areas can be modeled as a linear filter in which the positive areas respond positively to luminance and the negative areas respond negatively as shown in Figure 1a. The output of the linear filter is the linear summation of responses from excitatory and inhibitory regions. Therefore, only when the bright and dark areas of the stimulus align with the positive and negative areas of the linear filter does its output become strongly positive (Figure 1b). Linear filters are also selective for orientation and spatial frequency corresponding to the orientation and size of the receptive fields. Figure 1 shows that for gratings of different orientation (Figure 1c) or spatial frequency (Figure 1d) other than the optimal orientation and spatial frequency of the linear filter, the output of linear summation is very weak. For the same reason, diffuse light that covers the whole receptive field is ineffective

at evoking a strong response (Figure 1e). The linear filter model does a good job at explaining the processing of first-order luminance-defined information and integrating the results from neurophysiological studies.

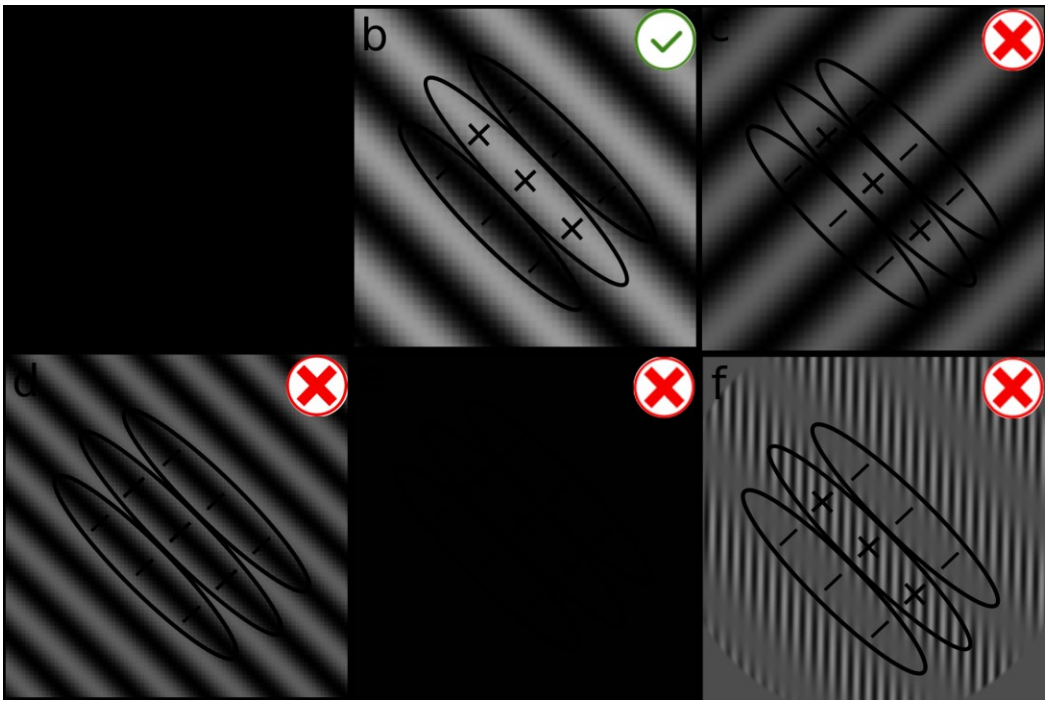

Figure 1. Linear filter model for first-order luminance-defined information processing showing linear filter and its selectivity for orientation and spatial frequency. (a) a linear filter; (b) The linear filter responds strongly to a first-order stimulus with the correct spatial frequency and orientation; (c) It does not respond when the orientation is not correct; (d) It does not respond strongly when the spatial frequency is not correct; (e) It does not respond to diffuse light; (f) It does not respond to a second-order contrast-modulated stimulus.

Contrast sensitivity

According to the linear filter model, one should be able to predict the responses of a certain receptive field to different levels of first-order information. The level of first-order

information is quantified by luminance contrast. In the literature, responses of either the visual system as a whole or of specific neurons are often characterized by gratings or filtered random noise in which the bright and dark areas are nearly equivalent. Because of this, the luminance contrast often takes the form of Michelson contrast (Michelson, 1927). The Michelson contrast is defined as

$$C_m = \frac{L_{max} - L_{min}}{L_{max} + L_{min}}, \qquad \text{Equation 1}$$

where L_{max} and L_{min} represent the highest and lowest luminance, respectively. Contrast sensitivity represents the ability to detect luminance variations, i.e. luminance contrast. Contrast sensitivity is calculated as *1/contrast threshold*. Contrast threshold is the lowest contrast level that is needed for the visual system to detect the contrast signal or for a neuron to respond. The contrast sensitivity function represents the extent to which contrast sensitivity varies with spatial frequency. The contrast sensitivity function is one of the most widely used measurements to characterize the function of normal and pathological visual systems. Many early measurements (Campbell & Green, 1965; Campbell & Robson, 1968; Robson, 1966; Westheimer, 1960) of contrast sensitivity function of human visual system demonstrated that it has a band-pass bell shape when plotted in log-log scale and it is thought to represent the envelope of the tuning of all the underlying cellular responses. Early neuro-physiological studies also have reported contrast sensitivity functions of similar shape in cat retina ganglion cells (Enroth-Cugell & Robson, 1966) and cortical neurons (Campbell, Cooper, & Enroth-Cugell, 1969). The contrast sensitivity functions of cat cortical neurons also show that cortical neurons are tuned to a narrow band of spatial frequency (Campbell et al., 1969).

Contrast response function

The linear filter model implies that the output of the filter has a linear relationship with the contrast level of the stimulus. However, many neurophysiology studies have measured the contrast response function (CRF) of single neurons, no matter whether simple or complex cells, in cat or primate visual cortex and found it to be nonlinear in form (Albrecht & Hamilton, 1982; Barlow, Kaushal, Hawken, & Parker, 1987; Dean, 1981; Maffei & Fiorentini, 1973; Ohzawa, Sclar, & Freeman, 1982, 1985). The nonlinearity mainly consists of two parts, the thresholding behavior at the low contrast levels and the saturation at high contrast levels. In Figure 2, a typical contrast response function is plotted with hypothetical data in log-log scale.

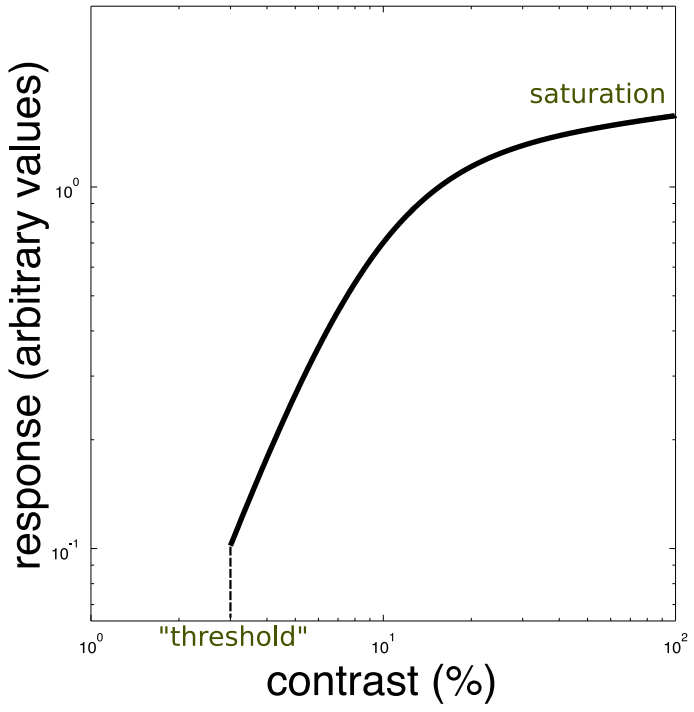

Figure 2. The contrast response function of primary cortex neurons in its typical shape. The curve is plotted with hypothetical data. The curve shows the “threshold” at which contrast level

the neurons start to response, and the saturating part of the response function at high contrast levels.

Extensive efforts have been made to model this nonlinear response function. Some chose a linear function to model the response function on log contrast scale (Maffei & Fiorentini, 1973) or to model only a part of the response function below a certain contrast level on a linear contrast scale (Dean, 1981). Others (Albrecht & Hamilton, 1982) model the nonlinearity with a hyperbolic ratio function:

$$R = R_{max} \frac{c^n}{\sigma^n + c^n},$$

Equation 2

where R represents is neuron's response, R_{max} is the maximum attainable response, c the is contrast level of the grating and σ^n is the semisaturation constant. When σ^n is not zero, the response R will vary between zero and $R_{max.}$

Divisive Normalization

A divisive normalization model was developed (David J. Heeger, 1992) to account for the nonlinearity of the contrast response function as well as to explain more physiological data about contrast adaptation and suppression. In this model, the response gain of a certain cortical neuron is normalized by pooled responses of nearby neurons that have different spatial frequency tuning and different spatial phases. This normalization can be calculated globally, over all spatial positions and all spatial frequencies, or locally, over an arbitrarily chosen spatial frequency bands and four phases in steps of π/2. The normalized response of a model simple cell is expressed as:

$$R_i^{\emptyset} = R_{max} \frac{A_i^{\emptyset}}{\sigma^2 + \frac{1}{4}\sum_i \sum_{\emptyset} A_i^{\emptyset}},$$

Equation 3

where $R_i^{\emptyset}$ represents the response of a model simple cell with phase $\emptyset$ and spatial frequency tuning i, $A_i^{\emptyset}$ is the half-squared output of the linear operator that corresponds to the model simple cell, σ^2 represents the semisaturation constant. The half-square operation to the linear response (D. J. Heeger, 1992) is a special feature of this divisive normalization model. It means taking the square value of the half-wave-rectification of the linear response. This feature enables the model cell to account for the nonlinearity in the CRF. What's more, this feature makes the model function equivalent to $R=R_{max}\frac{c^n}{\sigma^n + c^n}$, Equation 2 when n equals to 2 because the half-squared output is proportional to c^2 . Heeger (1992) showed that this divisive normalization model can explain most of the neurophysiology data about CRF, contrast adaptation and suppression available at that time.

Intercortical inhibition

There is plenty of evidence from neurophysiology studies to support the divisive normalization model. Cells in the cat striate cortex have been reported to receive divisive inhibitory input from a pool of neurons (Bonds, 1989; De Valois & Tootell, 1983). A mask grating superimposed on a base grating was found to modify the base response of a striate cortical cell (Bonds, 1989; Morrone, Burr, & Maffei, 1982). When this mask grating is not at optimal orientation, the effect is usually inhibition. This inhibition effect can be orientation-selective for narrowly tuned cells and more broad band for broadly tuned cells. The spatial frequency tuning of this inhibition effect is much broader than the spatial frequency passband of a typical cell. These effects suggest that inhibition is derived from a pool of neurons, not one. The inhibition is often referred to as cross-orientation or cross-spatial frequency inhibition (Carandini, Movshon, & Ferster, 1998). In another neurophysiological study, Robson (1988)

suggested that the mutual inhibition among striate neurons normalize effectively the responses of them with respect to overall contrast level (David J. Heeger, 1992). This intercortical inhibition is also thought to be the mechanism for striate neuron orientation selectivity (Bonds, 1989; Ringach, Hawken, & Shapley, 1997). Blocking the inhibition effect by the neurotransmitter gamma-aminobutyric acid (GABA) significantly reduces orientation selectivity of striate neurons (Sillito, 1977, 1979).

Dipper function

Behaviorally a phenomenon called "the pedestal effect", which was observed and studied for a long time (Barlow et al., 1987; Foley, 1994; Foley & Legge, 1981; Legge, 1979; Legge & Foley, 1980; Nachmias & Sansbury, 1974; Stromeyer & Klein, 1974) can also be modeled as the result of a nonlinear response system. The pedestal effect was found in contrast discrimination, contrast masking, or pattern masking studies in which the increment threshold for discrimination was found to be lower than detection threshold when the base contrast was at low level. Nowadays the contrast masking paradigm is often referred to as "the pedestal masking paradigm". It is often done by a 2-interval forced choice task (2IFC) in which observers need to identify the test interval that contains the target from two intervals that both contain the pedestal mask. The interval that only contains the pedestal mask is called null interval. Pedestal masking gets its name from the fact that it usually has the same spatial properties as the target. Measuring the increment thresholds at different base contrast levels and plotting them gives the increment threshold versus pedestal contrast (TvC) function. Because historically the TvC function has been used to also refer threshold versus external noise contrast in equivalent noise paradigm, to avoid confusion, in the current thesis I call the TvC function for patter masking experiment

"pedestal masking function". And the TvC function for equivalent noise experiments with this original term.

The pedestal masking function exhibits a "dipper" shape defined by the increment threshold decreasing when the pedestal contrast is low. However, at pedestal contrasts higher than the detection threshold, the increment threshold increases as the pedestal contrast increases. As shown in Figure 3 the pedestal masking function is composed of two parts; the facilitatory part and the inhibitory part. When the pedestal is of moderate level, it facilitates the detection of the increment contrast and when the pedestal gets much higher than the detection threshold, it inhibits the contrast discrimination task.

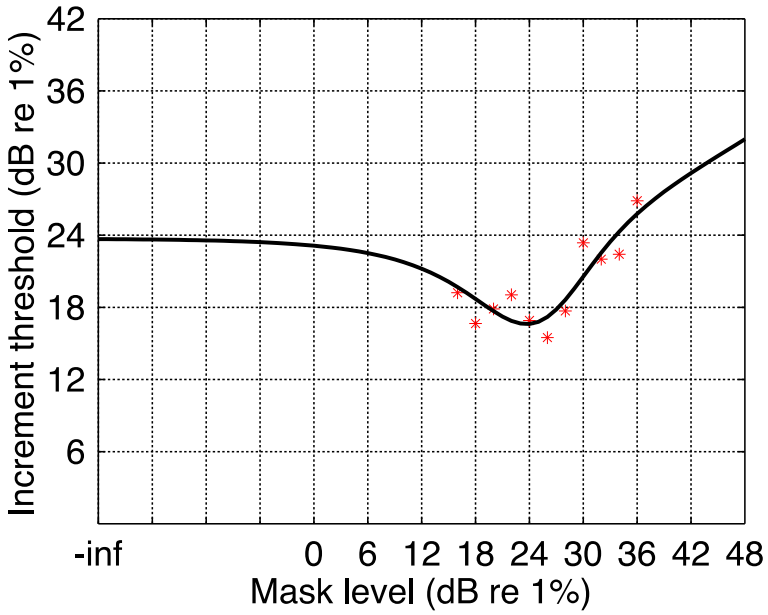

Figure 3. Pedestal masking function with the typical "dipper" shape. The figure is made by replotting Huang and Chen's (2014) data. The dots are the increment thresholds for their contrast-modulation condition with 40% contrast. The curve is made from fitting their increment threshold data with divisive normalization model (see Chapter 1).

The dipper shape of the Pedestal masking function implies that the contrast response system is not linear. If it was linear, the increment threshold should be independent from the

pedestal. The most popular explanations for the mechanism underlying this nonlinearity are: (1) a fundamental nonlinear transducer function with divisive inhibition, or (2) a change in uncertainty of the visual system together with increasing internal noise at high contrast levels. Both of these models can fit psychophysical data equally well.

Nonlinear transducer functions

Legge and Foley (1980) first developed a nonlinear transducer function model to account for the results from contrast masking experiments. An early form of their model included a linear response function, a nonlinear transducer function, and a decision process with additive internal noise. The nonlinear transducer function is expressed as such:

$$R = \frac{a_1|E|^{2.4}}{|E|^2+{a_2}^2}, \qquad \text{Equation 4}$$

where E is the excitatory input to the nonlinear transducer, a_1 and a_2 are constants. This nonlinear transducer is accelerating at low contrast levels and compressive at high contrast levels which correspond to the facilitatory and the inhibitory parts of the pedestal masking function, respectively (Legge & Foley, 1980). Foley (1994) later incorporated divisive inhibition (David J. Heeger, 1992) into the contrast masking model and modified the nonlinear transducer function into the following form:

$$R = \frac{E^p}{I^q+Z}, \qquad \text{Equation 5}$$

in which $I = \max(\sum_i C_i s_{I_i}, 0)$ represents the inhibitory input from a broadband of channels, p and q are constant exponents, and z is divisive gain control constant. The modification is mainly concerning the source of the inhibition. They also developed another model by raising the inhibitory activities from each channel to the power q before summing them. This modified version fits the data slightly better under some conditions. By manipulating the orientation of the pedestal masks and adding a second mask, the author demonstrated that the inhibition cannot be

a single mechanism; rather a divisive inhibitory mechanism that pools from a broadband of spatiotemporal channels to normalize the output fits the data much better. Thus the nonlinear transducer function for the contrast masking model developed in this study (Foley, 1994) is actually composed of two parts; the nonlinear accelerating excitation process to account for facilitatory effect of the pedestal mask and the divisive normalization process to account for the inhibitory effect.

Explanation with uncertainty and multiplicative noise

The other explanation for the dipper shape is also composed of two parts. The facilitatory effect is explained by the reduction of internal uncertainty in the visual system by the existence of the pedestal (Pelli, 1985). The inhibitory effect is accounted for by multiplicative noise that increases with contrast level of the stimulus only at high contrast levels (Nachmias & Sansbury, 1974; Sanborn & Dayan, 2011).

The uncertainty model was developed by combining a probability summation assumption and a decision variable assumption (signal detection theory, see next paragraph for introduction) (Pelli, 1985). When the uncertainty is high, the decision system has to monitor multiple channels, the relevant ones and the irrelevant ones, to pick one that has the largest decision variable. If the decision variable is larger than a certain subjective criterion, the system responds. When the pedestal is presented, the uncertainty is lower due to the information about position, spatial frequency, orientation etc. Reduced uncertainty results in reduced increment thresholds. Pelli has shown that the uncertainty model can explain the facilitatory effect but not the masking effect. The multiplicative noise that depends on the contrast level generates a larger increment contrast to be necessary for the discriminating task.

Nonlinear transducer model prevails

Now I would like to come back to the discussion about nonlinear transducer function and uncertainty. There have been a few studies that have tried to distinguish these two potential mechanisms and they favored the nonlinear transducer. Some (Barlow et al., 1987) tried to manipulate the level of uncertainty by presenting the targets at a designated location or in a range of various sizes. Knowledge of the specific location of the stimulus reduced increment thresholds at all mask levels in general but did not eliminate the dip. However, location uncertainty is most likely not the only source of uncertainty. The uncertainty from spatial frequency and orientation channels could still cause the dipper shape. They also compared the human contrast discrimination data with measurements of contrast response function from monkey primary cortex single neuron recording and found promising similarities. These results suggest that the nonlinear transducer function is supported by neurophysiological data of the contrast response function of single neurons (Westrick & Landy, 2013).

Another study (Kontsevich & Tyler, 1999) concluded that uncertainty cannot be the sole source of nonlinearity because pedestal masking functions of positive-signed and negative-signed pedestal masks are very different phenomena. If uncertainty is the sole source of nonlinearity, the nonlinear functions from these two kinds of masks should be similar.

While trying to determine the efficacy of their observer model-perceptual template model (PTM), Lu and Dosher (2008) also compared uncertainty and nonlinear transducer functions and favored the latter. In a PTM, besides the perceptual template which acts like a filter tuned to the stimulus, additive noise, and the decision making stage, they employed a nonlinear transducer function (half-wave rectified followed by an expansive transformation) and a multiplicative noise to account for the nonlinearity in the contrast response function and the equivalent external

noise results. They compared different observer models by fitting them to double-pass results and triple TvC results.

The triple TvC method was introduced and incorporated into the equivalent noise paradigm. It is a method used to calculate internal noise level by adding different levels of external noise, created by the same authors (Lu & Dosher, 2008). The TvC function here in the equivalent noise paradigm refers to detection or discrimination thresholds versus external noise contrast. Three TvC functions at three different performance levels (represented by signal-to-noise ratio d' or equivalently percent correct, see explanation in the next section Signal Detection Theory) are measured. From these three TvC functions, two threshold ratios are calculated and plotted at each external noise level. Results from this method reflect the nonlinearity in the visual system.

The double-pass procedure, on the other hand, was developed to estimate the internal noise relative to external noise (D. M. Green, 1964). In this procedure, the same sequence of trials, which contain both signal and external noise, is repeated twice for each observer. It has been used to conclude that the internal noise is not a constant; rather it increases with the external noise and signal contrast levels (Burgess & Colborne, 1988; Lu & Dosher, 2008). However, it has been proved that the PTM with multiplicative internal noise and a contrast gain control model with constant internal noise are mathematically equivalent (Dao, Lu, & Dosher, 2006) and both can account for the double-pass results (Lu & Dosher, 2008).

Although both nonlinear transducer function and uncertainty models can explain the triple TvC results, surprisingly the PTM with nonlinear transducer function outperforms uncertainty models in fitting double-pass results (Lu & Dosher, 2008). As for distinguishing between the multiplicative noise and the gain control mechanism, the current psychophysical

data that are available are not enough to decide whether internal noise changes with the stimulus level (F, 2016). Both the PTM and a nonlinear transducer function of the form of divisive gain control can account for the results from pattern-masking experiments, as well as double-pass and triple TvC experiments.

To determine whether the internal noise is constant (additive noise) or variable with the signal strength (multiplicative noise), current available data derived from contrast discrimination tasks including pedestal masking paradigm are simply not mathematically powerful enough. Either additive or multiplicative noise could possibly account for the pedestal masking functions. In his recent review, Kingdom (2016) proposed an approach to study this question by comparing data of discrimination experiments to difference-scaling experiments. The principle of difference-scaling experiment is to adjust the stimulus level until the differences between the two upper and lower stimuli are perceived as identical. This difference-scaling performance is not subject to the influence of internal noise. Thus, if the shapes of the transducer functions generated by discrimination and scaling paradigms are same, the internal noise is constant for the current stimuli and task. In the review, Kingdom showed that the transducer functions from two early studies (Whittle, 1986, 1992) about discrimination and scaling , respectively, are almost identical. This suggests constant internal noise for perceived luminance in the studies. This approach provides a possible solution for determining whether perceptual internal noise is constant. Applying it to second-order processing can be an interesting future research topic.

Based on the aforementioned studies that favor contrast-gain control over uncertainty models, I chose the nonlinear transducer model with a constant internal noise assumption when modeling second-order nonlinearity.

Signal detection theory

Regardless which mechanism is used to explain the dipper shape of the pedestal masking function which reflects the underlying nonlinearity in the visual system, one can take $f(c)$ as the output/response of the processing system. *c* denotes the stimulus contrast level. When this response gets to the decision-making stage, it is subjective to internal noise from various sources, which is a fundamental feature of the brain (Faisal, Selen, & Wolpert, 2008). In this thesis, the internal noise at the decision making stage is modeled as a whole; its specific source will not be mathematically studied. The signal detection theory (SDT), originated from engineering field, describes the distribution of internal noise as a Gaussian distribution with zero mean and constant standard deviation σ (constant additive noise assumption). Thus in the 2-interval forced choice (2IFC) task of the pedestal masking paradigm, the responses to the stimuli in the test intervals and the null intervals can be described by Gaussian distributions with means *f(m)* and *f(m+t)*, respectively, and a standard deviation σ. *m* is the contrast of the pedestal mask and *t* is the contrast of the target. In each trial, response to both the target and the pedestal mask in the test interval under the effect of internal noise is

$$r_t = f(t + m) + N_{int}\ ; \qquad \text{Equation 6}$$

and in the null interval response to only the mask is

$$r_t = f(m) + N_{int}\ , \qquad \text{Equation 7}$$

where $N_{int} \sim N(0, \sigma^2)$ is a random variable sampled from the normal distribution of internal noise.

In Figure 4(a), the probability density distributions of test-interval responses and null-interval responses are shown in standard deviation units. The two distributions are normalized in a way that the null-interval distribution is centered on zero while the test-interval distribution on

$f(t+m)-f(m)$. In standard deviation unit, the standard deviations of both distributions are 1. The decision variable is defined as the signal-to-noise ratio that is

$$d' = \frac{f(t+m)-f(m)}{\sigma}. \qquad \text{Equation 8}$$

In the standard deviation units, *d'* is the distance between two means.

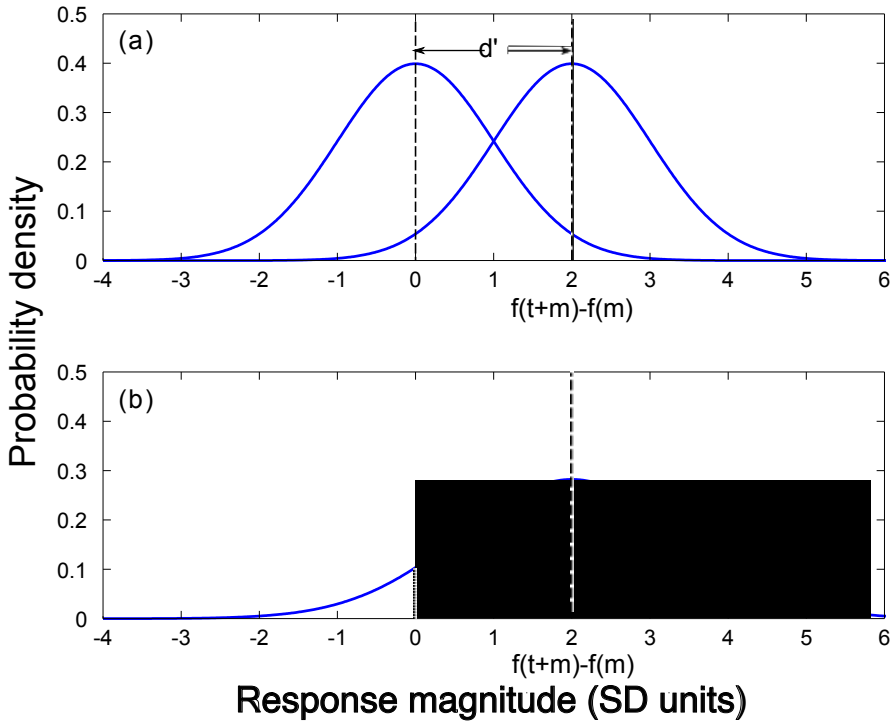

Figure 4. Illustration of how *d'* and percent correct are related under the SDT. The probability density functions are plotted against response magnitude on the standard deviation (SD) units. (a) The probability density function of the response magnitude to the pedestal mask is centered on zero and that to the target plus mask is centered on the response difference between the test and the null intervals. The SD is equal for the two distributions and has a value of 1. (b) The probability density function of the difference between the two distributions. It is centered on the difference of responses and has a SD of $\sqrt{2}$. The signal-to-noise ratio *d'* equals to f(t+m)-f(m). The probability that the response magnitude is larger in test interval is the grey area in (b) which can be calculated as $\Phi(\frac{d'}{\sqrt{2}})$.

The SDT provides a way of linking the percent correct to the magnitude of the stimuli in psychophysical experiments so that one can mathematically model the data (F. A. A. Kingdom & Prins, 2016). In the 2IFC task, the observer's criterion is to choose the interval with larger response. Then if the response in the test interval is larger than the null interval, the answer is correct. That is to say, percent correct on the task, which is the probability that a certain observer picks the test interval correctly, is equal to the probability that the response of test interval minus null interval is larger than zero. The probability density distribution of the difference of the two distributions of the two intervals is shown in Figure 4(b) in the same standard deviation units. According to the variance sum law, the mean of the difference distribution equals to the difference of the two means, and the standard deviation of it equals to $\sqrt{\sigma^2 + \sigma^2} = \sqrt{2}\sigma$ that is $\sqrt{2}$ on the standard deviation unit. Therefore, the probability of the difference distribution function having a value larger than zero is $\Phi(\frac{d'}{\sqrt{2}})$. $\Phi(x)$ is the cumulative probability distribution. This value is also the percent correct of the task overall. Because *d'* is a function of stimulus magnitude, in this way, the percent correct and the stimulus magnitude are linked. For each arbitrarily chosen performance level *d'*, there is a percent correct value corresponding to it.

By incorporating the SDT into the modeling process, one can build a complete observer model as well as studying the internal noise level under different task and perceptual conditions.

Second-order processing

Although neurons with simple receptive fields have been studied extensively, the physiological mechanism of second-order processing is not very clear. Second-order processing cannot be mediated by these neurons with separate excitatory and inhibitory regions in their

receptive fields. Such linear filter model cannot account for second-order processing because the average luminance level is identical on both sides of a second-order boundary so that the activation and inhibition within a linear receptive field are equal. Figure 1f shows that a linear filter tuned to the spatial frequency of the second-order information will give no response.

Second-order information is by definition a modulation of first-order information. In the literature, a second-order stimulus comprises two components; a carrier that consists of first-order information and an envelope, which modulates the carrier. The modulation can be contrast-defined, texture-defined, motion-defined, etc. The kind of second-order information that has been most studied is contrast-modulation.

Different mechanism than first-order processing

Psychophysical results

It is generally agreed that second-order processing is done by a different mechanism to that responsible for first-order processing. Psychophysical methods to investigate whether two kinds of stimuli are processed with the same mechanism include employing masking, facilitation and adaptation paradigms between these two stimuli. The existence of any of these effects between two different stimuli could be evidence for identical mechanism. With the masking approach, we found no mutual masking effect between first-order and second-order stimuli regardless of which one constitutes the mask (Allard & Faubert, 2007). Similarly, we found no facilitation between the two kinds (Schofield & Georgeson, 1999). Adaptation to one kind of stimulus does not elevate the threshold of the other (Nishida, Ledgeway, & Edwards, 1997). Furthermore, alternating between luminance-defined and contrast-defined frames in a multi-frame motion sequence makes observers unable to tell the motion direction (T. Ledgeway &

Smith, 1994). Likewise, second-order motion has no effect on extracting first-order global motion (Edwards & Badcock, 1995).

Neurophysiological and imaging results

Neurophysiology also provides support for separate mechanisms for first- and second-order processing. Although no neurons were found to respond exclusively to second-order envelope information (C. L. Baker, Jr. & Mareschal, 2001), about 50% of the neurons in cat A18 and less in A17 (Mareschal & Baker, 1998b; Zhou & Baker, 1993), and about 30% of neurons in primate V2 (G. Li et al., 2014) respond to second-order envelope information. However, these envelope-responsive neurons also respond to luminance gratings. The spatial frequency and orientation tuning to first-order luminance grating matches that was found for the envelope, however the carrier tuning is 5-30 times higher than that of the envelope. (G. Li et al., 2014; Mareschal & Baker, 1999; Zhou & Baker, 1996). There is no fixed ratio between the optimal spatial frequencies of the carrier grating and either the luminance grating or envelope grating in cat Area 17,18, and primate V2. This independence of first-order luminance, second-order carrier and second-order envelope tuning even within the same cells suggests separate processing streams (C. L. Baker, Jr. & Mareschal, 2001). Furthermore, recent studies by Rosenberg and colleagues found that this dual processing of first-order and second-order carrier information while having different tuning properties in cortex may be inherited from LGN Y cells (Rosenberg, Husson, & Issa, 2010; Rosenberg & Issa, 2011). Human fMRI studies also reported that different areas in the visual cortex respond differently to first- and second-order motion (Smith, Greenlee, Singh, Kraemer, & Hennig, 1998). fMRI adaptation of one kind does not reduce the response level of the other kind (Ashida, Lingnau, Wall, & Smith, 2007; Larsson et al., 2006). In a lesion study, selective deficits for first- and second-order motion processing were reported in two human patients (Vaina, Cowey, & Kennedy, 1999).

Temporal properties

In terms of temporal properties, second-order processing has been reported to be more sluggish than its first-order counterpart by some authors (Lu & Sperling, 1995) but not by others (Schofield & Georgeson, 2000). Although there is no consensus in the temporal properties from psychophysical studies, in two electrophysiological studies, one using visually evoked potentials (VEP) (Calvert, Manahilov, Simpson, & Parker, 2005) and another single cell recording (Mareschal & Baker, 1998a) found longer latency for second-order processing. These latter results imply that first-order and second-order processing undergo different processes.

Brain locus of processing

Unlike first-order processing whose neural substrate is attributed to the linear receptive fields of the simple neurons in the primary visual cortex (V1 or cat A17), results about the location where second-order processing occurs are of less consistent form. Nevertheless, it is generally agreed that second-order processing involves higher visual areas downstream from V1 though V1 may still make an important contribution. The techniques researchers have employed to investigate this question include neurophysiology, brain imaging and lesion analysis.

One interesting question to ask when studying second-order processing is whether different kinds of second-order information are processed by the same neurons in the same cortical area, a so called cue-invariant area (Self & Zeki, 2005). This question is not only about understanding the processing mechanism(s) for second-order information in general. It also provides insights about whether one can generate his or her conclusion based on results from studying a certain kind of second-order stimulus to second-order processing in general. In terms of different kinds of second-order stimuli, there is an important distinction between second-order

motion and motion-modulated (or motion-defined) second-order information. Second-order motion information represents spatiotemporal variations in second-order features, such as contrast and texture. A typical second-order motion stimulus that was used early in the literature is a patch of flickering dots moving on the background of similar static dots. The average luminance is the same for the moving patch and the background. Motion-defined second-order information, on the other hand, is created by different motion velocities. For example, a motion-modulated boundary has components on each side of it moving at different velocities. I believe categorizing second-order information with respect to the specific type of modulation is a more reasonable approach. Because it corresponds to the Linear-nonlinear-linear model for second-order processing (see introduction in the later section) in terms of the responses of the first-stage linear filters fed into the second-stage linear filters. In the Literature Review, I survey both of these two kinds of second-order information. However, in three of the four articles that compose this thesis, the stimulus is second-order motion-modulation instead of second-order motion.

Previous studies about the locus or physiological basis of second-order processing have almost all found that it starts from the primary visual cortex (V1) and extends to involve higher visual areas in the extra-striate cortex. For second-order motion, the earliest finding is that neurons in the middle temporal (MT) area are responsive to texture-modulated motion and are direction-selective (Albright, 1992). Also using single neuron neurophysiological technique, Zhou and Baker found neurons in cat A17 and A18 responded to the contrast-modulated moving envelope (Zhou & Baker, 1993, 1994). In an early human fMRI study, many areas including V1, V2, V3, VP, V3A, V3B and MT are all found to respond to second-order; and only V3, VP, V3A and V3B respond stronger to second-order than first-order motion. For motion-modulated second-order boundaries, selective response over first-order boundaries was found in V1, V2, V3

and VP (Reppas, Niyogi, Dale, Sereno, & Tootell, 1997) in a human fMRI study. Likewise, areas V3A, V3B, LO1, LO2 and V7 show orientation-selective adaption in another fMRI study (Larsson et al., 2010). For stationary second-order information, Larsson and colleagues (2006) reported orientation-selective adaptation in many areas for both contrast- and orientation-modulated second-order gratings using a human fMRI approach. In a few areas including VO1, V3A, V3B and LO1, the adaptation value was also found to be larger than V1. This result suggests that there are additional processes involved in static second-order processing after V1 (Larsson et al., 2006). Also using fMRI methods, areas V4 and V3A were found to exhibit stronger activities for texture-defined boundaries than plain textures without boundary (Kastner, De Weerd, & Ungerleider, 2000). Neurons in areas V1, V2, V3 and V4 have also been reported to be selective to spatial frequency (Hallum, Landy, & Heeger, 2011). A lesion study in monkeys also reveals the critical role of V4 for second-order texture discrimination (Merigan, 2000).

In summary, all the results about selective responses and selective adaptation to one or other kinds of second-order information, as well as to a certain attribute of it (such as spatial frequency or orientation) collectively imply that second-order processing stems from early visual areas V1 and V2 and involves multiple areas, depending on the type of second order modulation, in the extra-striate cortex.

Second-order models

Modulation transfer function

In psychophysical studies characterizing the properties of second-order processing, researchers have measured the modulation transfer function (MTF). Similar to the contrast sensitivity function for first-order processing, the MTF is the sensitivity across different

modulation (envelope) spatial frequencies. Although there are several inconsistencies due to the choice of stimuli and the range of spatial frequencies of the carrier and the envelope, the MTF was found to be generally a low-pass one for both contrast-modulation (Jamar & Koenderink, 1985; Schofield & Georgeson, 1999; Sutter, Sperling, & Chubb, 1995) and orientation modulation (F. A. Kingdom, Keeble, & Moulden, 1995; Landy & Oruc, 2002). A smooth MTF could signify a single second-order mechanism that operates on the whole spatial frequency range with preference on a portion of that whole range. It could also be, similar to first-order contrast sensitivity function, the summation of various modulation sensitivity functions of multiple second-order mechanisms each tuned to a specific narrower spatial frequency bandwidth.

Linear-nonlinear-linear model

This idea is consistent with the linear-nonlinear-linear (LNL) model. This modeal originates from the observation that second-order motion or texture information which could not be accounted for by a single linear filter model could be captured by a three-stage model that involves a first linear filter followed by a nonlinearity of any format and a second linear filter that process the nonlinearly transferred output of the first linear filter (Chubb & Sperling, 1988; Sutter, Beck, & Graham, 1989). The model is widely used to explain second-order processing (N. Graham & Sutter, 1996, 1998, 2000; N. Graham, Sutter, & Venkatesan, 1993; N. Graham, Sutter, Venkatesan, & Humaran, 1992; Sutter & Graham, 1995; Sutter et al., 1995; Wilson, 1994).

Tuning properties of the linear filters

Second-order mechanisms that are selective to spatial frequency and orientation (Arsenault, Wilkinson, & Kingdom, 1999; N. Graham et al., 1993; Kwan & Regan, 1998; Landy & Oruc, 2002; Sutter et al., 1995), like their first-order counterparts, were found with various

methods, such as adaptation (Kwan & Regan, 1998), masking (Arsenault et al., 1999) and sub-threshold summation (Landy & Oruc, 2002). A relatively recent study from our lab employed the discrimination at detection threshold approach to show that the bandwidth of these spatial frequency and orientation tuning channels are 1-2 octaves for spatial frequency and 30° for orientation (Alexandre Reynaud & Hess, 2012).

It has also been shown that second-order mechanisms are tuned to the carrier spatial frequency and orientation. Psychophysics studies using narrow-band (N. Graham et al., 1993) or band-pass (Dakin & Mareschal, 2000) carriers reveal that the first stage filter is tuned to both spatial frequency and orientation. In neurophysiology, Baker and colleagues (Mareschal & Baker, 1999; Zhou & Baker, 1996) found that envelope-responsive neurons are tuned to carrier spatial frequencies that are much higher than their optimal envelope spatial frequency. These neurons also show broad bandpass tuning to carrier orientation (Mareschal & Baker, 1998a, 1999).

Intermediate nonlinearity

The intermediate nonlinearity between the two linear filter stages is necessary because otherwise pooling outputs from different first-stage linear filter will cancel, and the two linear filters will collapse to only one linear filter. The second-order modulation will not be extracted by this one linear filter. Mathematically, however, almost any kind of nonlinearity would serve the purpose (Huang & Chen, 2014) and often researchers simply employed point-wise half-wave or full-wave rectification, it has been suggested that an expansive spatial nonlinearity (N. Graham, 1994; N. Graham & Sutter, 1998) and a compressive nonlinearity of the divisive normalization form between first-order channels (N. Graham & Sutter, 1996, 1998, 2000; Olzak & Thomas, 1999) are involved as well.

In studies about texture segregation, the "element arrangement textures" are often used. These are stimuli in which the texture boundaries are created only by different arrangements of the elements. Elements can vary in size, contrast, spatial frequency and orientation in different stimuli. It is believed that square element textures are processed by first-order simple cells whereas Gabor element textures are processed by second-order complex cells tuned to the fundamental spatial frequency of the texture information. An area experiment was used to study the spatial nonlinearity by investigating the area-contrast trade-off (N. Graham & Sutter, 1998). For square element textures, the trade-off is linear. Gabor element textures, on the other hand, exhibit a trade-off between area size and Gabor contrast level. This shows that the spatial nonlinearity is a power function with an exponent in the range from 2 to 4. In a later study by the same authors, a series of "constant-difference" experiments with element arrangement textures were conducted in the effort to distinguish between an early local compressive nonlinearity before the first-order channels and a normalization network in the form of divisive inhibition after the first-order channels. In the experiment, the amount of contrast difference between two types of elements is constant while they both vary together. By comparing the results with the results from area experiments, they found that only the divisive normalization model can explain the results from both experiment. When contrast is in the middle-high range, compressive nonlinearity overwhelms the expansive nonlinearity, thus in the constant-difference experiment, the ends of the segregation curves show clear compressiveness. In the same contrast range, because the spatial nonlinearity is decided by the spatial pooling within complex channels, it is independent from the normalization network. Thus, an intermediate nonlinearity of expansive form would explain the result of expansive power functions in the area experiment. Graham and colleagues showed that the nonlinearity of a divisive normalization form as well as an expansive

nonlinearity between channels are needed for second-order element-arrangement texture segregation.

Canonically (F. A. Kingdom et al., 1995; Landy & Oruc, 2002; Sutter et al., 1995), it is assumed that the modulation information in the envelope is successfully and faithfully demodulated by the first two stages-the first linear filters followed by the intermediate nonlinear stage. Then the second linear filters can successfully extract the modulation information. My studies about second-order nonlinearity are also based on this assumption. When modeling the nonlinearity, the input to the nonlinear transducer function is equal to the modulation contrast.

Identical or different mechanisms for different second-order stimuli?

In a classical LNL model, the second linear filters will respond to spatiotemporal variations in any second-order modulation dimension (F. A. Kingdom et al., 2003). This flexibility implies that different types of second-order modulations are processed by the same mechanism. Indeed, there is evidence in the literature from psychophysics, neurophysiology and imaging studies that supports this idea of identical mechanism for different types of second-order modulations. Usually, studies that bear upon this topic are done with the goal of investigating the processing of second-order, complex boundaries. Complex boundaries that were studied could be contrast-defined, texture-defined (which includes orientation-, size, spatial frequency-defined), motion-defined etc. Studying the processing of complex boundaries is essentially the same as studying second-order modulation.

For boundary processing, the idea of "cue-invariant" processing has been advocated for many years. Weak mutual facilitation between the processing of contrast-modulation and orientation-modulation was reported in a psychophysical study (Schofield & Yates, 2005). There is also cross-adaptation effect between luminance- and contrast-defined boundaries, as well as between luminance- and orientation-defined boundaries (Filangieri & Li, 2009; Hawley &

Keeble, 2006). Tilt after effect was also found between pairs of motion-, luminance-defined boundaries and illusory contours (Berkley, Debruyn, & Orban, 1994). Neurophysiological experiments have also shown that there are neurons in various regions in the visual cortex that respond in a cue-invariant manner to more than one types of contours, for example primate V2 (Leventhal, Wang, Schmolesky, & Zhou, 1998; Marcar, Raiguel, Xiao, & Orban, 2000) and inferior temporal (IT) region (Sary, Vogels, Kovacs, & Orban, 1995) and cat Area 18 (Gharat & Baker, 2012; Song & Baker, 2007). Specifically in cat Area 18, neurons show similar selectivity to spatial frequency and orientation for both envelope and carrier between contrast-modulation and motion-modulation (Gharat & Baker, 2012). In an fMRI study, boundaries defined by luminance and motion showed similar radial biases that involved a stronger blood oxygen level-dependent (BOLD) signal in the parts of the retinotopic map that have radial orientations with respect to the fixation point. Although motion processing was shown to involve a separate pathway to that of static luminance information (Derrington, Allen, & Delicato, 2004; Goodale & Milner, 1992), all the aforementioned studies suggest that there is one general mechanism for second-order modulation/boundary processing.

However, there is also evidence that second-order stimuli are processed by at least partly separate mechanisms. A study that tested the pedestal effect between different types of second-order modulations (F. A. Kingdom et al., 2003) found no facilitative effect when the pedestal mask was of different type as the target. In a later study, however, Schofield and Yates (2005) argued that the lack of facilitation is due to the phase relationship between the carrier and envelope and pedestal levels that Kingdom et. al. used.

In an EEG study, visual evoked potentials (VEPs) were used to compare second-order modulations of different types (Babenko & Ermakov, 2015). The authors found that contrast-,

orientation- and spatial frequency-modulations had all different parameters for their evoked response. This result implies that different second-order modulations involve different brain processes suggesting separate mechanisms for various second-order modulations.

Evidence also comes from neuroimaging results. Two fMRI studies done by Larsson and colleagues (Larsson et al., 2010; Larsson et al., 2006) showed that orientation-selective adaptation to different types of second-order boundaries is elicited in different cortical visual areas. Overlap exists but is very limited. For motion-modulation, fMRI adaptation exhibits in areas including V3A/B, LO1 (lateral occipital), LO2 and V7; while for contrast-modulation and orientation-modulation, the areas are V1, V2, V3, V3A/B, LO1, hV4 and VO1. Beyond this, a monkey lesion study reported that the removal of MT affected the processing of kinetic boundaries but not luminance-defined boundaries (Marcar & Cowey, 1992). Importantly, this is not due to local motion processing being impaired – when the two motion directions are orthogonal and not opposite, the ability of using motion-defined boundaries in shape discrimination remains intact.

Whether different kinds of second-order modulations are processed by a single mechanism is still an open question. In this thesis, the first, second and fourth chapters all contribute to the resolution of this question by investigating the nonlinearities involved in these different types of second-order processing.

Second-order nonlinearity

The pedestal effect that is the dipper shape in TvC function has also been found in second-order processing (Huang & Chen, 2014; F. A. Kingdom et al., 2003; Schofield & Georgeson, 1999; Schofield & Yates, 2005). In second-order pedestal masking experiments, the

TvC function refers to increment threshold of the modulation versus contrast of the pedestal modulation. The existence of such a dip implies that the output of second-stage filters is also subjected to a nonlinearity which is accelerate/expansive at low modulation levels and decelerate/compressive at high modulation levels.

The earliest application of pedestal masking paradigm to second-order processing is probably the study in which gain control mechanisms in first- and second-order motion processing was studied (Lu & Sperling, 1996). However, a static pedestal grating was used to mask a second-order motion grating (contrast-modulated) and no facilitative or inhibitory effect was found. I think it is reasonable that no pedestal effect was found because the target (moving grating) and the pedestal (static grating) are not processed by the same mechanism, it makes sense that they do not undergo a same nonlinearity. Contrary to what the authors' claim, I think this result cannot prove that the envelope modulation is not involved in the gain control network in second-order processing.

The facilitatory part of the pedestal effect can be used to investigate whether the target and mask stimuli are processed by the same mechanism. If facilitation exists when the mask and the target represent different types of information, one can conclude that they are processed by at partially overlapping mechanisms. If cross-facilitation does not exist, the mask and the target are probably processed separately. Following this rationale, first-order luminance-modulation and second-order contrast modulation have been shown to be processed by different mechanisms (Schofield & Georgeson, 1999). Similarly, three types of second-order stimuli, contrast-, orientation- and spatial frequency-modulations, are reported to be processed by independent mechanisms (F. A. Kingdom et al., 2003). These two studies, although they reported the

existence of second-order pedestal effect, they did not specifically try to mathematically model the nonlinearity involved in second-order processing.

The only study (Huang & Chen, 2014) that has systematically studied second-order nonlinearity did so recently by modeling the pedestal masking functions of first-order luminance-modulation and second-order contrast-modulation, respectively. The model they built for second-order processing is composed of five stages: 1. Early linear filters that extract carrier information; 2. Early nonlinear response that is half-wave rectification followed by a nonlinear transform of divisive inhibition form; 3. Late linear filters that operates on the contrast-modulation information; 4. Late nonlinear response that is of same form of the earlier one; 5. Decision making stage that accords to signal detection theory with internal noise of fixed value 1. Even though they state that contrast-modulation may not need the late linear filters and the late nonlinear response to be extracted, these two stages are of important interest for the current thesis. One important conclusion of this study is that divisive normalization is needed for both first- and second-order processing.

The second-order nonlinearities of other types of second-order modulations besides contrast-modulation have not been studied and modeled. Modeling the second-order nonlinearity not only contributes to understanding the full picture of second-order processing, it can also provide insights about the question of whether different types of second-order information are processed by identical or separate mechanisms. The form of the nonlinear transducer function represents the shape of the nonlinearity which reflects the underlying divisive normalization network and interneuron connectivity. Thus different nonlinearities could suggest different mechanisms for different second-order modulations. In this thesis, I will present the pedestal masking functions of three different kinds of second-order modulations; contrast-modulation

(CM), orientation-modulation (OM) and motion-modulation (MM) in Chapter 1 and Chapter 2. Through modeling the data with a nonlinear transducer function of divisive normalization form, I found the same shape of nonlinearity for CM and OM, but a different nonlinearity for MM.

Amblyopia

Besides investigating the second-order processing in normal human vision, this thesis also studied second-order vision of amblyopic patients because it provides a better understanding of this neural developmental deficit as well as provides an insight into understanding normal visual function and neural plasticity.

General Introduction

Amblyopia is a neural developmental disorder of visual system. It is caused by disrupted or abnormal visual input in early life. Clinically amblyopia is often diagnosed by reduced visual acuity in the disrupted eye without any organic ocular disorder. Usually an interocular difference of two lines or more in an eye chart when both eyes are optically corrected to their best, is enough for the diagnosis. Amblyopia is typically categorized into three types-strabismus, anisometropia and deprivation, according to the specific cause of the disorder. Strabismus, also referred to as “crossed eyes”, is a vision disorder due to misalignment of the two visual axes that causes uncorrelated visual input from the two eyes. Anisometropia is a condition where two eyes have unequal refractive errors. Deprivation occurs because of a physical obstruction, such as cataract blocking the view of one eye or both. For some patients, more than one condition may apply. The most common combination is strabismus and anisometropia (Simons, 2005).

Low-level deficits

Although the typical diagnosis is done according to visual acuity loss, amblyopia has been reported to affect a wide range of visual functions from low level to higher levels, mainly in the amblyopic eye (AE). Low-level AE deficits include not only first-order contrast sensitivity loss (Bradley & Freeman, 1981; Hess, 1979; Hess & Howell, 1977; Levi & Harwerth, 1977), but also spatial distortion (Bedell & Flom, 1981; Hess, Campbell, & Greenhalgh, 1978; Lagreze & Sireteanu, 1991).

Higher-level deficits

Higher-level, more complex visual functions are also affected extensively and many of which have been reported to show deficits in the fellow-fixing eye (FE) as well (see introduction in the later session). Higher-level deficits include multiple object tracking (Ho et al., 2006; Levi & Tripathy, 2006; Tripathy & Levi, 2008), global motion integration (Aaen-Stockdale & Hess, 2008; Hess, Mansouri, Dakin, & Allen, 2006; Ho et al., 2005; C. Hou, Pettet, & Norcia, 2008; M. R. Joshi, Simmers, & Jeon, 2016; Meier, Sum, & Giaschi, 2015; Simmers, Ledgeway, Hess, & McGraw, 2003), global form processing (Dallala, Wang, & Hess, 2010; Hess, Wang, Demanins, Wilkinson, & Wilson, 1999; Husk & Hess, 2013; M. Joshi, Simmers, & Jeon, 2015; M. R. Joshi et al., 2016; Lewis et al., 2002; Mansouri & Hess, 2006; Rislove, Hall, Stavros, & Kiorpes, 2010; Simmers, Ledgeway, & Hess, 2005), second-order perception including contrast-modulation (CM) (Mansouri, Allen, & Hess, 2005; E. H. Wong, Levi, & McGraw, 2001), second-order motion processing in which the stimuli can be contrast-, orientation, texture-modulated (Aaen-Stockdale, Ledgeway, & Hess, 2007; Ellemberg et al., 2005; Simmers et al., 2003; Simmers, Ledgeway, Hutchinson, & Knox, 2011; Simmers, Ledgeway, Mansouri, Hutchinson, & Hess, 2006a; Tang et al., 2014), as well as motion-defined form which I think is largely the same as second-order motion-modulation (MM) (D. Giaschi, Chapman, Meier,

Narasimhan, & Regan, 2015; D. E. Giaschi, Regan, Kraft, & Hong, 1992; Hayward, Truong, Partanen, & Giaschi, 2011; J. Wang, Ho, & Giaschi, 2007), texture-defined form (Aaen-Stockdale & Hess, 2008; J. Wang et al., 2007). Although it is argued that pure integration of motion directions or element orientations can be normal in amblyopia, deficit for global processing only occurs when external noise is added (Hess et al., 2006; Mansouri et al., 2005; Mansouri, Allen, Hess, Dakin, & Ehrt, 2004). Even higher-order abnormalities in amblyopia have been reported for attention (Popple & Levi, 2008) and decision making (Farzin & Norcia, 2011).

What's more, amblyopic patients often have poor binocular vision as well. Many studies have shown that amblyopes have poor binocular summation of at contrast detection threshold (Levi, Harwerth, & Manny, 1979; Levi, Harwerth, & Smith, 1980; Pardhan & Whitaker, 2000). It was thought that binocular mechanism may be lost in amblyopia. However in a later study, binocular summation in strabismic amblyopia was found to be intact when the contrast level was normalized to equalize detectability in the two eyes (D. H. Baker, Meese, Mansouri, & Hess, 2007).

There are many recent reviews (Bretas & Soriano, 2016; Hamm, Black, Dai, & Thompson, 2014; Joly & Franko, 2014; Levi, 2013; Meier & Giaschi, 2017; Tsirlin, Colpa, Goltz, & Wong, 2015) that have good introduction about diagnosis, causes and clinical symptoms. What is of main concern in this thesis, is that the amblyopic deficit for second-order processing and its implications for neural basis of the disorder as well as any implication this might have for second-order mechanisms of normal vision.

Neural substrates for amblyopic deficits

Primary visual cortex deficit

As mentioned earlier, the AE shows deficits for contrast sensitivity, particularly at high spatial frequencies (Hess & Howell, 1977; Levi & Harwerth, 1977; Bradley & Freeman, 1981). This loss in contrast sensitivity is thought to occur in the striate cortex. Neurons in the striate cortex show similar reduced contrast sensitivity. In human primary visual cortex (V1), the AE shows reduced activity in VEP (Levi & Harwerth, 1978) especially at high spatial frequencies. Lower resolution and contrast sensitivity are also found in cat striate cortex neurons (Eggers & Blakemore, 1978). Besides reduced activity, there is also an imbalance in terms of the interconnections between regions in the visual system. Much fewer cells in cat striate cortex are driven by the eye that was deprived since birth (Kiorpes, 2006; Wiesel & Hubel, 1963). Also in the striate cortex of strabismic cats, there are fewer binocular neurons (Chino, Smith, Yoshida, Cheng, & Hamamoto, 1994; Hubel & Wiesel, 1965). Synchronization of population response is also reduced in AE-driven neurons (Lowel & Engelmann, 2002; Roelfsema, Konig, Engel, Sireteanu, & Singer, 1994) as well.

Extra-striate cortex deficits

As reflected by higher-level deficits, amblyopia does not only affect primary visual cortex. Similar to the striate cortex, neurophysiological studies found that ocular dominance in the extrastriate cortex also shifted towards the FE for (Schroder, Fries, Roelfsema, Singer, & Engel, 2002). The level of ocular dominance change is not equivalent in regions that belong to the dorsal and ventral pathways respectively (Schroder et al., 2002). Another neurophysiological study compared the behavioral and neuronal performance in area MT/V5 of macaque monkeys. The authors (El-Shamayleh, Kiorpes, Kohn, & Movshon, 2010) found that, unlike normal MT neurons which are binocular, most MT neurons of amblyopic monkeys have strong preference

for FE input and their response to coherent motion in the AE greatly reduced compared with the FE. Furthermore, an fMRI study (Barnes, Hess, Dumoulin, Achtman, & Pike, 2001) demonstrated that the cortical deficit affected large regions of the extrastriate cortex. A recent study involving multiple-object tracking found less BOLD activity in MT complex in both eyes of the amblyopes and reduced activity in the AE in anterior intraparietal sulcus and frontal eye fields (Secen, Culham, Ho, & Giaschi, 2011).

Since second-order processing is thought to involve extrastriate cortex (see earlier introduction about second-order processing), studying second-order processing in amblyopia provides a good way to speculate deficits in the extrastriate cortex.

Second-order processing deficits

Many studies have reported that amblyopia shows second-order deficits that cannot be accounted to the loss of first-order sensitivity (Ellemberg et al., 2005; E. H. Wong et al., 2001). Wong and colleagues (2001) inferred that amblyopia exhibits extra loss for second-order contrast-modulation from the results that both AEs and NAEs showed increased detection threshold for second-order stimulus when the carrier visibility was equated for the amblyopes and normal control eyes. The evidence suggests that when first-order loss is accounted for by equating the detectability of first-order carrier for AEs, FEs, and the normal eyes (NEs), amblyopia still shows deficits in processing second-order contrast modulation for both detection (Mansouri et al., 2005; E. H. Wong et al., 2001) and orientation-discrimination (Mansouri et al., 2005).

Ellemberg et al. (2005) measured the motion direction discrimination for both first-order luminance-modulated and second-order contrast-modulated sine-wave gratings in patients with

early monocular or binocular visual deprivation due to congenital cataracts. Sensitivity loss for second-order motion was greater than its first-order counterpart (Ellemberg et al., 2005). Global motion deficits are also found to exist for both first-order and second-order elements (Aaen-Stockdale et al., 2007; Simmers, Ledgeway, Mansouri, Hutchinson, & Hess, 2006b). In a relatively more recent study (Simmers et al., 2011), the sensitivity for second-order motion defined by contrast-, flicker-, size- or orientation-modulation in a large spatial and temporal frequency range was measured in strabismic amblyopia. It was found that the "window of visibility" of second-order motion in the AE reduced more than that of the first-order motion for all four kinds of modulations. What's more, second-order motion defined by some texture modulations, e.g. orientation, are almost invisible for severe amblyopes (Simmers et al., 2011). The same second-order motion (contrast-modulated gratings) deficit was found in a group of anisometropic amblyopes as well (Tang et al., 2014).

For second-order motion-modulation, an early study found that both the AEs and the FEs of amblyopic children shows reduced ability to recognize motion-defined letters (D. E. Giaschi et al., 1992). In adults, the deficit also exists for the AEs (D. E. Giaschi et al., 1992). More studies have found the ability to detect motion-defined simple shapes is degraded in both eyes of the amblyopes (Hayward et al., 2011; J. Wang et al., 2007). A clinical study (D. Giaschi et al., 2015) followed the occlusion treatment process of a group of amblyopic children and measured their ability to detect motion-defined forms. What they found out was that occlusion therapy does not resolve the deficit in motion-defined form processing even when the visual acuity and contrast sensitivity are greatly improved. For second-order orientation modulation, the amblyopic eye deficit has also been reported for detecting orientation-modulated form (J. Wang et al., 2007).

Motion- and texture-defined form processing is a complex process in which the amblyopic deficit could be due to either specifically second-order processing or form processing in general. One study that tested motion-defined form, texture-defined form and global motion tasks in the same group of amblyopic children claim that figure-ground segregation might be the reason behind the deficit in motion- and texture-defined form (J. Wang et al., 2007). Their reason for this was that performance on the global motion task was not significantly worse compared with normal, while performance for both motion- and texture-defined form was reduced. However, their finding of no global motion deficit somewhat contradicts the results of other studies, as mentioned earlier. In order to study the amblyopic deficit for second-order modulations, purer second-order stimuli are needed. In this thesis, I employed motion-modulated and orientation-modulated gratings to study amblyopic second-order vision.

Before my paper (Gao et al., 2015), which constitutes Chapter Three in this thesis, was published, there was no study that systematically investigated amblyopic deficits for various kinds of second-order modulations. In this paper, we wanted to ask whether amblyopia shows general deficits for all kinds of second-order modulations and to what degree the fellow eye is also affected in processing second-order modulations. I tested the orientation-discrimination sensitivity monocularly for contrast-modulation (CM), orientation-modulation (MM) and motion-modulation (MM) in 28 patients including both strabismic and anisometropic amblyopes. This study answered the two questions by finding reduced sensitivity in the AEs for all three kinds of modulations, especially at high spatial frequencies. Furthermore, only for MM, the FEs showed reduced peak sensitivity. Thus amblyopic deficit for second-order processing is general but the FE is affected in processing only some types of modulations.

Fellow eye deficit

A deficit in the FE for amblyopes is not only found in my study. It has been reported for various higher-level visual functions. Global motion is the task that was most reported to show FE deficit (Aaen-Stockdale & Hess, 2008; Aaen-Stockdale et al., 2007; C. Hou et al., 2008; Kiorpes, Tang, & Movshon, 2006; Simmers et al., 2003; Simmers et al., 2006b). This deficit for global motion processing cannot be explained by contrast sensitivity loss (Aaen-Stockdale et al., 2007; Simmers et al., 2003; Simmers et al., 2006b). It exists for translational, rotational and radial components of the global motion task (Simmers et al., 2006b). When the components are contrast-defined (second-order), the deficit in the FE is comparable to that in the AE (Aaen-Stockdale & Hess, 2008; Aaen-Stockdale et al., 2007).

Motion-defined form perception has also been reported to show FE deficit especially in children (D. Giaschi et al., 2015; Hayward et al., 2011; J. Wang et al., 2007). The presence of amblyopic deficits in both eyes is reported for a structure-from-motion task as well (Aaen-Stockdale & Hess, 2008; Husk, Farivar, & Hess, 2012). What's more, the FE is affected in multiple-object tracking task which reflects a binocular deficit in not only passive viewing condition but also in active motion tracking system (Ho et al., 2006; Secen et al., 2011).

This higher-level motion-related binocular deficit is consistent with the neurophysiological finding that the dorsal pathway is more binocular than the ventral pathway in strabismic amblyopic cats (Schroder et al., 2002). According to the parallel processing hypothesis (Goodale & Milner, 1992; Haxby et al., 1991; Van Essen & Gallant, 1994), the extra-striate cortex is organized into two parallel processing streams-the "dorsal" or "action" pathway and the "ventral" or "form" pathway. The dorsal pathway is specialized for processing location and motion of objects while the ventral pathway is specialized for processing form and pattern.

Correspondingly, deficits for global form perception (Dallala et al., 2010; Hess et al., 1999; M. R. Joshi et al., 2016; Levi, Yu, Kuai, & Rislove, 2007) and second-order contrast-modulation perception (Mansouri et al., 2005) have mostly been found to affect only AE function. FE deficits have been reported in contour integration across space, but it is much less severe compared with the AEs and only exists in a small portion of the amblyopic observers (Kovacs, Polat, Pennefather, Chandna, & Norcia, 2000; Levi et al., 2007). Furthermore, only two out of five patients (E. H. Wong et al., 2001) and one out of seven patients (Tang et al., 2014) FEs showed slightly higher CM detection threshold.

The fact that FE deficit was consistently found for motion-related higher-level visual functions suggests that dorsal and ventral pathways may be affected by amblyopia to different degrees. In the last Chapter, I studied whether second-order nonlinearity, which reflects divisive normalization (according to our model), can account for the different deficit patterns for the processing of second-order motion- and contrast-modulation.

Manuscript 1: The response nonlinearity to second-order contrast and orientation modulation characterized using pedestal masking

Yi Gao, Alex S. Baldwin, Robert F. Hess

Abstract

Second-order processing in the visual system can be modeled by a linear non-linear linear (LNL) process. There is evidence that the second-order modulation signals extracted by the LNL process undergo a gain-control nonlinearity. This study systematically investigates and models this second-stage nonlinearity in the processing of contrast-modulation (CM) and orientation-modulation (OM) using data from a pedestal masking paradigm. The basic model describes the nonlinear modulation response function in a divisive inhibition form with three parameters including two exponents and a gain parameter, followed by the decision-making process with one internal noise parameter. The pedestal masking functions of both CM and OM have the typical dipper shape. Model fitting reveals that OM has the same internal noise and transducer exponents as CM, but a four-fold larger gain parameter. The similarity of the transducer exponents suggests that OM processing goes through identical second-stage nonlinearity and decision-making process as CM. The difference in the gain parameter would be consistent with the output from the OM channels receiving greater divisive inhibition, or smaller effective carrier contrast due to cross-orientation suppression between the carrier orientations.

Introduction

Information about objects and structures in the retinal image can be extracted from both first- and second-order features (Cavanagh & Mather, 1989; Chubb & Sperling, 1988). First-order features are defined by changes in luminance or chromaticity. Second-order features are changes in those first-order features, such as changes in contrast, orientation or motion properties. The most basic second-order feature that has been investigated is contrast-modulation

(CM). Stimuli that test CM processing can be constructed by modulating a first-order carrier stimulus defined by luminance changes (e.g. a high spatial-frequency grating or visual noise) by a lower spatial frequency envelope grating(Huang & Chen, 2014). Second-order stimuli are thought to be processed by separate mechanisms from that of their first-order counterparts. This notion is supported by a number of previous studies employing various methods including psychophysics (Edwards & Badcock, 1995; T. Ledgeway & Smith, 1994; Schofield & Georgeson, 1999, 2003), electrophysiology (C. L. Baker, Jr., 1999; Mareschal & Baker, 1998a, 1999), brain imaging (Smith et al., 1998) and visually evoked potentials (VEP) (Calvert et al., 2005).

A commonly-used model for second-order processing involves a three-stage process: i) the input image is filtered by in a set of first-stage linear filters, ii) the filter outputs are transformed by a non-linearity, iii) the transformed filter outputs are filtered again by a final-stage linear filter. This is the linear non-linear linear (LNL) model (N. Graham & Sutter, 1998, 2000; N. Graham, Sutter, et al., 1992; Wilson, 1994). In this model, the first-stage linear filters are tuned to orientation and spatial frequency. These extract the luminance-defined structure. The form of the nonlinear operation applied to their output has been suggested to be either a simple full-wave or half-wave rectification followed by a gain-control (N. Graham, Beck, & Sutter, 1992; N. Graham & Sutter, 1998, 2000; Olzak & Thomas, 1999). The final-stage filters, also tuned to orientation and spatial-frequency (Arsenault et al., 1999; Landy & Oruc, 2002; Mareschal & Baker, 1998a, 1999; Alexandre Reynaud & Hess, 2012; Sutter et al., 1995), extract the modulation at the scale of the envelope.

In a typical LNL model the final-stage linear filters will respond to spatiotemporal variations in any second-order modulation dimension (F. A. Kingdom et al., 2003). This

flexibility implies that different types of second-order modulations can be processed by the same LNL mechanism. Evidence from neurophysiological studies (Gharat & Baker, 2012; Song & Baker, 2007) shows that neurons in cat early visual cortex respond to different types of second-order contours in a form-cue invariant manner. A psychophysical study found mutual facilitation, although weak, between the processing of contrast-modulation (CM) and orientation-modulation (OM) (Schofield & Yates, 2005). However, there is also evidence that second-order stimuli are processed by at least partly separate mechanisms from psychophysics (F. A. Kingdom et al., 2003), VEP (visual evoked potential) (Babenko & Ermakov, 2015) and fMRI studies (Larsson et al., 2010; Larsson et al., 2006).

Psychophysical studies have provided evidence that the response to the second-order modulation bears a nonlinear relationship to the input (N. Graham & Sutter, 2000; Norma Graham & Wolfson, 2004; Huang & Chen, 2014; F. A. Kingdom et al., 2003; Schofield & Georgeson, 1999; H. X. Wang, Heeger, & Landy, 2012). The form of this nonlinearity is consistent with a gain-control process. One study (Huang & Chen, 2014) has investigated the form of the gain-control nonlinearity for CM processing and compared it to that for first-order luminance-modulation counterpart. They found that, similar to first-order processing, divisive inhibition is necessary to explain the nonlinearity involved in CM processing. No study has systematically investigated the second-stage nonlinearity involved in OM and determined whether it is of the same form as that for CM.

The pedestal masking paradigm can be used to examine the response nonlinearity in first-order mechanisms (C. Chen, Foley, & Brainard, 2000a, 2000b; C. C. Chen & Tyler, 2008; Foley, 1994). Observers discriminate between a null interval containing a mask stimulus with a certain "pedestal" modulation alone, and a test interval that contains that pedestal mask with an

increment added to it. Plotting discrimination threshold against mask level gives a pedestal masking function. In a linear system the pedestal mask level would not affect the discrimination threshold. In the nonlinear visual system, the pedestal masking function often has a "dipper" shape (e.g. Fig. 1). At low pedestal mask levels (where the mask itself is around detection threshold) the increment threshold first decreases ("dips"). At high mask levels the discrimination threshold increases with the mask level. The shape of the dipper function is consistent with a nonlinearity that is accelerating at low stimulus levels and saturating at high stimulus levels. The dipper function has been shown not only in first-order processing but also in second-order CM (Huang & Chen, 2014; F. A. Kingdom et al., 2003; Schofield & Georgeson, 1999) and texture segregation (F. A. Kingdom et al., 2003; Landy & Oruc, 2002).

Here, we employ the pedestal masking paradigm to study the form of the second-stage nonlinearity in the processing of two kinds of second-order modulations: contrast-modulation (CM) and orientation modulation (OM). The nonlinear transform we utilize here is a gain control function(Foley, 1994; N. Graham, Beck, et al., 1992; N. Graham & Sutter, 1998, 2000; Huang & Chen, 2014; Legge & Foley, 1980) popularly used for contrast processing. In our model the outputs of this function are considered in the context of signal detection theory (D. M. Green, Swets, J. A., 1988; Gregory & Cane, 1955). The typical contrast response function (CRF), has the form of

$$f(c)=\frac{c^p}{c^q+z}, \tag{1}$$

where c is the contrast level, p and q are exponents controlling the shape of the expansive and compressive regions of the response function, and z represents general inhibition from divisive gain control process. We assume the second-order modulation response function (MRF) also takes the same form and we replace c with m, representing the strength of modulation. Under

signal detection theory, discrimination of different modulation strengths is limited by internal noise from various sources in the brain (Faisal et al., 2008). Samples of this noise are drawn on an interval-by-interval basis from a Gaussian distribution with zero mean and constant standard deviation σ.

Hence in the pedestal masking experiment, the modulation responses in the two intervals are both Gaussian distributions with means *f(m)* and *f(m+t)*, respectively, and the same standard deviation σ(C. C. Chen & Tyler, 2008). On each trial the response in the test interval is

$$r_t = f\left(t+m\right)+N_{\text{int}}, \tag{2}$$

and in the null interval

$$r_n = f\left(m\right)+N_{\text{int}}, \tag{3}$$

where m is the pedestal modulation level, t is the increment added in the test interval, and $N_{int} \sim N(0, \sigma^2)$ is a random variable sampled from a normal distribution representing internal noise. According to signal detection theory, the signal-to-noise ratio (d') is

$$d' = \frac{f\left(t+m\right)-f\left(m\right)}{\sigma}. \tag{4}$$

The percent correct at a threshold *d'* level, $d' = 1$, is $\Phi\left(\frac{d'}{\sqrt{2}}\right) = 76.02\%$.

Therefore, in our model, there are four parameters, namely σ, p, q and z. We used the maximum likelihood method to fit the data from CM and OM pedestal masking experiments simultaneously with a set of models. There was a model with completely independent gain control functions for CM and OM, a model with identical gain control functions for the two conditions, and a range of intermediate models with some shared parameters. These models were compared using a twenty-fold cross-validation method to find which one best explained the data without overfitting(Baldwin, Schmidtmann, Kingdom, & Hess, 2016). We find the typical dipper

shape for the pedestal masking functions of both CM and OM. Through our model selection operation, we find that the only critical modeling difference between CM and OM is in the divisive inhibition parameter *z*. The response functions for CM and OM both have the same shape (defined by the exponents *p* and *q*).

Results

Pedestal masking functions

Incremental thresholds from four observers are plotted as dots against pedestal modulation depth in the four panels of Figure 1. The left-most points are the detection thresholds obtained without a pedestal mask. Both threshold and pedestal modulation levels are in the dB log unit calculated as $20 \cdot \log10(m)$. For both CM and OM, the pedestal masking functions show the typical dipper shape. Incremental threshold initially decreases as pedestal level increases, showing a facilitative effect of the pedestal at low modulation depths. In general, the greatest facilitation occurs when the pedestal level is around the detection threshold (*d'*=1). This dipper shape is consistent with the contrast response functions derived from both first-order contrast processing(C. Chen et al., 2000a, 2000b; C. C. Chen & Tyler, 2008; Foley, 1994; Schofield & Georgeson, 1999) and the second-order CM processing(Huang & Chen, 2014; Schofield & Georgeson, 1999).

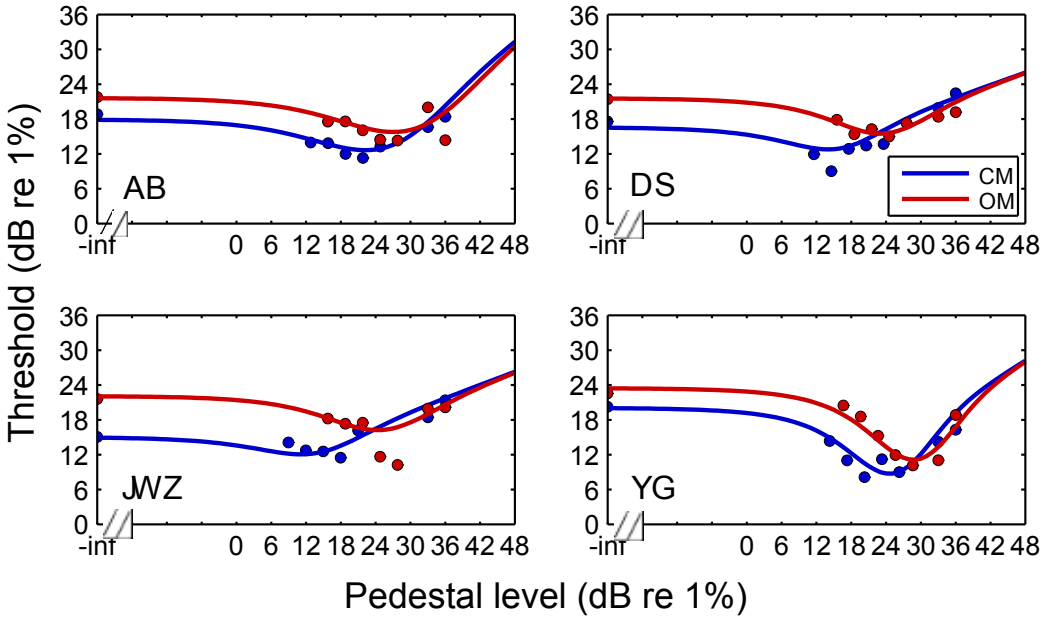

Figure 1. Results from the observers in the pedestal masking experiments. Symbols show increment thresholds obtained from psychometric function fitting at each pedestal modulation level. Curves show the threshold prediction from the modulation response function that provides the best fit to the data at all pedestals (see *Cross-validation model selection*, below).

The magnitudes of the dip for each observer are shown in Table 1. The mean magnitude across four observers is 10.64 dB for CM and 9.44 dB for OM. The dip magnitude for both CM and OM are similar to the values found in first-order contrast processing(Baldwin, Baker, & Hess, 2016) as well as for CM(Huang & Chen, 2014) in previous studies. There is no significant difference between these two values (paired t-test: $p = 0.55$). After the dip, increment thresholds increase with the pedestal level. We obtained the slopes of the increasing region (handle) of the pedestal masking function by fitting the points to the right of the deepest point to a straight line. The handle slopes for each observer are shown also in Table 1. On average the handle slope of OM is steeper than CM, although paired t-test showed no significance ($p = 0.14$). These slopes

are not very well constrained as they are based on fits to only a few values. There is a limit to the range of mask levels above the dip we can measure, because we are limited in the modulation depths we are able to produce. For this reason, only two observers in CM have thresholds at the highest pedestal level that are higher than their detection thresholds. This limitation also affected the previous pedestal masking study that used CM (Huang & Chen, 2014).

	AB	DS	JWZ	YG	Mean +/- ste
CM dip size (dB)	7.5	8.6	3.6	12.1	8.0 +/- 1.7
OM dip size (dB)	7.5	6.4	11.4	12.4	9.4 +/- 1.5
CM handle slope	0.48	0.57	0.44	0.48	0.49 +/- 0.03
OM handle slope	1.08	0.33	1.30	1.11	0.95 +/- 0.21

Table 1. The magnitude of dip and the slope of the masking handle of the dipper function are shown for each observer. We also show their mean with the standard error. When calculating the handle slope of OM for observer AB, we omitted the last threshold at mask level 36 dB, because this drop is due to the poor psychometric function fit that occurred as a result of lack of modulation space at high mask levels. However, the trail-by-trial data from this mask level still made a contribution to maximum likelihood fitting.

Cross-validation model selection

We employed a twenty-fold cross-validation method to a set of candidate models in order to find that which best accounted of our data. This allowed us to compare models with different degrees of independence between CM and OM. The cross-validation method is a standard procedure that allows for different models to be compared while avoiding over-fitting. Our approach develops from that described in Baldwin et al.(Baldwin, Schmidtmann, et al., 2016). We provide the details of our cross-validation procedure in the methods section.

The eight candidate models are constructed by varying the number of shared parameters between the two conditions. The basic MRF model has four free parameters – σ, p, q and z for each condition. Therefore, when all parameters are the same for CM and for OM the model will have four free parameters, when all parameters are allowed to vary between CM and OM there will be eight free parameters.

We quantify the quality of the model fits using the deviance, which indicates the deviation between the model under consideration and one that fits the data perfectly (the saturated model, which has as many parameters as there are conditions in the experiment). The best-fitting model will have the smallest deviance. Deviances from the eight candidate models are plotted in Figure 2. On average, the model that has the lowest test deviance is Model 3. In this model CM and OM have identical internal noise σ, and transducer exponents p and q, but different values for the divisive inhibition constant z. Letting z varying freely between the two conditions increases the quality of the model fit compared to Model 1 where it is fixed. Beyond Model 3, the deviances are actually very similar for models with greater numbers of parameters. Letting more parameters other than z vary between CM and OM did not lead to a reduction in the deviance. In summary, the selection of Model 3 suggests that the differences between CM and OM are accounted for by changes in only the divisive inhibition parameter z.

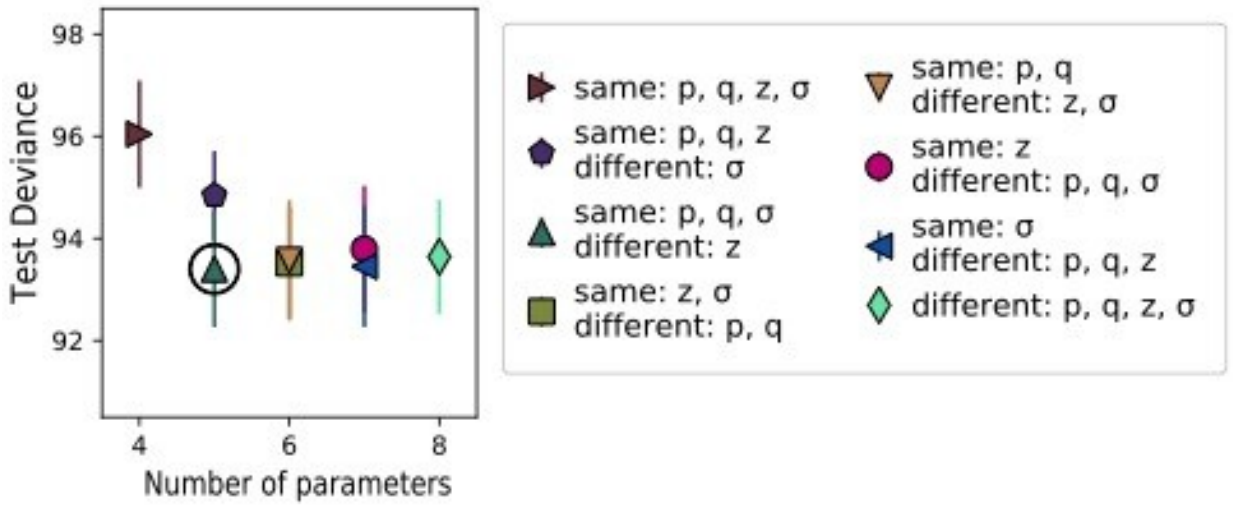

Figure 2. Test deviances from cross-validation model selection procedure. The mean and standard error of the test deviances across the four observers are plotted for eight candidate models. The eight models vary in the number of identical parameters between CM and OM. The model with the lowest test deviance is indicated by a ring. In this model, CM and OM has same nonlinear exponents and internal noise, but different values for the divisive inhibition parameter.

Best model fit result

We then fitted the data of CM and OM to the best model (Model 3) using a maximum likelihood method to find the best-fitting parameter values. The curves of the best model fit to the raw data in each condition for each observer are plotted in Figure 1. There are noticeable individual differences between the observers in terms of the shape of the dipper functions as well as the absolute values of the incremental thresholds in the full pedestal range. For all observers however the pedestal masking functions of both CM and OM showed the typical dipper shape. And the model selected above fitted the data of both CM and OM well.

To investigate the reliability of our parameter estimates we also performed fitting to simulated data obtained through nonparametric bootstrapping of the raw data (generating 500 sample datasets). This analysis is provided in Table 2. Individual observer values are the median and standard error from the bootstrap samples. The internal noise σ and the divisive inhibition parameter z are given in the log unit dB. The 13 dB increase in the value of z between CM and OM is equivalent to a factor of 4.4x in linear units.

	N (dB)	p	q	Z_{CM} (dB)	Z_{OM} (dB)	Deviance
AB	-11.0 +/- 2.5	1.82 +/- 0.14	1.50 +/- 0.11	42.3 +/- 2.7	49.1 +/- 2.8	176.7
DS	4.7 +/- 2.6	2.56 +/- 0.29	1.92 +/- 0.27	31.6 +/- 4.8	46.7 +/- 6.4	143.5
JWZ	3.8 +/- 2.0	2.36 +/- 0.29	1.74 +/- 0.27	25.1 +/-4.8	45.0 +/- 6.4	176.8
YG	-8.7 +/- 3.6	2.86 +/- 0.22	2.46 +/- 0.16	64.8 +/- 3.8	74.7 +/- 4.2	183.4
Mean	-2.8 +/- 2.1	2.40 +/- 0.11	1.90 +/- 0.10	40.9 +/- 4.4	53.9 +/- 3.5	170.1 +/ 18.0
PCH	9.4	2.40	1.78	46.1		
CWC	7.0	3.17	2.63	67.3		
Mean_H&C	8.2	2.78	2.21	56.7		

Table 2. Bootstrap analysis from the best model-Model 3. The median parameters for each observer are shown, with the standard error given by the bootstrap samples. We also provide the mean across observers with standard error. The deviance of fitting the best model to the combined data for both CM and MM of each subject as well as the mean and standard deviation across subjects are shown in the last column. The parameter values from fitting our basic model to Huang and Chen's data(Huang & Chen, 2014) of two observers-PCH and CWC as well as their mean are also shown in the table.

Using the mean parameters from Table 2, we plot pedestal masking functions for CM and OM, in Figure 3. The blue dashed line represents CM and the red solid line represents OM. The larger z for OM is manifested as an up-right shift of the pedestal masking function from CM. The grey curves show fits to the CM data (grey symbols) from Huang and Chen's study (Huang &

Chen, 2014). As shown in Figure 3, our model describes Huang and Chen's CM data as well. The four parameters obtained from fitting their data to our basic model are shown in Table 2 as well. The difference in the position of the pedestal masking functions and in the parameters may be due to different experiment settings especially the different spatial frequencies used in the stimuli. What's worth noticing is that the values of the exponents p and q are 2.78 and 2.21, although slightly larger than the mean values in our study, they are in the range of the values we obtained. This similarity in the exponents confirms the same nonlinearity for CM.

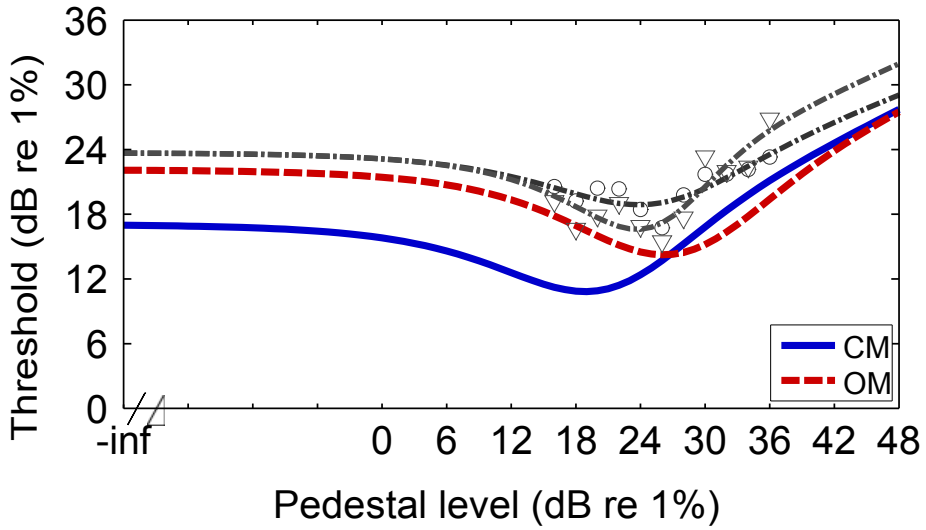

Figure 3. Pedestal masking functions of CM (blue) and OM (red) constructed from the mean values of the fitted parameters of best model-Model 3. The grey curves with corresponding incremental thresholds are pedestal masking functions from fitting our basic model to the CM data of two observers in Huang and Chen's study (Huang & Chen, 2014).

Discussion

We find the expected dipper shape for pedestal masking functions for both contrast-modulated (CM) and orientation-modulated (OM) second-order stimuli. This implies that a gain

control nonlinearity exists not only for the processing of CM(N. Graham & Sutter, 2000; Norma Graham & Wolfson, 2004; Huang & Chen, 2014; F. A. Kingdom et al., 2003; Schofield & Georgeson, 1999; H. X. Wang et al., 2012), but also for the processing of OM. This is consistent with the idea that nonlinear normalization processes (e.g. surround suppression) operate on the representation of second-order texture modulations, as proposed by Wang and colleagues(H. X. Wang et al., 2012).

The dipper function has been shown for CM in former studies(Huang & Chen, 2014; F. A. Kingdom et al., 2003; Schofield & Georgeson, 1999). Specifically, Huang and Chen(Huang & Chen, 2014) demonstrated that a divisive inhibition process after the second-stage linear filters explains the dipper function they found for CM. The dipper function of OM was also shown in two former studies(F. A. Kingdom et al., 2003; Landy & Oruc, 2002), but the current study is the first one to systematically model and compare the second-stage nonlinearity for CM and OM processing.

Within our model, the difference between CM and OM processing is accounted for solely by an increase in the gain-control parameter *z* for OM. The internal noise parameter and the exponents controlling the shape of the modulation response function (MRF) are shared between the two conditions. The shared shape of the response functions for CM and OM would be consistent with their reliance on the same second-order mechanisms. It is also compatible with the finding of form-cue invariant responses in cat early visual cortex(Gharat & Baker, 2012; Song & Baker, 2007) to boundaries defined by second-order modulation. This suggests that the CM and OM are processed either by a single generalized second-order mechanism, or at least pass through the same nonlinearity.

A number of studies(Dakin & Mareschal, 2000; N. Graham, Sutter, et al., 1992; Mareschal & Baker, 1998a, 1999; Motoyoshi & Nishida, 2004; N. Prins, 2008; N. Prins & Kingdom, 2002, 2006) have shown that the first-stage linear filters, which provide the input to the second-stage filters, are tuned to carrier orientation and spatial frequency. This would allow OM to be detected by comparing the outputs of sets of second-stage filters that process the contrast variations in the two orthogonal orientations. Prins (N. Prins, 2008) showed that OM textures that contain CM in two orientation bands are processed by three mechanisms: two of which only detect CM within each modulated orientation band, while the other integrates contrast across all orientations to detect overall contrast modulations. Two other earlier studies(Motoyoshi & Kingdom, 2007; Motoyoshi & Nishida, 2004) also supported the idea of an isotropic mechanism that detects the overall contrast modulations in all orientation-tuned channels. When there is no overall contrast variation over space, like in our OM stimuli, Prins' study supports probability summation between the two mechanisms, whereas Motoyoshi and Nishida's results suggests that the two mechanisms are integrated(Motoyoshi & Nishida, 2004). However, Kingdom and colleagues(F. A. Kingdom, Baldwin, & Schmidtmann, 2015) has questioned the use of high threshold theory that was used to model probability summation in Motoyoshi and Nishida's study and suggested as an alternative, signal detection theory. Therefore, how the two mechanisms tuned to orthogonal carrier orientations are combined is still an open question.

The larger *z* we found in OM and CM, could imply greater divisive inhibition to the responsible second-order channel (s) from other relevant second-order channels. This implication makes sense because in the carrier of OM there are two orientations involved instead of only one as in the carrier of CM. Therefore, for OM there are more channels activated by the stimuli

presented on the screen that could have a divisive inhibitory input on the target channel. Another potential explanation is that cross-orientation suppression(Foley, 1994; Morrone et al., 1982) between the two orthogonal orientations in the carrier of OM stimuli could reduce the response of the first-stage linear filters. This would reduce the effective carrier contrast. From fitting Huang and Chen's data to our model and comparing the values of the *z* parameter in two conditions of different carrier contrasts, we find that smaller carrier contrast results in z values increasing from 67.33 dB for carrier contrast at 0.40 to 104.61 dB for carrier contrast at 0.16.

The other three parameters in our model, the internal noise and the nonlinear exponents are similar between CM and OM. The same internal noise would be compatible with CM and OM judgments occurring at a common decision stage and being affected by the same level of internal noise, notwithstanding the idea that different types of second-order modulations are processed by, at least partially, separate mechanisms(Babenko & Ermakov, 2015; F. A. Kingdom et al., 2003; Motoyoshi & Nishida, 2004; N. Prins & Kingdom, 2003). The shared values of exponents p and q between the two conditions are compatible with the idea that the OM responses could be built up from the CM responses. Perhaps surprisingly, the fitted values of p and q that we find are very close to typical values 2.4 and 2 that researchers have been using in modeling first-order, luminance-modulation(D. H. Baker & Meese, 2013; Legge & Foley, 1980). This common nonlinearity could suggest that the first-order and second-order modulations are processed by the same, or partially common mechanism. This idea is compatible with the findings that in cat early visual cortex Area 18(Gharat & Baker, 2012, 2017; Song & Baker, 2007; Zhou & Baker, 1993) and LGN Y pathway(Rosenberg et al., 2010), as well as primate V2(G. Li et al., 2014), there are a substantial fraction of neurons responding to boundaries defined by first-order or second-order modulations. Together with the neurophysiological

evidence, our result of a common nonlinearity challenges the previous idea that first-order and second-order features are encoded by independent mechanisms(Edwards & Badcock, 1995; T. Ledgeway & Smith, 1994; Mareschal & Baker, 1998a, 1999; Schofield & Georgeson, 1999, 2003; Smith et al., 1998).

In summary, we find that pedestal masking functions for second-order contrast-modulation and orientation-modulation both have the typical dipper shape. The basic model we propose for second-order processing, which is a linear non-linear linear model (LNL) plus a gain-control nonlinearity and a decision stage consistent with the signal detection theory, accounts for the data of both CM and OM well. The only difference between the two conditions is the larger gain control parameter in the case of OM, which suggests greater divisive inhibition for the responsible second-order channels for OM than CM or smaller carrier contrast gain due to cross-orientation suppression. The invariant internal noise and nonlinear exponents suggest identical nonlinearity and decision process between the two second-order conditions-CM and OM.

Method

Apparatus

Stimuli were generated by a Macintosh computer running Matlab (Mathworks) under OS X, and presented on a gamma-corrected Compaq CRT monitor (30 cm × 40 cm, refresh rate: 85 Hz; resolution: 1280 × 960 pixels; mean luminance 20 cd/m^2). Observers viewed the stimuli from 86 cm in a dimly lit room. At this distance, there were 48 pixels per degree of visual angle. A Bits++ box (Cambridge Research System) provided 14 bits of digital to analog converter

(DAC) depth. The experiment software utilized functions from the Psychophysics Toolbox(Brainard, 1997). Data analysis and model fitting were performed in MatLab. The Palamedes toolbox 2(N. K. Prins, F. A. A. , 2009) was used to fit the psychometric functions.

Participants

Four experienced psychometric experiment observers including two of the authors, YG and AB, participated in the current experiment. Observers gave written informed consent. They all have normal or corrected-to-normal vision. All procedures were conducted in accordance with the Declaration of Helsinki, and approved by the Ethics Review Board of the Montreal Neurological Institute.

Stimuli

The constructions of the second-order contrast-modulation (CM) and orientation-modulation (OM) stimuli in both cases involves multiplying a carrier *C(x,y),* which is a high-spatial-frequency tilted sinusoidal grating, by an envelope *G(x,y)*, which is a low-spatial-frequency horizontal sinusoidal grating. The carrier and the envelope are defined as $C\left(x,y\right)=\sin\left(2\pi f_c x\right)$ and $G\left(x,y\right)=\sin\left(2\pi f_e x\right)$, where f_c and f_e are spatial frequencies of the carrier and the envelope, respectively. Figure 4 illustrates the construction of CM and OM stimuli.

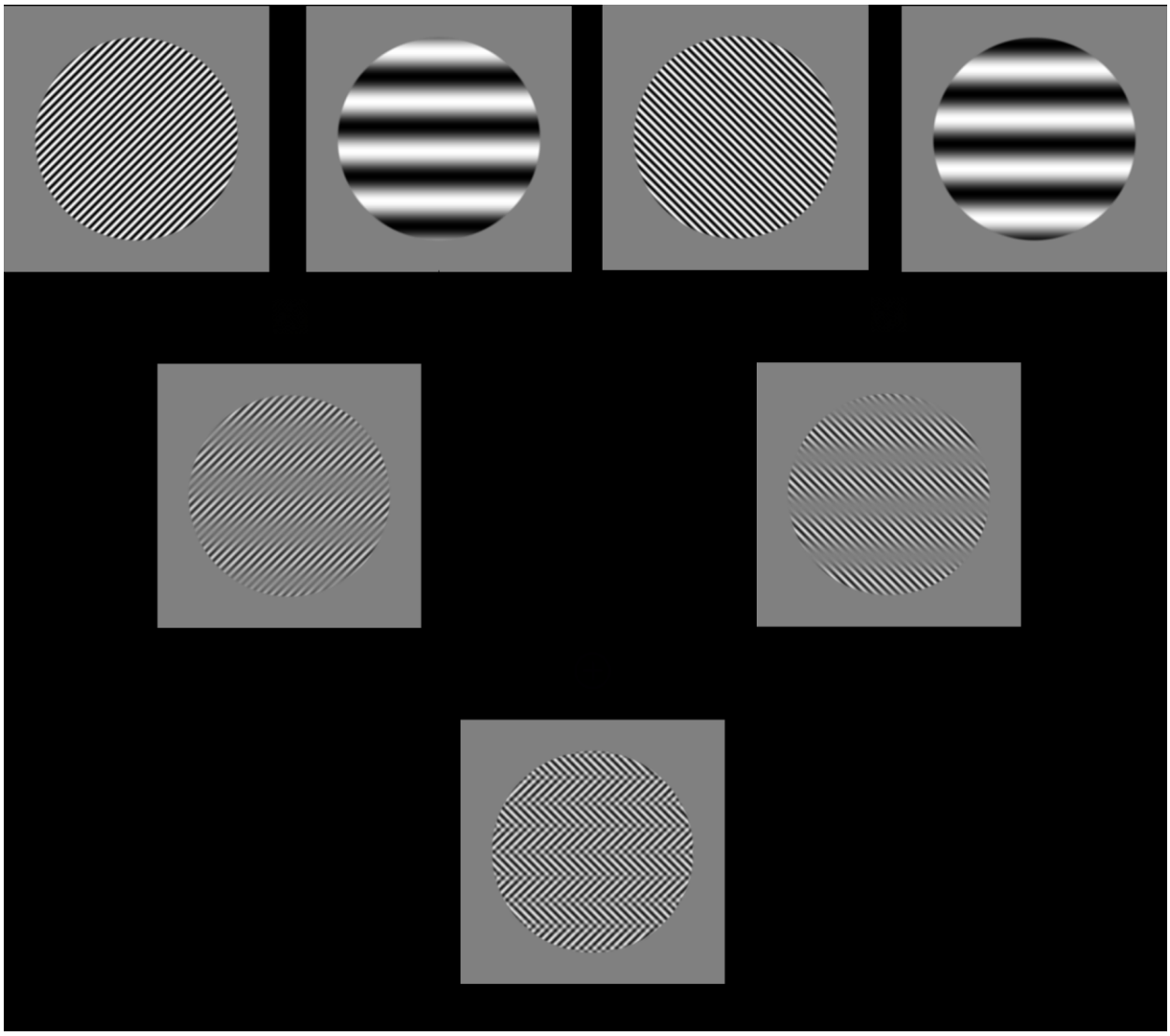

Figure 4. Construction of second-order CM patterns by multiplying an envelope grating by a carrier grating. This is followed by construction of an OM pattern by adding two CM stimuli with opposite phases and orthogonal carrier orientations together. The CM1 stimulus is the one that is used in the current experiment.

The CM stimulus is constructed by the modulation of the contrast of one carrier by one envelope. In the null interval, the stimulus, that only contains the pedestal mask *m*, can be described by

$$N(x,y)=C(x,y)\left[c+c\times mG(x,y)\right]\omega(x,y), \tag{5}$$

where c is the contrast of the carrier, m is the modulation depth of the pedestal, and ω(x, y) is a raised cosine window with a blur width of 0.5º to soften the edge of the stimulus. The CM stimulus in the target interval, which contains both the pedestal mask and the target, is described by

$$T(x,y)=C(x,y)\left[c+c\times(m+t)G(x,y)\right]\omega(x,y), \quad (6)$$

where t is the modulation depth of the target.

The OM stimuli involve the addition of two CM patterns which have carrier gratings of orthogonal orientations, 45° and -45°, as well as envelope gratings of opposite phases. The OM stimuli in the null interval and the target interval can be described by

$$OM(x,y)=\left\{C_1(x,y)\left[c+c\times mG_1(x,y)\right]+C_2(x,y)\left[c+c\times mG_2(x,y)\right]\right\}\omega(x,y), \quad (7)$$

and

$$OM(x,y)=\left\{C_1(x,y)\left[c+c\times(m+t)G_1(x,y)\right]+C_2(x,y)\left[c+c\times(m+t)G_2(x,y)\right]\right\}\omega(x,y) \quad (8)$$

All of the carriers have a spatial frequency of 4 cycles per degree and all of the envelopes have a spatial frequency of 0.5 cycles per degree. The contrast of carrier is kept constant at 0.40 in all conditions. Figure 5 shows examples of CM (a) and OM (b) stimuli.

Procedure

The two-interval forced-choice (2IFC) paradigm was employed to measure the increment thresholds. During each trial, the target and null stimuli were presented, each for 500 ms, in a random order with a 400 ms inter-stimulus interval between them. To reduce temporal uncertainty, an auditory tone was given at the onset of each interval. The task was to identify which interval was the target containing the greater modulation. The observer responded with a

button press on a keyboard. Auditory feedback informed observers whether they responded correctly on each trial.

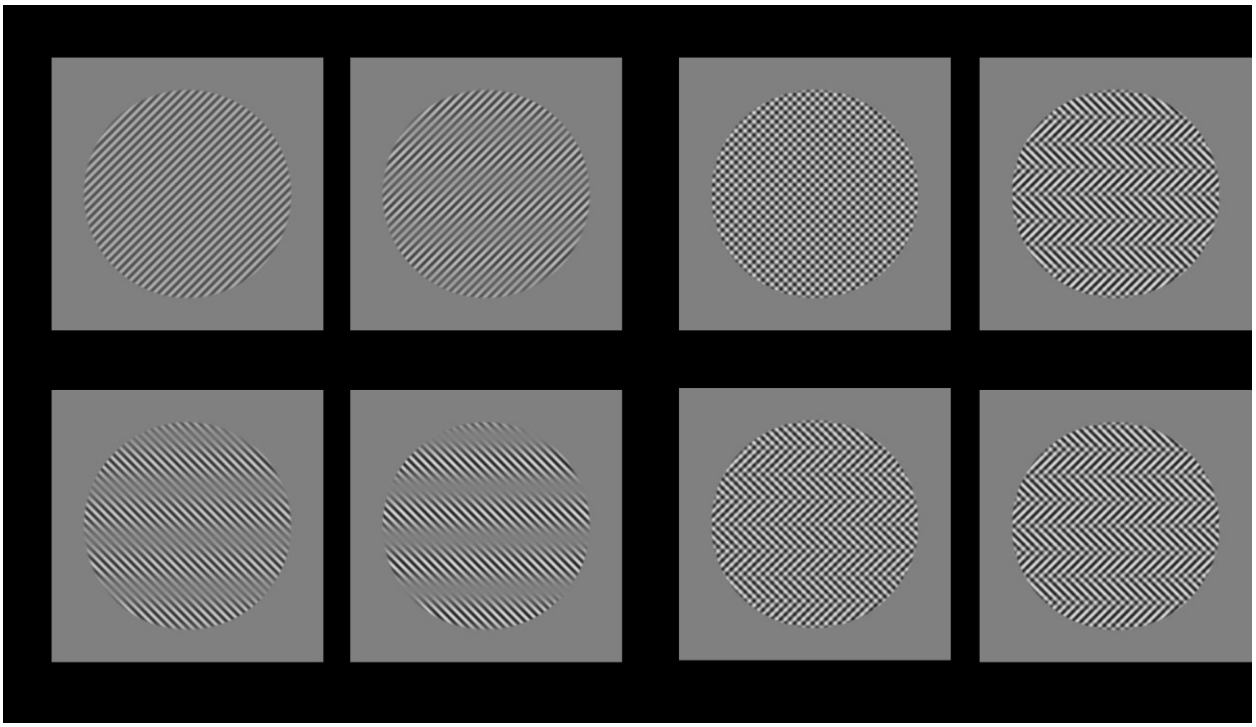

Figure 5. Examples of the stimuli-CM (a) and OM (b) gratings. The upper row shows the stimuli in the blocks of zero mask level and the lower row shows the stimuli in the blocks of 36dB mask level. In both (a) and (b), the left figure shows the stimuli in the null interval while the right one shows the stimuli in the target interval.

The experiment was conducted in blocks of pedestal modulation levels with two repetitions for each block. The pedestal levels were adjusted for each observer to give an informative sampling of the masking function. First, the detection threshold (*T*) was measured. Then this *T* determined the seven pedestal mask levels: (*T-12*), (*T-6*), (*T-3*), (*T+3*), (*T+6*) and (*T+12*) *dB*. The unit *dB* is *20*log10(c)*, where *c* represents the modulation depth. At each pedestal level, a psychometric function was measured with two interleaving staircases and a

threshold was obtained by fitting the psychometric function. One staircase was one-up-three-down and the other one was one-up-two-down, both terminated after 60 trials. Therefore, there were 60 x 2 x 2 x 8 = 1920 trials in each of the two conditions-CM and OM. The two conditions were measured alternately and the sequence of the two was balanced among observers.

To test whether the observers used a second-order strategy to do the task, there were 10 trials blended in each block where the modulators were half-wave rectified. These trials were split evenly into positive (+) and negative (-) modulators. For the positive modulators, the modulating envelopes had only the "positive parts"-values between the crest and the mean, while the "negative parts"-values between the trough and the mean - were set to zero. By examining performance on the three modulators it is possible to infer the strategy that the observers adopted. If the observers did not use a second-order strategy, instead focusing on a positive stripe of the stimulus and discriminate its first-order contrast level, the performance for (+) modulators should be much better than (-). Figure 6a shows average percent correct values for (+) and (-) modulators under different pedestal mask levels for all four observers. There are 29 points higher than the unit line and 27 dots lower. This indicates that there was not an advantage for detecting increments on the positive regions of the stimulus, suggesting that observers made use of the whole stimulus in the main task. Following the same logic, if the observers did use the whole stimulus to do the task, the performance for full modulator should be better than either (+) or (-) modulators. In Figure 6b we plot the average percent correct values for (+) and (-) modulators separately against those for full modulators. The green-blue points are for (+) and the yellow-brow ones are for (-) modulators. 48 out of 56 points for the (+) modulator and 46 out of 56 points for the (-) modulator are lower than the unit line. This also indicates that observers generally used the whole stimulus to perform the task with a second-order strategy.

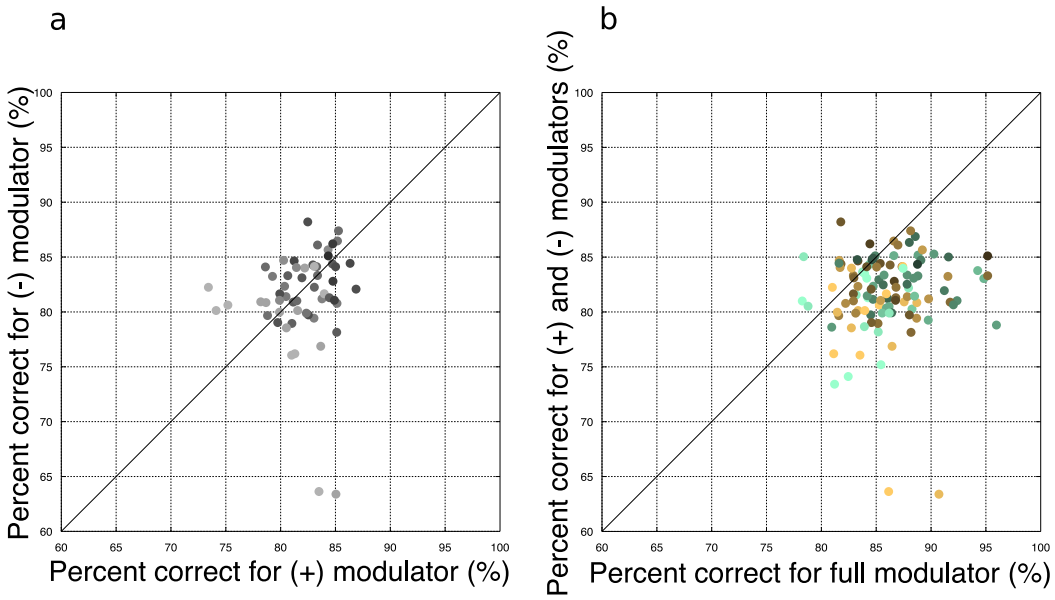

Figure 6 a: The percent correct values for positive (x axis) and negative (y axis) modulators. Each point represents the mean percent correct values of all trials of positive and negative modulators, in the form of (+,-), under each pedestal mask level for each observer. b: The percent correct values for positive (green-blue points) and negative (yellow-brown points) modulators on the y axis again those for full modulators on the x axis. The color shade represents pedestal mask levels-the lighter the color, the higher the pedestal mask level.

Data Analysis

A model selection procedure seeks to answer the question of which of a number of candidate models best accounts for the data. We did so using a cross-validation analysis. This relies on splitting the data up and then using fits to some of the data to try to predict other data that were excluded from the fitting. In our analysis, we partitioned the data into 20 sets. Each was used as the holdout test set once, and the remaining 19 sets were combined together and used to fit the model. Parameters were obtained by fitting to the fit dataset. The predictions from

these fits were tested against the holdout test dataset in order to calculate the deviance. Our 20 iterations of this procedure gave us 20 deviance values (one for each test set).

Considering the comparison between the processing mechanisms of the two types of second-order modulation, namely contrast-modulation (CM) and orientation-modulation (OM), we identified eight possible models to fit. As in the equation (1) and (2), the models to explain the second stage nonlinearity and decision making of CM and OM each has four free parameters, internal noise n, p, q, and z. Depending on the number of same and different parameters between the two conditions CM and OM, there are eight possible models in total. Here p and q are restricted to be either both same or both different between the two conditions. Therefore, the eight models are:

1. Four parameters are all the same between CM and OM;
2. Except for σ, the other three parameters p, q and z are same;
3. Except for z, the other three parameters σ, p and q are same;
4. σ and z are same, p and q are different between two conditions;
5. σ and z are different, p and q are same;
6. σ, p and q are different, only z is the same;
7. Except for σ, the other three parameters p, q and z are different;
8. Four parameters are all different between CM and OM.

The data (fit sets) of CM and OM were brought together and fitted simultaneously with each of these eight models using the method of maximum likelihood. The best model is defined as the model with the smallest deviance:

$$D = -2\left(\log L_{test} - \log L_{sat}\right) \tag{9}$$

Where L_{test} is the test likelihood of the candidate model and L_{sat} is the likelihood of the saturated model(Baldwin, Schmidtmann, et al., 2016). To calculate the deviance of each candidate model, from the maximum likelihood fitting with each fit set, we obtained the best fit values of the parameters. Then we calculated the test likelihood of the candidate model by calculating the likelihood of the data in the corresponding test set(Baldwin, Schmidtmann, et al., 2016) within the model having the fitted parameters from the fit set.

Data Availability

The datasets generated and analyzed during the current study are available from the corresponding author on reasonable request.

Acknowledgements

We would like to thank Pi-Chun Huang for providing the data from Huang & Chen (2014)(Huang & Chen, 2014). This work was supported by Natural Sciences and Engineering Research Council of Canada grant (NSERC #46528) to Robert Hess.

Additional Information

Author Contribution Statement

YG conducted the experiment, analysed the data and wrote the main manuscript text with extensive discussion with AB. AB prepared Figure 2. AB and RH reviewed and edited the manuscript.

Competing Financial Interests

The authors declare no competing financial interests.

Manuscript 2: Different nonlinearity in the processing of contrast- vs motion-defined boundaries

Yi Gao, Alex S. Baldwin, Robert F. Hess*

Abstract

To extract information from the outside world, the visual system detects boundaries where there are changes in the retinal image. In the simple case of first-order contrast these might be boundaries between light and dark regions. One interesting question is whether the

boundaries defined by different features, e.g. changes in luminance, contrast, texture or motion are processed by a general mechanism in a cue-invariant manner. The processing of two types of second-order modulation, contrast- and orientation-modulation has been reported to involve a nonlinear gain-control similar to that previously established for first-order processing. In the current study, we investigated the nonlinearity involved in processing second-order motion boundaries using a pedestal masking paradigm. This nonlinearity was then compared to that for contrast-defined boundaries. We find the typical dipper shape in the pedestal masking functions for motion-modulation. In our modeling however we find that the processing of motion-defined boundaries goes through a different nonlinearity compared to contrast-defined boundaries. Furthermore, this difference cannot be accounted for by the carrier's temporal properties. Our result challenges the view of a cue-invariant boundary processing mechanism.

Introduction

The natural scene comprises boundaries defined by changes in different types of visual features, including luminance, color, contrast, texture and motion. Boundary processing facilitates figure-ground segregation. This enables identification and discrimination of objects of interest within complex natural scenes. Specifically, motion-defined boundary processing plays an important role in extracting form from motion (Timothy Barnes & Ennio Mingolla, 2013), breaking camouflage (T. Barnes & E. Mingolla, 2013) and generating depth percepts (Yoonessi & Baker, 2011).

Among the different types of boundary contrasts, luminance- and color-defined visual features are classified as first-order or Fourier based. Their processing can be explained by a

linear filter model followed by a gain-control nonlinearity. While the other features (e.g. contrast-, texture- and motion-defined) are classified as second-order or non-Fourier and their processing can be modeled by a linear, nonlinear, linear model (LNL) (N. Graham, Beck, et al., 1992; N. Graham & Sutter, 1998; Wilson, 1994). The LNL model involves three stages: i) the input image is filtered by a set of first-stage linear filters, ii) the filter outputs are transformed by a nonlinearity, iii) the transformed outputs are filtered again by a final-stage linear filter. Some previous studies involving contrast-modulation (N. Graham & Sutter, 2000; Huang & Chen, 2014; Schofield & Georgeson, 1999) and orientation-modulation (Gao, Baldwin, & Hess, in review) suggest that the response to second-order modulation also goes through a gain-control nonlinearity. The relevance of this to second-order motion defined boundary processing is not known.

The processing of a motion-defined boundary has been considered to involve two stages; first, the extraction of local motion and second, the integration of local motions (Durant & Zanker, 2009; Sinha, 2001). Variations in both motion direction and motion speed generate detectable motion-defined boundaries (Durant & Zanker, 2008). However these two kinds of information are probably processed by separate mechanisms (Hess & Ledgeway, 2003) with direction difference having a greater influence in boundary localization (Durant & Zanker, 2008). Tuning properties of motion-defined boundary processing depend on the specific stimuli used. Spatial frequency tuning to the local motion signal is band-pass for boundary stimuli constructed with grating carriers and grating envelopes (Gharat & Baker, 2012). The contrast of the carrier has been shown to positively contribute to the discrimination of boundary orientation (Regan, 1989). Then in the motion integration process, the second-stage filter is shown to be elongated with the length of 4-5 degrees of visual angle (Durant & Zanker, 2009). Orientation

discrimination of boundaries defined by combining direction and speed differences among dot elements has been shown to be low-pass for spatial frequency (Durant & Zanker, 2009). While using grating carriers and envelopes, Gharat et al. (Gharat & Baker, 2012) showed band-pass tuning for envelope spatial frequency as well as orientation. Moreover, numerous studies have reported neurons that are selective for the orientation of motion-defined boundaries in different areas, such as middle temporal (MT) (Albright, 1992), V1,V2 (Marcar et al., 2000) ,V3A and V3B (Larsson et al., 2010), and V4 (Mysore, Vogels, Raiguel, & Orban, 2006). These neurons could be the neural substrates for extracting the orientation of motion-defined boundaries.

One interesting question about boundary processing is whether it is done in a cue invariant manner, or are motion-defined boundaries processed by a mechanism that is separate from that involved in the processing of luminance-, contrast- or orientation-defined boundaries? Many previous studies support the former view. Psychophysical studies have shown mutual facilitation between the processing of contrast-defined and orientation-defined boundaries (Schofield & Yates, 2005). Adaptation effect was found between luminance- and contrast-defined boundaries, as well as between luminance- and orientation-defined boundaries (Filangieri & Li, 2009; Hawley & Keeble, 2006). Tilt after-effect was also shown between pairs of motion-defined, luminance-defined and illusory contours (Berkley et al., 1994). Our previous study (Gao et al., in review) modeled the second-order nonlinearity for contrast- and orientation-defined boundaries and found it to be identical. Neurophysiological experiments have also shown that there are neurons in various regions in the visual cortex that respond in a cue-invariant manner to more than one type of contour, for example primate V2 (Leventhal et al., 1998; Marcar et al., 2000) and inferior temporal (IT) region (Sary et al., 1995) as well as cat Area 18 (Gharat & Baker, 2012). Although motion processing may involve a separate pathway to

that of static luminance information (Derrington et al., 2004; Goodale & Milner, 1992), the majority of studies suggest that there is one general mechanism for boundary processing which in turn leads to our hypothesis that there will be one common nonlinearity in motion- and contrast-defined boundary processing.

The purpose of current study is to investigate the second-stage nonlinearity in processing two types of second-order boundaries: motion-modulation (MM) and contrast-modulation. Insights about the nonlinearity will contribute to our general understanding about boundary processing as well as providing more evidence to decide whether motion- and contrast-defined boundaries are processed by a common mechanism. To study the nonlinearity, we employed the pedestal masking paradigm that has been widely used to investigate the nonlinearities in both first-order (C. C. Chen & Tyler, 2008; Foley, 1994) and second-order processing (Gao et al., in review; Huang & Chen, 2014; F. A. Kingdom et al., 2003; Landy & Oruc, 2002; Schofield & Georgeson, 1999). Observers discriminate between a null interval containing a mask stimulus with a "pedestal" modulation alone, and a test interval containing that pedestal mask with an increment target added to it. Plotting increment threshold against mask level gives a pedestal masking function. In the nonlinear visual system, the pedestal masking function often has a "dipper" shape (e.g. Fig. 1)-at low pedestal mask levels the increment threshold first decreases and as the mask level then increases, the increment threshold increases. These two parts of the pedestal masking function reflect facilitation and inhibition effects of the pedestal mask on the target discrimination. The shape of the dipper function is consistent with a nonlinearity that is accelerating at low stimulus levels and saturating at high stimulus levels.

Our basic model to describe the second-order nonlinearity involves a nonlinear transform as a divisive gain-control function (Foley, 1994; N. Graham & Sutter, 2000; Huang & Chen,

2014), and its outputs are considered in the context of signal detection theory (D. M. Green, Swets, J. A., 1988; Gregory & Cane, 1955). This basic model is the same as that of our recent study (Gao et al., in review). The typical nonlinear response function has the form of

$$f(c)=\frac{c^p}{c^q+z}, \tag{1}$$

where c is the modulation depth, p and q are exponents controlling the shapes of the expansive and compressive regions of the response function, and z represents general inhibition from divisive gain control process. Under signal detection theory, discrimination of different modulation depths suffers from internal noise from various sources in the brain[(Faisal et al., 2008)]. Samples of the internal noise in each interval are drawn from a Gaussian distribution with zero mean and constant standard deviation σ. According to signal detection theory, the signal-to-noise ratio (d') is

$$d'=\frac{f\left(t+m\right)-f\left(m\right)}{\sigma}, \tag{2}$$

where m is the pedestal modulation depth, t is the increment added in the test interval. The percent correct at a threshold level, d'=1, is $\Phi\left(\frac{d'}{\sqrt{2}}\right)$= 76.02%. Therefore, in our basic model, there are four parameters, namely σ, p, q and z.

The current study is composed of two parts. In Experiment 1 we measure the increment discrimination thresholds for boundaries defined by contrast- (CM) and motion-modulation (MM) where the CM has the standard static grating carrier. In Experiment 2, the carrier of the CM stimulus has the same motion properties as the MM stimulus. By comparing the pedestal masking functions for CM and MM and letting CM carriers vary between being static and

moving, we can gain insights into differences between MM and CM defined boundary processing and whether these differences are due to first or second-order processing.

We found the typical dipper shape in the pedestal masking functions for both contrast-defined and motion-defined second-order boundary processing. This indicates the existence of a nonlinearity of the divisive inhibitory form not only for second-order contrast-modulation but also for motion-modulation processing. However, larger nonlinear transducer exponents and larger divisive inhibition parameters were found in the case of motion-defined boundaries. This suggests a different response nonlinearity for motion-defined boundary processing compared to other types of boundary processing. This difference cannot be explained by the different temporal properties of the first-order carrier. What's more, varying the contrast level of the carrier does not change the fundamental properties of the response nonlinearities for either contrast- or motion-defined boundary processing.

Results

Pedestal masking functions

Increment thresholds plotted as dots against pedestal modulation depth are shown in Figure 1 for Experiment 1 and Figure 2 for Experiment 2. The increment threshold indicates the ability to detect the target modulation in the presence of the pedestal modulation at each pedestal mask level. The data at each pedestal mask level are fitted with a Quick psychometric function (Quick, 1974). The thresholds are calculated as the signal level at 76.02 percent correct (see introduction). The left-most point in each panel is the detection threshold obtained without a

pedestal mask. Both threshold and pedestal mask levels are in the dB log units calculated as $20 \log10(m)$.

In Experiments 1 and 2, for both CM and MM, the pedestal masking functions show the typical dipper shape. In general, the greatest facilitation occurs at the pedestal mask level that is around the detection threshold (*d'=1*). And in most cases, the inhibitory effect of the pedestal mask makes the increment thresholds at high mask levels higher than the corresponding detection thresholds. This dipper shape is consistent with the contrast response functions derived from first-order contrast processing (C. C. Chen & Tyler, 2008; Foley, 1994; Legge & Foley, 1980; Schofield & Georgeson, 1999), as well as second-order CM (Huang & Chen, 2014; F. A. Kingdom et al., 2003; Schofield & Georgeson, 1999; Schofield & Yates, 2005) and OM (Gao et al., in review; F. A. Kingdom et al., 2003; Schofield & Yates, 2005) processing.

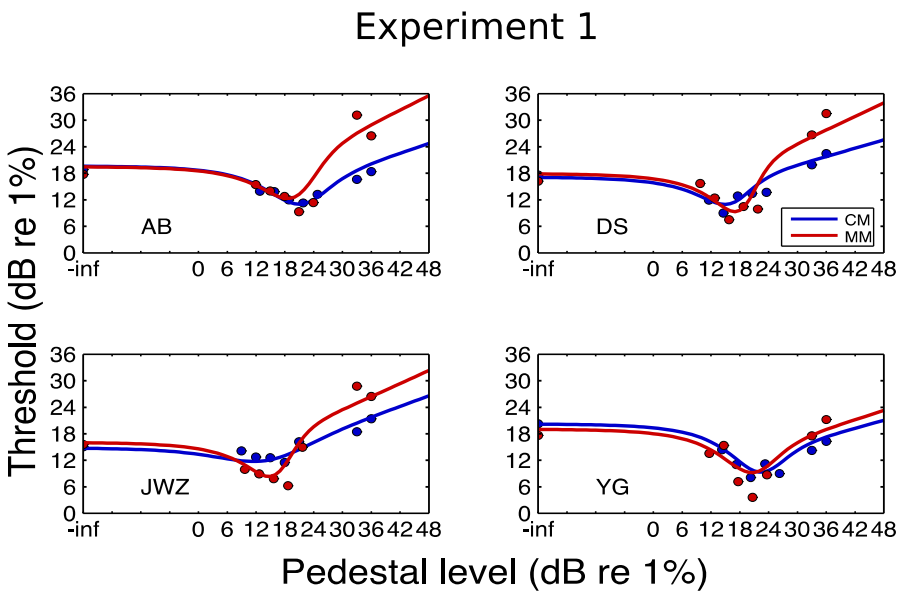

Figure 1. Results of four observers in Experiment 1. The dots- blue for CM and red for MM- show increment thresholds obtained by fitting a Quick psychometric function then calculating at 76.02% percent correct corresponding to d'=1 (see introduction) at each pedestal modulation

level. Curves represent the threshold prediction from the best model in which the four parameters are all different between CM and MM (see Data analysis in Methods section).

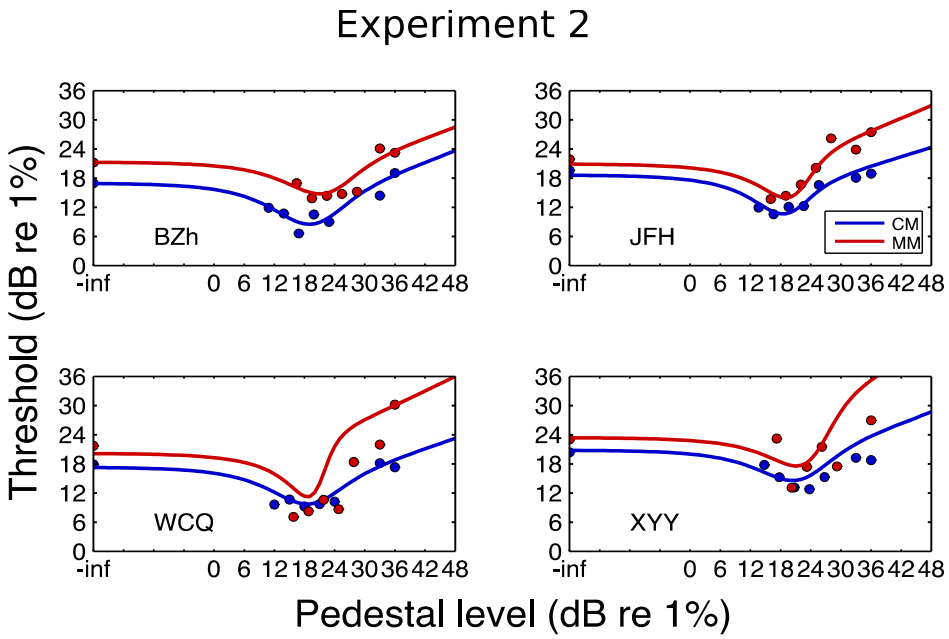

Figure 2. Results of four observers in Experiment 2. Figure caption is the same as Figure 1.

We then calculate two features of the dipper functions, the magnitude of the dip and the slope of the positively increasing region (the handle). The magnitude of the dip is defined as the difference between the smallest increment threshold and the detection threshold at zero mask level. The handle slope is obtained by fitting the points to the right of the lowest threshold to a straight line. As shown in Table 1, the mean dip magnitude for MM is larger than CM in both Experiment 1 (paired-samples t-test, $t(3) = -1.72$, $p = 0.18$) and Experiment 2 ($t(3) = -0.58$, $p = 0.6$), although the difference is not significant according to the t-test result. The mean handle slope is significantly steeper in MM than in CM in both Experiment 1 ($t(3) = -9.89$, $p = 0.002$) and Experiment 2 ($t(3) = -2.91$, $p = 0.05$). The effect size of the significantly different handle

slope is 6.99 for Experiment 1 and 1.99 for Experiment 2. The effect size was computed with pooled standard deviation, which is $SD = \sqrt{\frac{(n_1-1)\times SD_1^2 + (n_2-1)\times SD_2^2}{(n_1+n_2-2)}}$ (Coe, 2002).

The curves are the pedestal masking functions obtained from fitting the best model, in which all four parameters are different between CM and MM, to the raw data as a whole for both conditions. This is discussed further in the *Best model fit result* section below.

	Experiment 1					Experiment 2				
	AB	DS	JWZ	YG	Mean 1	BZ	JFH	WCQ	XYY	Mean 2
CM dip size (dB)	7.6	8.6	3.6	12.1	8.0 +/- 1.8	10.3	9.0	8.7	7.6	8.9 +/- 0.6
MM dip size (dB)	8.4	8.7	9.3	14.0	10.1 +/- 1.3	7.3	8.2	14.6	9.9	10.0 +/- 1.6
CM handle slope	0.47	0.57	0.43	0.48	0.49 +/- 0.03	0.55	0.44	0.54	0.52	0.51 +/- 0.02
MM handle slope	1.42	1.21	1.17	1.09	1.22 +/- 0.07	0.67	0.72	1.11	1.32	0.96 +/- 0.15

Table 1. The magnitudes of the dip and the values of handle slope of the dipper functions from four observers in Experiment 1 and four observers in Experiment 2. The mean and standard error are also shown for each group.

Model fit

We constructed eight candidate models from the basic model. These were composed of second-order divisive normalization, followed by a decision-making stage. The eights models differ from each other in the number of parameters varying between CM and MM processing. They range from Model 1 that has four free parameters that are shared between the two conditions, to Model 8 where each condition gets its own set of four parameters. To select a best

model, we employed a twenty-fold cross-validation method (see *Methods* for detail) and found that the model that best accounted of the data allows all four parameters to be different between CM and MM. This was the case for both Experiment 1 and Experiment 2. We then fitted the raw data of CM and MM to the best model using a maximum likelihood method to find the best-fitting values of the four parameters. The pedestal masking functions predicted by the parameter values from the best model fit in each condition for each observer are plotted as solid curves in Figure 1, superposed on the increment threshold data.

The mean parameter values are shown in Table 2, separately for Experiment 1 and Experiment 2. The internal noise σ and the divisive inhibition parameter z are in dB log units which is calculated as $20 \times log_{10}(x)$. First we compared the parameters from Experiment 1 and Experiment 2 for each condition. For CM, all four parameters are not significantly different between the two experiments (in t-test p values all larger than 0.35). For MM, only the internal noise is significantly larger in Experiment 2 ($p = 0.006$, $df = 3$). The other three parameters are not different (p values all larger than 0.32).

	Experiment 1				Experiment 2			
	p	q	Z (dB)	σ (dB)	p	q	Z (dB)	σ (dB)
CM	3.0 +/- 0.3	2.7 +/- 0.2	52 +/- 9	3.7 +/- 0.9	3.1 +/- 0.2	2.6 +/- 0.2	53 +/- 3	2.7 +/- 1.3
MM	3.9 +/- 0.2	3.4 +/- 0.2	65 +/- 3	0.8 +/- 0.5	4.0 +/- 0.3	3.5 +/- 0.4	75 +/- 9	3.5 +/- 1.0

Table 2. The mean values with standard error of four parameters from fitting the best model to the data of CM and MM together, for Experiment 1 and Experiment 2 separately.

Since the divisive gain control parameter and the exponents of the nonlinear transducer function do not vary with the change of carrier type (static or moving) or the change of carrier

contrast, we combined these three parameters of every observer from Experiment 1 and Experiment 2 to better compare CM and MM. Whereas the internal noise value is significantly different between the two experiments for MM, therefore we show its values separately for Experiment 1 and 2. The four parameters are plotted as bars to compare CM and MM (Figure 3). The nonlinear exponents *p* and *q* are both significantly larger for MM than CM (paired t-test, *df* = 7, *p1* = 0.05, *p2* = 0.04). The effect sizes are 1.20 for *p* and 1.31 for *q*, respectively. The gain control parameter *z* is also greater for MM than CM (*df* = 7, *p* = 0.02). The effect size is 1.40 for *z*. The fact that for MM the exponents *p* and *q* have larger values suggests different second-stage nonlinearities between the processing of contrast-modulated and motion-modulated boundaries. And this difference is not due to the temporal property of the carrier in MM. The much larger divisive inhibitory parameter in MM suggests larger divisive inhibition to the response of the responsible second-order channels.

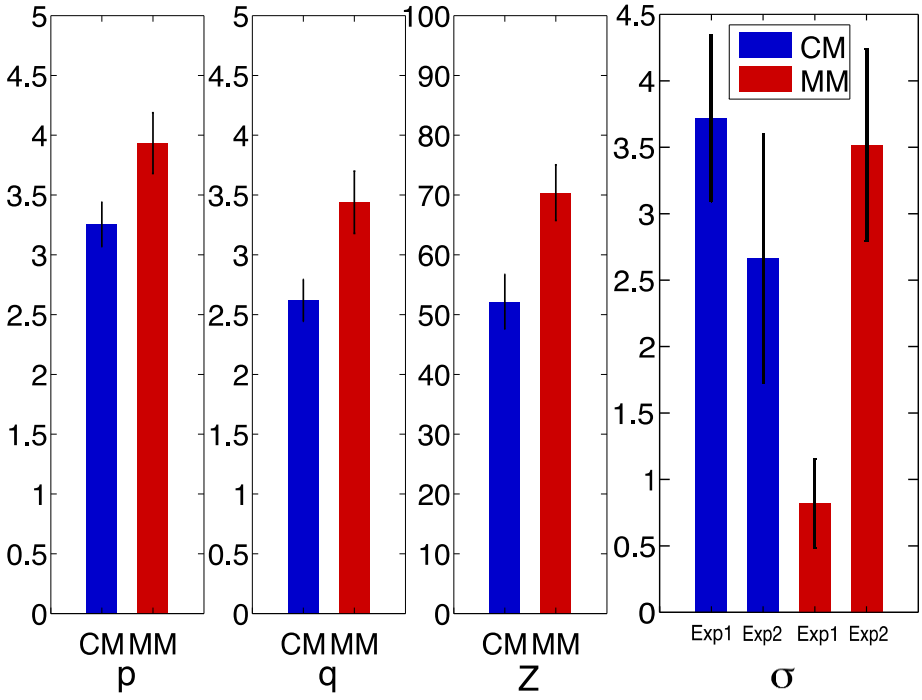

Figure 3. Three parameters-two exponents and the divisive gain parameter-are shown as means and standard error across all 8 observers combined from Experiment 1 and Experiment 2. Z is in

dB units. Red bars represent CM and the green ones represent MM. Stars indicate significant difference between the two conditions. Compared to CM, all three parameters have larger values for MM.

Using the mean parameters from Table 2, we plot the pedestal masking functions for CM and MM in Experiment 1 and Experiment 2, respectively, as shown in Figure 4. The blue dashed line indicates CM and the red solid line indicates MM. In both Experiment 1 and Experiment 2, the larger exponents for MM are manifested as a deeper dip in the pedestal masking function than that for CM. As shown in the figure, thresholds for MM are generally higher than those of CM across pedestal mask levels especially in Experiment 2. And there is no difference between Experiment 1 and Experiment 2 for CM. However, changing the carrier temporal properties affects the pedestal masking functions for MM. This difference is mainly expressed as an increased internal noise when the carrier is moving, as shown in the last section of Results about fitted parameters.

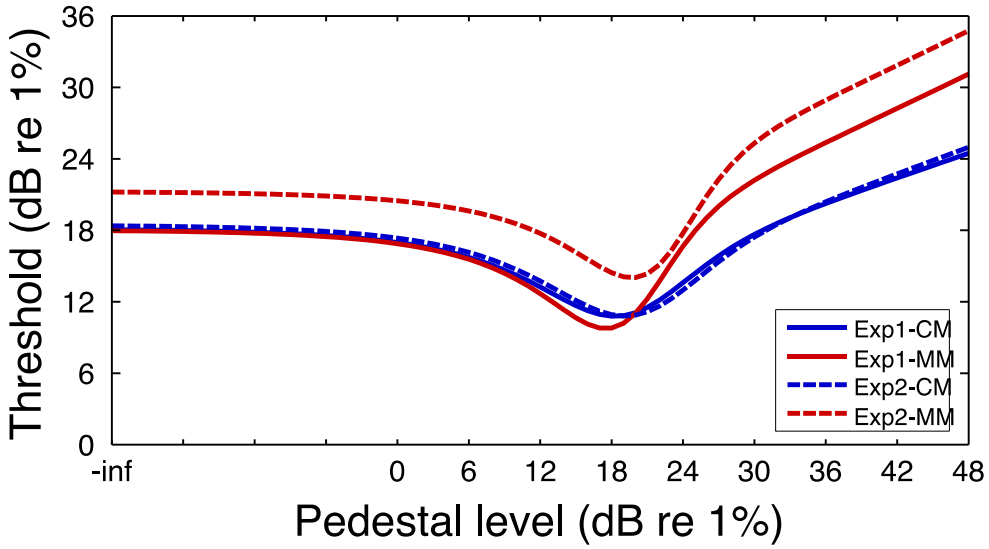

Figure 4. Pedestal masking functions of CM (blue) and MM (red) constructed with mean parameters from best model fit in Experiment 1 (solid curves) and Experiment 2 (dashed curves), respectively.

Discussion

We find the typical dipper shape for pedestal masking functions for motion-modulated (MM) second-order boundary processing. We also replicated its existence for contrast-modulation (CM) (Huang & Chen, 2014; Schofield & Georgeson, 1999). This dipper function implies the existence of a nonlinearity, which is consistent with a gain-control function of a divisive inhibitory form. Similar forms of nonlinearity have been found not only in first-order processing (Foley, 1994; Legge & Foley, 1980), but also in two types of second-order processing including contrast-modulation (N. Graham & Sutter, 2000; Huang & Chen, 2014; Schofield &

Georgeson, 1999) and orientation modulation(Gao et al., in review; F. A. Kingdom et al., 2003; Landy & Oruc, 2002). This divisive inhibition in MM processing could be explained by mutual lateral inhibition among the second-order spatial channels that are tuned to envelope spatial frequency and orientation (Durant & Zanker, 2009; Gharat & Baker, 2012). The channels may also differ in their tuning to different carrier spatial frequencies, orientations and motion velocities. Carrier spatial frequency and orientation tuning are reported in some previous studies (Durant & Zanker, 2009; Gharat & Baker, 2012; Timothy Ledgeway & Hess, 2006). For carrier velocity, a recent physiological experiment (Gharat & Baker, 2012) found very broad carrier temporal frequency tuning and no carrier motion direction tuning for motion-defined boundary processing in cat Area 18. In our stimulus, a motion-defined contour is defined solely by a motion direction difference between regions of the same carrier spatial frequency, orientation and speed. Therefore, the divisive inhibition among channels for processing motion direction or contrast-defined boundaries in our stimuli is probably from channels that are tuned to carrier or envelope spatial frequencies and orientations other than the ones we used, if the carrier tuning properties are similar between human and cat visual neurons.

The model we employed to explain the nonlinear process involved in second-order modulation processing is a nonlinear transducer function of the divisive gain-control form (Equation (1)). Outputs of this nonlinear transform are then considered under signal detection theory. Fitting our model to the data we find significantly larger nonlinear transducer exponents p and q for MM than CM. The exponents for MM are also larger than the typical values 2.4 and 2 that have been used in modeling first-order luminance modulation (D. H. Baker & Meese, 2013; Legge & Foley, 1980). In a recent study (Gao et al., in review) the exponents of second-order CM and orientation-modulation (OM) processing were found to be similar to those typical

first-order values. Since the shape of the nonlinear transducer function is determined by the values of the exponents, this difference in exponent values suggests a separate nonlinearity involved in motion-defined boundary processing.

Previous results have suggested common processing of different types of boundary. These include tilt after effect between any pair of motion-defined, luminance-defined and illusory contours(Berkley et al., 1994), similar selectivity to envelope spatial frequency and orientation for CM and MM(Gharat & Baker, 2012), similar carrier spatial frequency tuning between CM and MM(Gharat & Baker, 2012), and similar radial bias in processing motion- and luminance-defined boundaries(Clifford, Mannion, & McDonald, 2009). Neurons that respond to both motion-defined and other types of boundaries can be the neural substrates of the common part of the mechanism, including primate V2(Leventhal et al., 1998; Marcar et al., 2000) and inferior temporal (IT) region(Sary et al., 1995) and cat Area 18(Gharat & Baker, 2012). Our results suggest that the mechanism for motion-defined boundary processing must be at least partially separate from other types of boundary processing. In support of this idea, Morita et al.(Morita, Morita, & Kumada, 2003) have found performance to be particularly poor at detecting boundaries defined by combined motion and luminance variation or motion and color variation compared to single attribute defined boundaries. Additionally, two fMRI studies by Larsson et al.(Larsson et al., 2010; Larsson et al., 2006) showed that orientation-selective adaptation to different types of second-order modulation-defined boundaries is elicited in different cortical visual areas with limited overlap. Furthermore, the removal of MT affected the processing of kinetic boundaries but not luminance-defined boundaries(Marcar & Cowey, 1992). This is not due to local motion processing being impaired because when the two motion

directions are orthogonal not opposite, the ability of using motion-defined boundaries in shape discrimination remains intact.

Motion-defined boundaries require the use of moving carriers, which would possibly explain differences in processing, however here we also present contrast-defined boundary results with moving carriers. We found no difference in contrast-defined boundary processing between static or moving carriers. This implies that changing carrier type does not influence the shape of the nonlinear transducer function involved in second-order processing. What's more, comparison between the pedestal masking functions for a motion-defined boundary and a contrast-defined boundary comprising the same moving carriers gives significantly different values of exponents and divisive inhibitory parameter. This suggests that there is a different nonlinearity for motion-defined second-order boundary processing that is not explained by carrier differences.

In conclusion, our results indicate that motion-defined boundary processing has larger nonlinear transducer exponents and a larger divisive inhibitory parameter than those found for contrast-defined boundary processing. This suggests a separate nonlinearity for motion-defined boundary processing, rather than cue-invariant processing of different boundary types. Unsurprisingly, the carrier contrast does not affect the shape of the nonlinearity for either CM or MM.

Method

Stimuli

Experiment1

Both second-order boundaries, contrast-defined and motion-defined, are constructed multiplying an envelope *G(x,y)*, which is a low-spatial-frequency sinusoidal grating, to a carrier *C(x,y),* which is a high-spatial-frequency sinusoidal grating. The envelope and the carrier are defined as $C(x,y)=\sin(2\pi f_c x)$, and $G(x,y)=\sin(2\pi f_e x)$, respectively, where f_e and f_c are spatial frequencies of the envelope and the carrier.

The CM stimulus is constructed by the modulation of the contrast of one static carrier tilted 45° clockwise by one horizontal envelope. In the null interval, the stimulus, that only contains the pedestal mask m, can be described by

$$N(x,y)=C(x,y)\left[c+c\times mG(x,y)\right]\omega(x,y), \tag{3}$$

where c is the contrast of the carrier, m is the modulation depth of the pedestal, and $\omega(x,y)$ is an raised cosine window with a blur width of 0.5º to soften the edge of the stimulus. The CM stimulus in the target interval, which contains both the pedestal mask and the target, is described by

$$T(x,y)=C(x,y)\left[c+c\times(m+t)G(x,y)\right]\omega(x,y), \tag{4}$$

where t is the modulation depth of the target.

To construct a MM stimulus, we add two CM patterns which have orthogonal carrier motion directions, 45° and -45°, and opposite envelope phases. Note that the two carriers are drifting at 2 Hz instead of being static in the CM stimulus. Therefore the carrier function is

actually $C(x, y, t) = \sin(2\pi(f_c x + \omega t))$, where ω is the temporal frequency 2 Hz. The MM stimuli in the null interval and the test interval can be described as

$$MM(x,y)=\left\{C_1(x,y)\left[c+c\times mG_1(x,y)\right]+C_2(x,y)\left[c+c\times mG_2(x,y)\right]\right\}\omega(x,y), \quad (5)$$

and

$$MM(x,y)=\left\{C_1(x,y)\left[c+c\times(m+t)G_1(x,y)\right]+C_2(x,y)\left[c+c\times(m+t)G_2(x,y)\right]\right\}\omega(x,y). \quad (6)$$

The spatial frequency of all carriers is 4 cpd and the spatial frequency of all envelopes is 0.5 cycles per degree. The contrast of carrier is kept constant at 0.40 in all conditions.

Experiment 2

The differences in the stimuli are: 1) the carrier of CM is also drifting at 2 Hz instead of being static, to allow a better comparison between CM and MM; and 2), the carrier contrast of all stimuli is set to 0.48 (c.f. 0.40 in Experiment 1). A higher carrier contrast can lower increment thresholds to provide a greater modulation range above the dip to show the masking effect at high pedestal contrasts (Huang & Chen, 2014).

Figure 5 illustrates the construction of two CM stimuli and a MM stimulus. Among the two CM stimuli shown in Figure 5, only CM1 is actually used in the Experiment 2. And the CM stimulus used in the Experiment 1 has static carrier instead of a moving one shown in Figure 5. Adding two CM stimuli of opposite carrier moving directions and opposite envelope phases generates an MM stimulus.

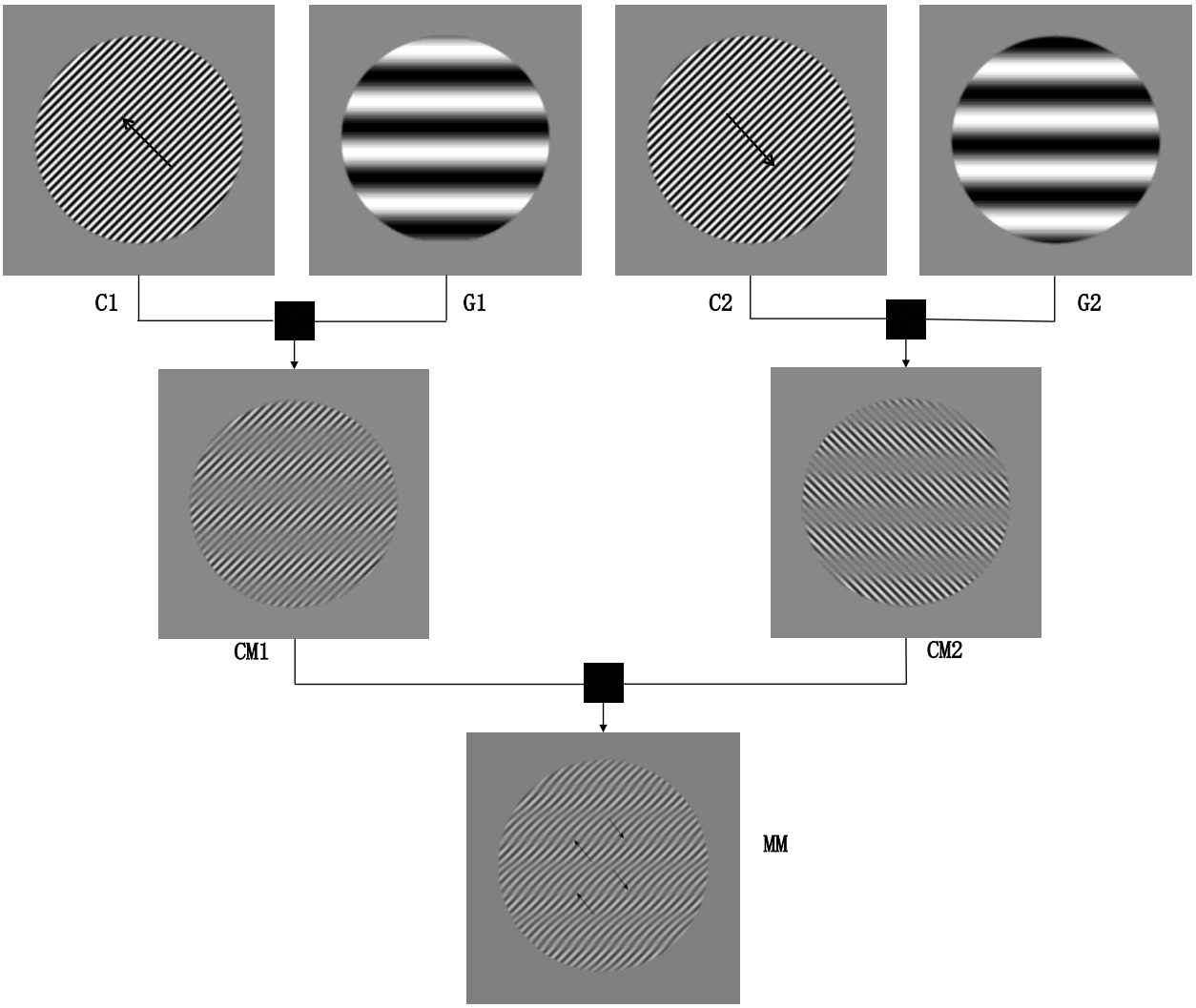

Figure 5. The process of constructing a MM stimulus from adding two CMs with moving carriers of opposite directions (C1 and C2) and envelopes of opposite phases (G1 and G2). In Experiment 2, the actual CM stimulus is CM1 which is constructed by multiplying a moving carrier grating of high spatial frequency with a static envelope grating of low spatial frequency. In Experiment 1, the CM stimulus has static carrier. The MM stimulus is the same for both Experiment 1 and Experiment 2.

Procedure

We employed the two-interval forced-choice (2IFC) paradigm to measure the increment thresholds. During each trial, the target and null intervals were presented, each for 500 ms, in a

random order with a 400 ms inter-stimulus interval between them. An auditory tone was given at the onset of each interval to reduce temporal uncertainty. The task was to identify which interval contained greater modulation. The observer responded with a button press on a keypad and were given auditory feedback as to whether they were correct for each trial. There is an inter-trial-interval of 1000 ms before the onset of next trial. We conducted the experiment in blocks of pedestal mask levels with two repetitions for each level. The pedestal levels were adjusted for each observer to give an informative sampling of the masking function. First, the detection threshold T was measured. Then the eight pedestal mask levels were calculated as: (T-*12*), (T-*6*), (T-*3*), T, (T+*3*), (T+*6*) and (T+*12*) *dB*. The unit *dB* is $20 \times log_{10}(c)$, where c represents the modulation depth (Eq. 10). At each pedestal level, a psychometric function was measured with two interleaving staircases and a threshold was obtained by fitting the psychometric function. One staircase was one-up-three-down and the other one was one-up-two-down, both terminated after 60 trials. Therefore, there were 1920 trials in each of the two conditions. The two conditions were measured alternately and the sequence of the two was balanced among observers.

Data Analysis

To compare the processing mechanisms of CM and MM, we identified eight candidate models. As in Eq. 1 and 2, the basic model to account for the second stage nonlinearity and the decision making process of second-order modulation processing has four free parameters, internal noise σ, exponents p and q, and divisive inhibition parameter z. The question was whether these parameters would be the same or different between CM and MM. By varying the

number of same and different parameters between the two conditions, we constructed eight candidate models. The exponents p and q were restricted to be either both same or different between the conditions. The eight models are, from least different parameters to most different parameters, shown in Table 3.

Models	Shared *p*	Shared *q*	Shared *z*	Shared σ	# free parameters
1	✓	✓	✓	✓	4
2	✓	✓	✓	✗	5
3	✓	✓	✗	✓	5
4	✗	✗	✓	✓	6
5	✓	✓	✗	✗	6
6	✗	✗	✓	✗	7
7	✗	✗	✗	✓	7
8	✗	✗	✗	✗	8

Table 3. The eight candidate models. The number of identical parameters between CM and MM varies among the models. This table shows whether the four parameters are same or different between CM and MM for each candidate model.

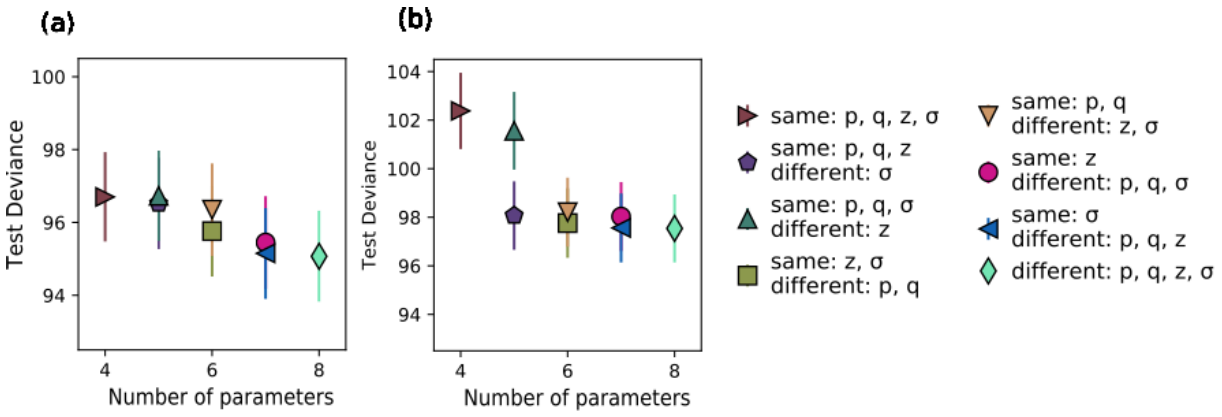

Figure 6. The mean and standard error of test deviances across 20 partitions of cross-validation are plotted for eight candidate models, for Experiment 1-(a) and Experiment 2-(b). Each candidate model is represented by a symbol of unique shape and color. The model that has the smallest test deviance is shown with a ring on its symbol. For both groups Model 8, in which all four parameters are different between the two conditions, has the smallest test deviance among the candidate models.

A twenty-fold cross-validation analysis was employed to perform model selection procedure. The cross-validation analysis relies on splitting the data and then using fitting parameters from fitting some of the data to try to predict other data that were excluded from the fitting. First, we partitioned the data for each condition of each observer into 20 sets. Each was used as the holdout test set once, and the remaining 19 sets were combined together to form the fit dataset and used to fit the model. Parameters were obtained by fitting to the fit dataset. The predictions from these fits were tested against the holdout test dataset in order to calculate the deviance. Our 20 iterations of this procedure gave us 20 deviance values (one for each test set). The best model is defined as the model with the smallest deviance:

$$D = -2 * (\log L_{test} - \log L_{sat}) \quad (7)$$

Where L_{test} is the test likelihood of the candidate model and L_{sat} is the likelihood of the saturated model(Baldwin, Schmidtmann, et al., 2016). To calculate the deviance of each candidate model, from the maximum likelihood fitting with each fit dataset, we obtained the best

fit values of the parameters. Then we calculated the test likelihood of the candidate model by calculating the likelihood of predicting the data in the corresponding test dataset(Baldwin, Schmidtmann, et al., 2016) with the fitted parameters from the fit dataset. After calculating the deviance of each of the twenty fit and test datasets, the mean and standard deviation across 20 partitions were obtained for each model. The mean test deviance values with standard deviation of all eight candidate models are shown in Figure 6. Experiment 1 (a) and 2 (b) are shown separately. The model which used the same set of parameters for CM and MM (Model 1) was the worst, especially in Experiment 2. Model 3, which would be compatible with a simple input gain difference between CM and MM (or difference in suppression) fared little better. We found that the best-performing model was Model 8, in which all four parameters can have different values between CM and MM. We fitted the whole data set of CM and MM to Model 8 to obtain the fitted curve and parameters shown in Figure 1 and Table 2.

Apparatus

For Experiment 1, stimuli were generated by a Macintosh computer running OS X and presented on a gamma-corrected Compaq CRT monitor (30 cm × 40 cm, refresh rate: 85 Hz; resolution: 1280 × 960 pixels; mean luminance 20 cd/m^2). Observers viewed the stimuli from 86 cm in a dimly lit room. A Bits++ box (Cambridge Research System) was used to provide 14 bits of digital to analog converter (DAC) depth and was running in mono mode. For Experiment 2, a computer running Windows 7 and a Multiscan G220 monitor (32 × 24 cm, refresh rate: 60 Hz, resolution 1024 × 768, mean luminance: 60 cd/m^2) were used to generate and present the stimuli. The viewing distance is 86 cm in order to keep the same value of pixel per degree. For both

experiments, the experiment and data analysis software was written in Matlab (Mathworks) using functions from the Psychophysics Toolbox(Brainard, 1997). The Palamedes toolbox 2(N. K. Prins, F. A. A. , 2009) was used to fit the psychometric functions.

Participants

For Experiment 1, four experienced psychometric experiment observers including two of the authors, YG and AB, participated. The other two observers are naïve to the purpose of the experiment. For Experiment 2, there are four observers as well, all university students in China. Two of them are experienced observers. All eight observers had normal or corrected-to-normal vision at the time of testing. All four observers are naïve to the experimental purpose and signed written informed consent. All procedures were conducted in accordance with the Declaration of Helsinki, and approved by the Ethics Review Board of the Montreal Neurological Institute.

Appendix

Effect of carrier contrast

In the current study, we also tested the effect of carrier contrast on the second-order nonlinearity for processing motion-defined boundaries. Two of the authors, YG and AB, as well as a naïve observer completed the same pedestal masking task for MM with two carrier contrast levels-3 and 10 times of the first-order detection threshold respectively. As shown in Figurea, fitting the same model to these data shows that none of the four parameters is significantly

different (paired-t test, $p > 0.05$) between the two carrier contrast levels. We then reconstruct the pedestal masking functions of each observer with their fitted parameters and plot the mean pedestal masking function with standard deviation of each carrier contrast level in Figure 7b. As shown in Figure 7b, although it seems that the pedestal masking function of the 3 times condition (blue) is shifted up-right from that of the 10 times condition (red), which corresponds to an increase in z parameter, the areas of standard deviation of each condition overlap with each other. Thus the pedestal masking function for MM is not affected by the change in carrier contrast. This means that the second-order nonlinearity for MM is unaffected by carrier contrast.

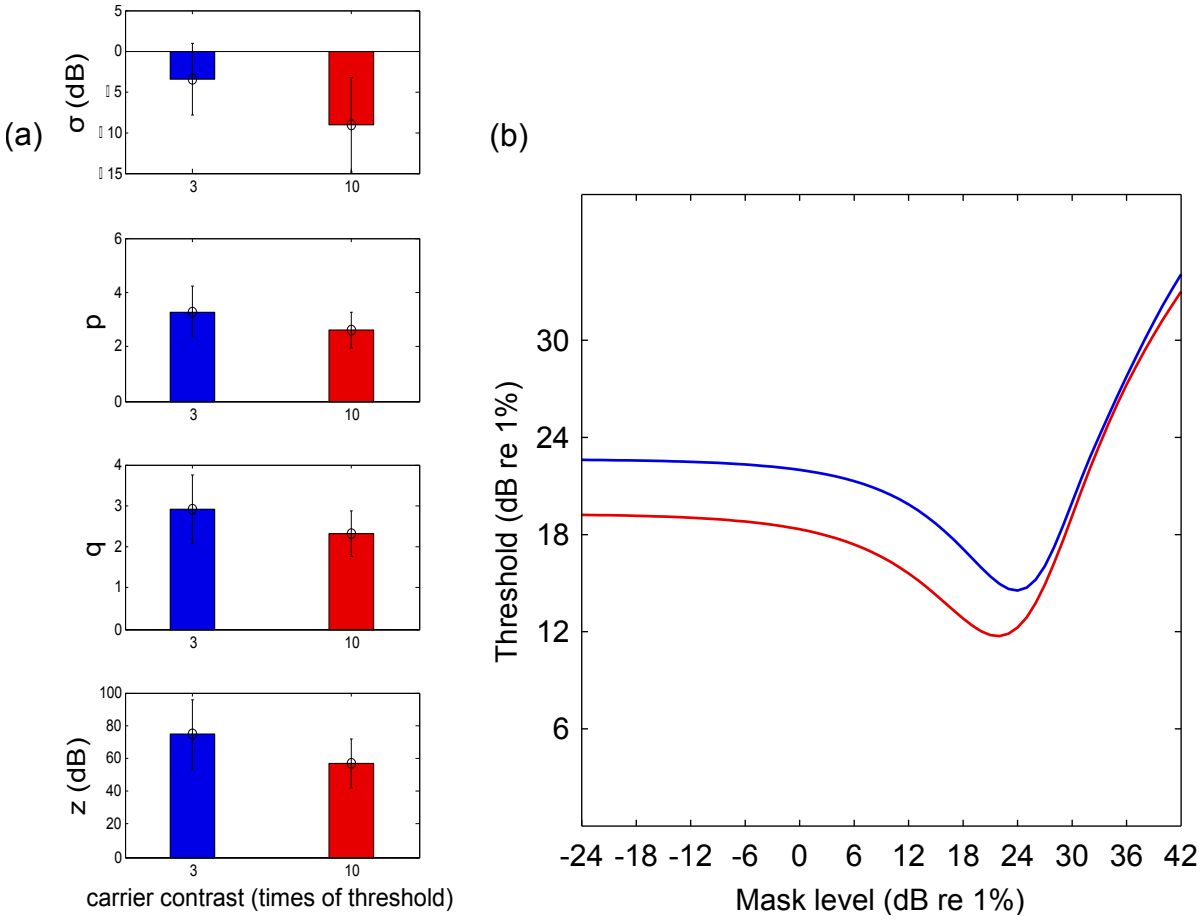

Figure 7. The results of studying the effect of carrier contrast on second-order nonlinearity of MM. The pedestal masking functions were measured with two carrier contrast levels-3 times (blue) and 10 times (red) of first-order detection threshold. (a) Mean parameters with their standard deviations are plotted for two carrier contrast levels. (b) The mean pedestal masking functions of two carrier contrast levels with their standard deviations are reconstructed from

fitted parameters. The difference of four parameters between two levels are not significant. And the standard deviations of the two pedestal masking functions overlap.

Considering the effect of carrier contrast on CM processing, we can have a look at a previous study of Huang and Chen (Huang & Chen, 2014) in which the pedestal masking functions of CM gratings were measured with two different levels of carrier contrast. Fitting our second-order gain-control nonlinear model to the data in that study reveals that the internal noise and the shape (nonlinear exponents) of the nonlinearity do not vary considerably under different carrier contrast levels (values change between 16% and 23%). The gain control parameter z increased over 40 times when the carrier contrast was reduced from 0.40 to 0.16. None of the parameters show significant difference between two carrier contrast levels. This might partially due to low statistical power with merely two observers. The mean values of parameters from fitting our model to their data are shown in Table 4.

Carrier contrast	σ (dB)	p	q	Z (dB)
0.16	8.80	3.68	3.21	100.67
0.40	6.96	3.17	2.63	67.21
Change	0.23	0.16	0.22	47.11

Table 4. The mean values of the parameters from fitting our model to Huang and Chen's data(Huang & Chen, 2014). Only z parameter increased dramatically when the carrier contrast is reduced.

In conclusion, for both MM and CM, the carrier contrast appears to have no effect on the shape of the second-order processing nonlinearity.

Manuscript 3: The amblyopic deficit for 2nd order processing: Generality and Laterality

Yi Gao, Alexandre Reynaud, Yong Tang, Lixia Feng, Yifeng Zhou, and Robert F. Hess

Abstract

A number of previous reports have suggested that the processing of second-order stimuli by the amblyopic eye (AE) is defective and that the fellow non-amblyopic eye (NAE) also exhibits an anomaly. Second-order stimuli involve extra-striate as well as striate processing and provide a means of exploring the extent of the cortical anomaly in amblyopia using psychophysics. We use a range of different second- order stimuli to investigate how general the deficit is for detecting second order stimuli in adult amblyopes. We compare these results to our previously published adult normative database using the same stimuli and approach to determine the extent to which the detection of these stimuli is defective for both amblyopic and non-amblyopic eye stimulation. The results suggest that the second order deficit affects a wide range of second-order stimuli, and by implication a large area of extra-striate cortex, both dorsally and ventrally. The NAE is affected only in motion-defined form judgments, suggesting a difference in the degree to which ocular dominance is disrupted in dorsal and ventral extra-striate regions.

Introduction

The natural environment is composed of luminance-defined (first-order) as well as contrast/motion/stereo-defined (second-order) features. It is widely accepted that the first-order information is processed by the neurons in early visual cortex (V1) with receptive fields tuned for orientation (Hubel & Wiesel, 1962) and spatial frequency (Campbell, Cooper, & Enroth-Cugell, 1969; DeValois & DeValois, 1988) of the luminance-defined stimuli. However, there are two conflicting views for where second-order visual features are processed, though it is widely accepted that it involves additional processing in extra-striate cortex. There is some debate over whether all second-order stimuli are processed in one cue-invariant area in extra-striate cortex, such as V3A (Zeki & Shipp, 1988) or whether multiple different areas are involved for the different varieties of second-order stimuli (e.g. contrast-defined, motion-defined and orientation-defined). For example, for motion-defined stimuli, there is evidence supporting the involvement of V1, V2 and V3 in representation of motion boundaries (Reppas, Niyogi, Dale, Sereno, & Tootell, 1997). There are also reports that MT (V5) responds to second-order motion stimuli (Smith, Greenlee, Singh, Kraemer, & Hennig, 1998), as well as reports that V3 and VP respond stronger to second-order than first-order stimuli. For orientation (texture)-defined stimuli, single cell studies suggest the involvement of areas downstream from V2 (El-Shamayleh & Movshon, 2011), while human fMRI studies suggest the involvement of many areas including V1, V2, V3, V3A/B, LO1, hV4 and VO1 (Larsson, Landy, & Heeger, 2006). There is also evidence from lesion study for the involvement of V4 in texture discrimination (Merigan, 2000). For contrast-defined stimuli, there is evidence for the involvement of V1/A17 and V2/A18 (Hallum, Landy, & Heeger, 2011; Zhou & Baker, 1993, 1994).

The psychophysical deficit in amblyopia is extensive involving not only contrast sensitivity (Hess & Howell, 1977; M. Levi & R. S. Harwerth, 1977) but also the encoding of spatial position (Bedell & Flom, 1981; Hess, Campbell, & Greenhalgh, 1978; Lagreze & Sireteanu, 1991), global motion (Aaen-Stockdale & Hess, 2008; Ho et al., 2005; Simmers, Ledgeway, Hess, & McGraw, 2003), global form (Simmers, Ledgeway, Hutchinson, & Knox, 2011; Husk & Hess, 2013; Simmers, Ledgeway, & Hess, 2005), contrast-defined form (Hong, Levi, & McGraw, 2001) and motion-defined form (Giaschi, Regan, Kraft, & Hong, 1992; Farivar, & Hess., 2011). The site of the amblyopic deficit is thought to be primarily in the striate cortex (Kiorpes & McKee, 1999) but the extent to which the extra-striate cortex is separately affected is not clear (Kiorpes, Kiper, O'Keefe, Cavanaugh, & Movshon, 1998). Although it is true that second-order processing is thought to involve extra-striate areas, it is not always possible to exclude an explanation based on a reduced feedforward input from striate cortex for reduced second order function. Simmers and colleagues (Simmers et al., 2005; Simmers et al., 2003; Simmers, Ledgeway, Mansouri, Hutchinson, & Hess, 2006) specifically separated contrast from global integrative effects and argue for a primary deficit in ventral as well as dorsal extra-striate function. Wong and colleagues (Wong, Levi, & McGraw, 2001) also show that the deficit for contrast-defined form is not simply due to reduced visibility of the carrier, suggesting extra-striate involvement. Similarly, Husk and colleagues (Husk, Farivar, & Hess, 2012) argue that deficits for motion-defined form remain even after correcting for low-level differences in contrast sensitivity.

Thus there is support for defective second order processing in amblyopia that is not explicable in terms of striate function, suggesting extra-striate involvement. Here we address the nature of this extra-striate involvement with the following questions;

1. How general is this deficit? For example, are only some types of second order processing affected in amblyopia or are all types of second order processing affected equally?

2. How lateral is this deficit? For example, is this deficit specific to the AE information or is information from the NAE equally affected?

An answer to the first question bears upon the extent of the extra-striate deficit as there is evidence from both single cell neurophysiology (Zhou & Baker, 1993, 1994) and human fMRI (Reppas et al., 1997; Hallum et al., 2011) that separate ventral and dorsal extra-striate regions underlie the processing of different second-order stimuli. On the basis of the suggested developmental vulnerability of the dorsal extra-striate cortex (Braddick, Atkinson, & Wattam-Bell, 2003), one might expect a greater loss of motion-defined form compared with either contrast- or orientation-defined form. The answer to the second question has been partly answered by previous studies (Giaschi et al., 1992; Ho et al., 2005; Wong et al., 2001), information through the NAE is affected to some extent. The numbers of amblyopes studied to date does not allow us to gauge how general a finding this is and whether both eyes are affected equally. Also this effect seems clear in children but less clear in adults (Giaschi et al., 1992; Ho et al., 2005). By using a larger number of adult subjects and comparing results to a large database

of normal adult responses collected using the same psychophysical approach, we hope to answer both of these questions for the adult population.

We used the quick Contrast Sensitivity Function (qCSF) approach (Lesmes, Lu, Baek, & Albright, 2010) to measure two types of first-order contrast sensitivity and three types of second-order sensitivity that relied on form judgments (i.e. contrast-, orientation- and motion-defined form).

The qCSF method has been successfully applied to measuring second-order sensitivity of normal observers (A. Reynaud, Tang, Zhou, & Hess, 2014) as well as first-order sensitivity of amblyopes (F. Hou et al., 2010). This is the first time that qCSF model is applied to second-order sensitivity of amblyopes and we are relatively confident that the model is valid based on its previous successful applications. The stimuli used for the first order measurements served as the carriers for the second order measurements. The results on 28 adult amblyopes were compared with a normative database from 52 adult subjects using an identical approach (Reynaud et al., 2014).

Methods

Subjects

In total 28 subjects (17 males and 11 females, average age=26.3 ± 9.69 years, range: 13 – 55 years) volunteered in the main experiment which included two first-order conditions: static and moving stimulus conditions, and three second-order conditions: contrast-modulation,

orientation-modulation, motion-modulation (see *Stimuli*). There are two groups-the first group includes 21 subjects (9 males and 12 females, average age=22.0 ± 3.62 years, range: 13 – 27 years) that were tested in Hefei; the second group includes 7 subjects (4 males and 3 females, average age=38.5 ± 11.40 years, range: 23 – 55 years) that were tested in Montreal. All of the subjects were diagnosed with amblyopia (6 with strabismus) and the visual characteristics are detailed in Table 1. 24 (16 males and 7 females, average age=28.5 ± 9.38 years, range: 21- 55 years) of them also did a normalized contrast-modulation condition (see Stimuli). Informed consent was obtained from all participants. This research project has been approved by the Ethics Review Board of the Montreal Neurological Institute and by the Ethics Committee in University of Science and Technology of China. It was performed in accordance with the ethical standards

laid down in the 1964 Declaration of Helsinki.

Subjects	Refraction Error	Visual Acuity	Strabismus	CMn
EL	NAE -0.25/ -0.50*120° AE +0.50/ -1.00*0°	20/ 20 20/ 40	L eso 10°	Y
KM	NAE plano AE -1.25/ -0.50*90°	20/ 20 20/ 40	R exo 20°	Y
GH	NAE -1.25/ -0.50*30° AE +2.50/ 1.50*75°	20/ 20 20/ 50	L exo 6°	Y
EC	NAE plano AE +2.50 / -0.50 * 180°	20/ 12.5 20/ 100	None	Y
EV	NAE plano AE -0.75/ -0.50*60°	20/ 20 20/ 63	R exo 15°	Y
MG	NAE plano AE -1.00	20/ 12.5 20/ 63	Microtropia eso 6!	Y
JF	NAE +0.50/ -0.50*60° AE +2.00	20/ 16 20/ 160	L exo 15°	Y
CS	NAE plano AE +2.00/ +1.00*90°	20/ 20 20/ 63	None	Y
LS	NAE -0.50 DS AE +2.50/ 0.50*90°	20/ 20 20/ 50	None	Y
ZH	NAE plano AE +2.50/ 1.50*85°	20/ 16 20/ 50	None	Y
YX	NAE plano AE +1.00/ +1.50*95°	20/ 20 20/ 40	None	Y
YFZ	NAE -0.50*165° AE +2.00/ +3.00*70°	20/ 25 20/ 50	None	Y
YJ	NAE -2.75 DS AE +1.50 DS	20/ 20 20/ 50	None	Y
WS	NAE plano AE +4.00/ +1.00*85°	20/ 20 20/ 160	None	Y
XL	NAE plano AE +3.00/ +2.00*100°	20/ 20 20/ 80	None	Y
SJ	NAE -2.00/ -1.00*10° AE -1.00/ +3.50*85°	20/ 20 20/ 40	None	Y
XCX	NAE +0.50/ 1.50*180° AE +4.00/ +1.00*170°	20/ 25 20/ 63	None	Y
DJY	NAE plano AE +1.00/ +0.25*90°	20/ 20 20/ 80	None	Y
ZY	NAE -2.25 DS AE +3.00/ +1.50*75°	20/ 25 20/ 100	None	Y

Table 1. Clinical details of amblyopic subjects

Apparatus

All of the procedures and the analysis were processed with Matlab (© the MathWorks) using the psychophysics (Brainard, 1997; Pelli, 1997), Palamedes (Prins & Kingdom, 2009) and qCSF (Lesmes et al., 2010) toolboxes. Stimuli were presented on a gamma-corrected Sony G220 CRT monitor for the first group of subjects and on a gamma-corrected Compaq CRT monitor for the second group. For the first monitor the display area was 24.4 x 32.5 cm with the mean luminance 40 cd/m^2, the refreshing rate 75 Hz and the resolution 1600 x 1200 pixels. For the second monitor the display area was 30 x 40.5 cm with the mean luminance 20 cd/m^2, the refreshing rate 120 Hz and the resolution 1024 x 768 pixels. Subjects viewed the stimuli monocularly in a dimly lit room with a viewing distance of 60 cm.

Stimuli

The visual stimuli presented in this experiment on amblyopes were the same as the ones in our previous study on normals (Reynaud et al., 2014) except that in addition to the five existed conditions, namely first-order oriented luminance modulation (subsequently denoted as LM1d), first-order moving luminance modulation (denoted as LM2d), second-order non-normalized contrast-defined modulation (denoted as CM), second-order normalized orientation-defined modulation (denoted as OM) and second-order normalized motion-defined modulation (denoted as MM), an additional normalized contrast modulation condition (denoted as CMn) was added.

The two types of first-order stimuli were then used as carriers to build the second-order stimuli.

To keep consistency, the contrast is always expressed as Michelson contrasts.

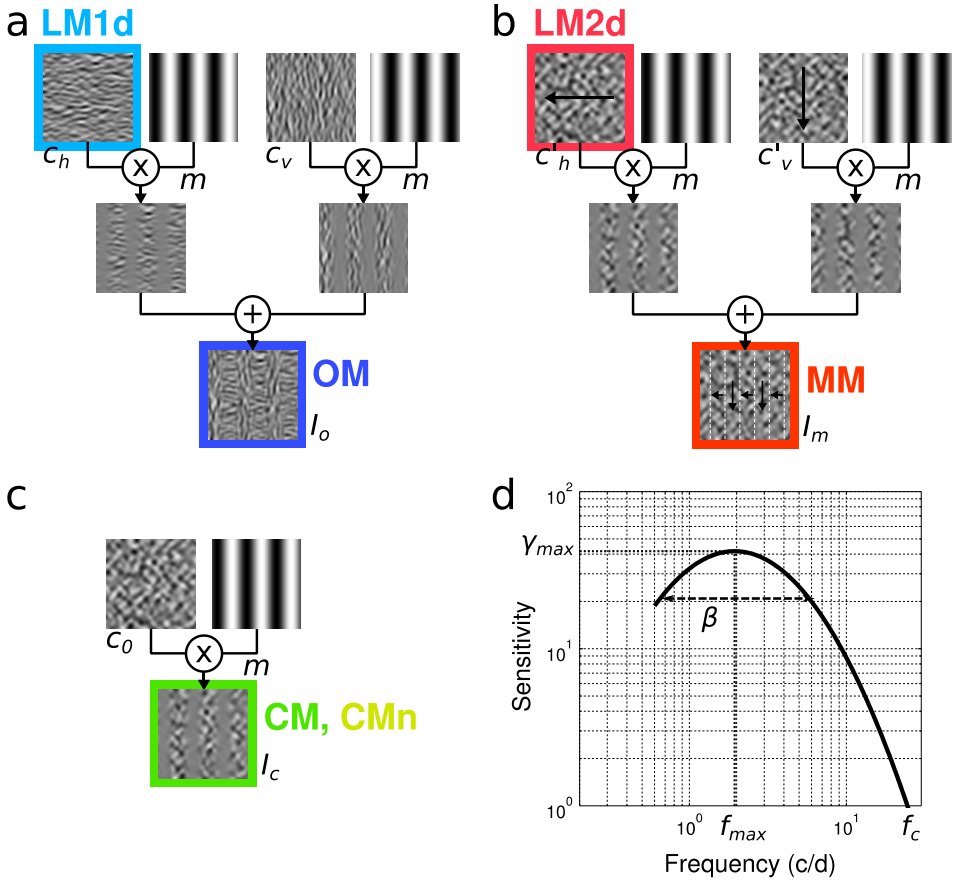

Figure 1. Stimuli and sensitivity functions. (a) Orientation case. The carrier is an oriented one-dimensional filtered noise (first-order orientation case, LM1d). Two carriers of orthogonal orientations are respectively modulated by out-of-phase sine-wave gratings and combined to generate the second-order orientation-modulated stimulus (OM). (b) Motion case. The carrier is a non-oriented two-dimensional filtered noise moving horizontally or vertically (first-order motion case, LM2d). Two carriers moving in random orthogonal directions are respectively modulated by out-of-phase sine-wave gratings and combined to generate the second-order motion-modulated stimulus (MM). (c) Contrast-modulation. The carrier is a non-oriented two-dimensional filtered noise, its contrast is modulated by a sinusoidal grating to generate the second-order contrast-modulated stimulus (CM), or contrast-modulated normalized stimulus (CMn). (d) The sensitivity is described by the truncated log-parabola model as a function of the spatial frequency. Four parameters are studied: the peak gain (γ_{max}), the peak frequency (f_{max}), the bandwidth (β), and the cutoff frequency (f_c). Stimuli are rendered here at 100% Michelson contrast, adapted from Reynaud, Tang, Zhou and Hess 2014.

First-order, carriers

In the case of LM1d and OM, the first-order carriers c_h and c_v (Figure 1a, first row) were generated by filtering white noises by the horizontal Gabor filter G_h or the vertical one G_v respectively in a two-dimensional space (x,y) with values ranging from -1 to 1 (Equation 1). The frequency and contrast of the Gabor filters were determined by the qCSF method (see Procedures) and the bandwidth was 3 octaves.

$$c_h(x,y)=w_1(x,y)*G_h(x,y)$$

$$c_v(x,y)=w_2(x,y)*G_v(x,y) \quad (1)$$

In the case of LM2d or MM, the carriers c'_h and c'_v (Figure 1b, first row) were functions of two-dimensional space and time (x,y,t) with a range of values between -1 and 1. They were generated by successively filtering white noises by both the orthogonally oriented Gabor filters G_h and G_v (Equation 2). The carriers were moving randomly leftward or rightward for the horizontal conditions and upward or downward for the vertical conditions, at a drifting rate of 2Hz. Note that the illustration Figure 1b only indicates leftward and downward arrows as examples.

$$c'_h(x,y,t)=w_1(x+t,y)*G_h(x,y)*G_v(x,y)$$

$$c'_v(x,y,t)=w_2(x,y+t)*G_h(x,y)*G_v(x,y) \quad (2)$$

The carrier of CM and CMn – c_0 was also generated by successively filtering white noise by both G_h and G_v but in a two-dimensional space (x,y) with a range of values between -1 and 1, as shown in Equation 3.

$$c_0(x,y)=w_1(x,y)*G_h(x,y)*G_v(x,y) \quad (3)$$

Second-order, modulation

The envelopes that were used to build the second-order stimuli were two half-cycle phase-shifted gratings with a frequency of 1/4 that of the carrier, m_1 and m_2 respectively (Equation 4). These envelopes took values between 0 and 1. They were weighted by a modulation parameter m ($0<m<1$) characterizing the blending applied between the two textures (Figure 1a and b, second rows), and could both be horizontal or both be vertical. These envelopes modulated the carriers in each second-order condition.

$$m_1(x)= 1/2\ (1 + m\ \sin(2\pi f_m x))$$

$$m_2(x)= 1/2\ (1 - m\ \sin(2\pi f_m x)) \qquad (4)$$

For the OM stimulus I_o consisted of the sum of the modulated oriented carriers c_h and c_v (Equation 5, Figure 1a third row). The MM stimulus I_m consisted of the sum of the modulated moving carriers c'_h and c'_v (Equation 6, Figure 1b third row). While for the CM and CMn the stimulus I_c contained only modulation of one carrier (Equation 7, Figure 1c).

$$I_o(x,y)= (c_h(x,y)\times m_1(x)) + (c_v(x,y)\times m_2(x)) \qquad (5)$$

$$I_m(x,y,t)= (c'_h(x,y,t)\times m_1(x)) + (c'_v(x,y,t)\times m_2(x)) \qquad (6)$$

$$I_c(x,y)= c_0(x,y)\times m_1(x) \qquad (7)$$

In all of the second-order stimuli, there is no relationship between the orientation of the carriers and that of the envelopes. In particular, for the motion-modulation case, the two carriers were moving in random orthogonal directions (one horizontally and one vertically). Thus the direction of motion never provided any cue on the envelope orientation. All the stimuli were showed on a grey background in a Gaussian aperture of 10° standard deviation (Reynaud & Hess, 2012). The filtered noise carrier has an RMS contrast of approximately 0.2 times that of

the Michelson contrast. The application of the Gaussian mask also has the effect of reducing the apparent contrast of the stimulus.

Procedures

Trial procedure

A single-interval identification task was employed to estimate the detection sensitivity. The subjects' task was to identify the orientation of the carrier for the first-order measurements or the orientation of the envelope for the second-order measurements: horizontal or vertical. The trial time course was as follows: (1) a green fixation dot appeared on the screen, (2) the dot turned red and the stimulus was presented for 1 s with an auditory cue, (3) the dot turned orange and indicated to the subject that a response was needed, (4) when the subject answered, the dot disappeared and audio feed-back about the correctness of the response was provided.

The first-order sensitivities were always measured before their second-order counterparts for each subject individually so that the contrast of the carrier for the subsequent OM and MM conditions could be set to 10 times the contrast threshold for detecting the respective carrier (LM1d and LM2d conditions). It was set to 1 if larger than 1. However, for the CMn condition the mean contrast was set to 5 times the contrast threshold. For the CM condition, the mean contrast was set to 50% to ensure that the full range of modulation was always available. Each run consisted of 100 trials preceded by 5 training trials, took approximately 7 minutes and was repeated two times. Sensitivity was measured monocularly with the sequence of first run of all measurements of the NAE, first run of the AE, second run of the NAE and second run of the AE. An extra run was performed in case these two repetitions showed a notable difference.

qCSF method

The sensitivity functions were determined using the quick contrast sensitivity function (qCSF) method (Hou et al., 2010; Lesmes et al., 2010). This method is a Bayesian adaptive procedure that estimates multiple parameters of the psychometric function at the same time. The qCSF jointly estimates thresholds across the whole spatial frequency range. For each trial, the method finds the optimal stimulus in order to maximize the expected information gain about the sensitivity function under study (Lesmes et al., 2010). The method estimates the sensitivity function with the truncated log-parabola model (Watson & Ahumada, 2005). The log-parabola function in Equation 8 can be described by three parameters: the peak gain γ_{max}, the peak frequency f_{max}, and the bandwidth β (full-width at half-maximum, Figure 1d).

$$S'(f) = log_{10}(\gamma_{max}) - \kappa\left(\frac{log_{10}(f) - log_{10}(f_{max})}{\beta\prime/2}\right)^2 \qquad (8)$$

with κ=$\log_{10}(2)$ and β'=$\log_{10}(2\beta)$.

The truncated log-parabola comes from the truncation imposed for low frequencies and described by the parameter δ. The log-sensitivity S is then expressed in Equation 9 :

$$S(f) = log_{10}(\gamma_{max}) - \delta \qquad \text{if } f < f_{max} \text{ and } S'(f) < \log_{10}(\gamma_{max}) - \delta$$

$$S(f) = S'(f) \qquad \text{else} \qquad (9)$$

We discarded the truncation parameter from our analyses because it was often out of the range of our measurements. Another parameter that we used in the analysis was the cutoff frequency f_c defined as the frequency for which the sensitivity is minimal S=0 (Equation 10).

$$f_c = f_{max}.10^{\frac{\beta\prime}{2}\sqrt{\frac{log_{10}(\gamma_{max})}{\kappa}}} \qquad (10)$$

For the qCSF measurements, the possible range for the modulation was 0.001 to 1. The frequency range was 1 to 14.16 c/d for first-order luminance and 0.25 to 3.54 c/d for second-order modulation frequency. The initial priors required by the qCSF were set manually: the gain prior was set to 100 for the first-order and to 10 for second-order; the peak frequency prior was set to 8 c/d for the first-order and to 2 c/d for the second-order; and the bandwidth prior was set to 3 octaves in both cases.

Data analysis

To check if the results of the two groups of subjects that were tested in the two different experimental set-ups were different from each other, we compared the shapes of the average contrast sensitivity function and the modulation sensitivity function as well as the four parameters of the qCSF function. There was no significant difference between the two groups. Therefore, in the following analysis we report combined data.

Because the carrier contrast could not exceed 1, the contrast of some carriers was less than 10 times their detection threshold. In order to assess the capacity of second-order processing per se, i.e. to make sure any reduced performance for second-order stimuli is because of second-order processing per se instead of a loss of visibility of first-order information, only data for which the carrier contrast was larger than 5 times its detection threshold are displayed. For the first-order conditions, we used only contrast sensitivity data that was above zero.

We then compared the qCSF parameters obtained from the amblyopes with those parameters obtained from normal adults from our previous study (Reynaud et al., 2014). Since

there was no significant difference between normal eyes and the NAE of amblyopes, we compared the parameters obtained from AE with those obtained from NAE.

Results

The averaged sensitivity functions of 28 subjects are shown in Figure 2a for non-amblyopic eyes (NAE) and Figure 2b for amblyopic eyes (AE). The two kinds of first-order stimuli and the three kinds of second-order stimuli (see Methods) are shown in different colors. There are four important observations from these results. First, the sensitivity functions for first-order and second-order stimuli present a low-pass bell shape in both eyes. The functions cluster into two groups: a first-order group with large max gain and high peak spatial frequency and a second-order one with smaller gain and reduced peak frequency. This result is consistent with previous studies in terms of the shape of the first-order contrast sensitivity function (Campbell & Robson, 1968), the shape of the second-order contrast sensitivity functions (Hutchinson & Ledgeway, 2006; Landy & Oruc, 2002; Meso & Hess, 2010, 2011; Schofield & Georgeson, 2003; Sutter, Sperling, & Chubb, 1995; Watson & Eckert, 1994) and the higher sensitivity to first-order stimuli than that to second-order stimuli (Hutchinson & Ledgeway, 2006; Sutter et al., 1995). Second, although the shapes of the sensitivity functions of the NAE and the AE are similar, the gain and the peak frequency are higher in NAE than in the AE for both first-order and second-order sensitivity functions. Third, the sensitivity functions of the two first-order stimuli, namely the static and the moving first-order noise stimuli, are very similar in terms of shape, gain and peak frequency. In the NAE, the peak frequency is about 1.9 c/d and the gain is

about 54, which is consistent with previous results (Campbell & Robson, 1968). In the AE, the functions peak at about 1.40 c/d and have a sensitivity of about 37. The fact that the peak frequency and the max gain of the AE is smaller than that of the NAE is consistent with the widely accepted idea that amblyopic eyes have reduced contrast sensitivity (Gstalder & Green, 1972; Hess & Howell, 1977; D. M. Levi & R. S. Harwerth, 1977). Fourth, the sensitivity functions of the three second-order stimuli, although having similar shapes, are different in gain and peak frequency. In the NAE, the contrast-modulation sensitivity function peaks at approximately 1.14 c/d and has a sensitivity of 6.20; the orientation-modulation sensitivity function peaks at 0.99 c/d and has a sensitivity of 4.8; and the motion-modulation sensitivity function has a peak frequency of 0.72 c/d and a gain of 3.67. While in the AE, the contrast-modulation sensitivity function peaks at approximately 0.67 c/d and has a sensitivity of 5; the orientation-modulation sensitivity function peaks at 0.61 c/d and has a sensitivity of 4.32; and the motion-modulation sensitivity function has a peak frequency of 0.4 c/d and a gain of 3.66. Therefore compared to the NAE, there is also a sensitivity deficit for second-order processing for

amblyopic eye stimulation.

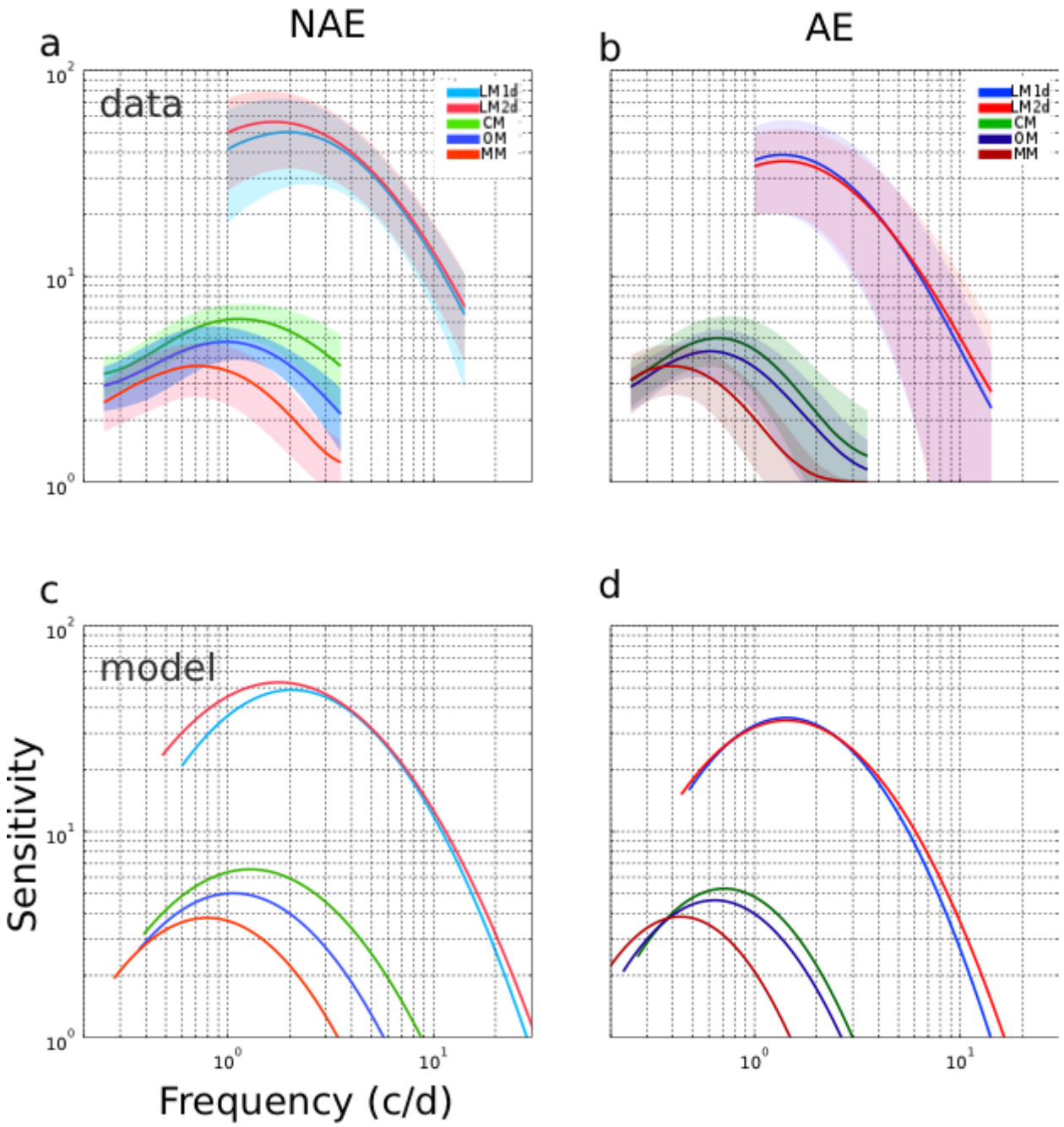

Figure 2: Data and model fits; a) averaged sensitivity functions from the data with standard deviation for the NAE; b) same functions for the AE; c) sensitivity functions reconstructed with the qCSF parameters using the log-parabola model for the NAE; d) the same functions as in c for the AE. In each figure five conditions are shown in different colors - first-order static luminance-modulated noise in light blue, first-order moving luminance-modulated noise in light red, second-order contrast-modulation in green, second-order orientation-modulation in darker blue and second-order motion-modulation in darker red.

The Figure 2c and 2d show the sensitivity functions reconstructed using the log-parabola model (Watson & Ahumada, 1985) with the parameters estimated by the qCSF model for the NAE and AE separately. The model representation was truncated to the delta threshold level of the qCSF (Lesmes et al., 2010) because this parameter is not of interest here, and the curve has been extrapolated to show the cutoff frequency (see Methods). As reflected in the data (figures 2a and b), the sensitivity functions derived from the parameters show that the AE has lower gain and peak frequency for both first-order and second-order sensitivity functions compared with that of the NAE. The cutoff frequency for the first-order functions is approximately 15 c/d in the AE and 30 c/d in the NAE. It is around 3, 2.6 and 1.5 c/d in the AE for second-order contrast-, orientation- and motion-modulation respectively. And in the NAE it is around 8.7, 5.7 and 3.4 c/d respectively.

Figure 3 shows the log threshold elevation ratios for the AE compared to the NAE in each condition as a function of spatial frequency for each subject separately. The data were fit by linear regression for each subject in each condition separately. The mean and standard deviation of the two regression parameters are shown in Table 2. Two features are noteworthy for the threshold elevation of the AE, first, the slopes of the regression lines in figure 3 are mostly positive and the mean of the slopes in every condition is positive. Second, in the two first-order conditions the intercepts are mostly at or above zero whereas for the three second-order conditions they are mostly below zero. Therefore, for both first-order and second-order processing the sensitivity of the AE declines relative to the sensitivity of the NAE as the spatial

frequency increases. For the first-order conditions, the contrast sensitivity of the AE is reduced relative to the NAE at all spatial frequencies including mid-low spatial frequencies. In the second-order conditions, however, the AE's sensitivity is worse than that of the NAE at high frequencies but better at mid-low frequencies.

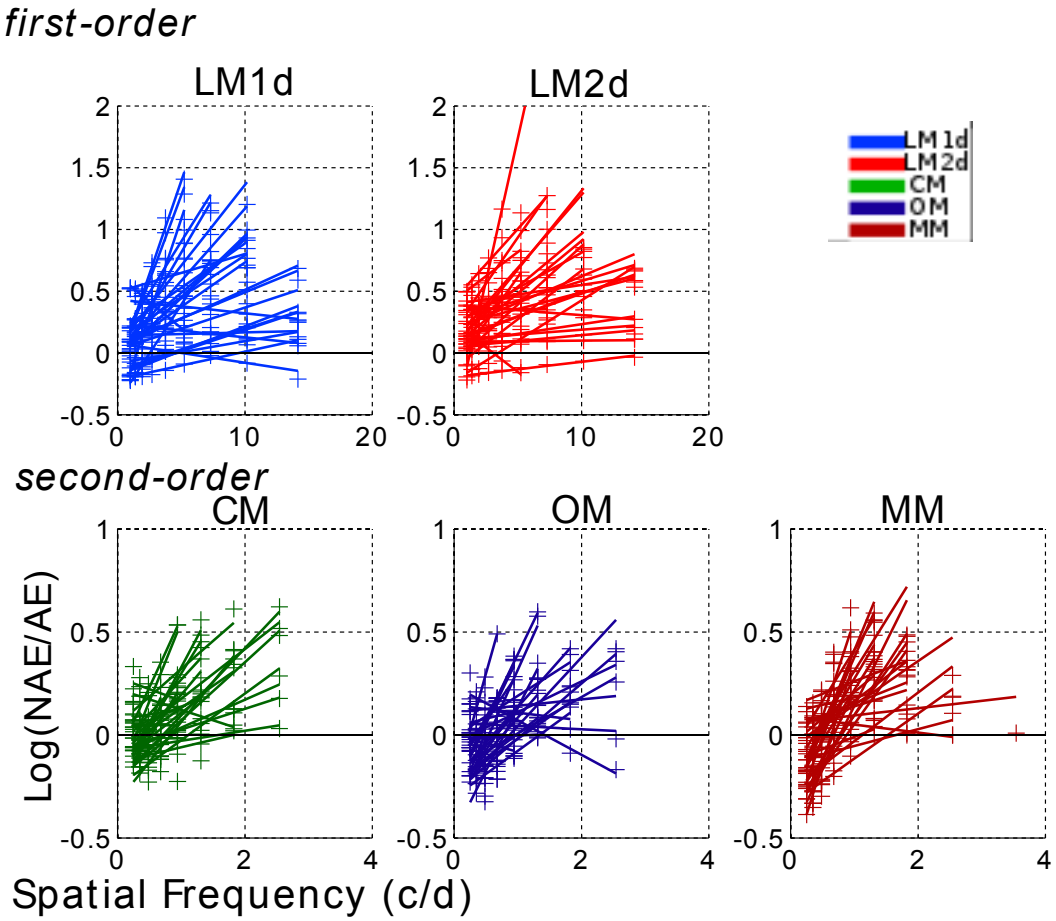

Figure 3. Logarithmic ratios of the sensitivity of the NAE to the AE against the spatial frequency. First row: first-order stimuli-LM1d (luminance-modulation orientation), LM2d (luminance-modulation motion); second row: second-order stimuli-OM (orientation-modulation), MM (motion-modulation), CM (contrast-modulation). The color of the symbols refers to the type of stimulus used from the color code of figure 2. Different number of points are shown for each subject because only the data that survived the truncation is shown (see Methods).

Condition	Slope mean	Slope std	Intercept mean	Intercept std
LM1d	0.2843	0.3595	0.0289	0.2379
LM2d	0.2135	0.2698	0.1255	0.1838
CM	0.274	0.2314	-0.0725	0.1843
OM	0.2999	0.2882	-0.1319	0.1656
MM	0.348	0.2954	-0.1868	0.2059

Table 2. The fitted parameters and their means and standard deviations.

Four parameters from qCSF model fits to the data are shown in figure 4, a – the gain, b – the peak frequency, c - the cutoff frequency and d - the bandwidth. For each parameter, averaged values are compared for 104 normal eyes, 28 NAEs and 28 AEs.

This parameter comparison is for the two first-order conditions and the 3 second-order conditions respectively. The data of the normal eyes are from our previous study (Reynaud et al., 2014) in which no significant difference was found between the sensitivity functions of the dominant eye and the non-dominant eye of normal subjects for either first-order or second-order stimuli. Therefore, in the current analysis the previous data of the dominant eyes and non-dominant eyes were averaged for comparison with those of the AE and the NAE.

Since it cannot be assumed that the NAE of amblyopia patients is absolutely normal, we used a Wilcoxon Rank Sum two-tail test for comparing the parameters between the NAE and the average of normal eyes. On the other hand, since our expectation is that the amblyopic eye will show a deficit, we used a one-tail test for comparing the parameters between the AE and the average of normal eyes. The difference between the AE and the normal eyes is significant for all parameters in all conditions ($p<0.05$). Hence compared to the normal eyes, the AE exhibits a deficit that is general for different types of first-order and second-order stimuli. On the other

hand, the parameters for the NAE are only significantly different from those of normal eyes in very few conditions ($p<0.05$). The gain and the cutoff frequency in the first-order motion condition and the bandwidth in the orientation-modulated second-order condition are superior to those for the normal eyes. However, the gain in the motion-modulated second-order condition is lower than that of normal eyes. Therefore, there is no general deficit in the NAE for either first-order or second-order processing, enabling further analysis to be done between the data of the NAE and the AE.

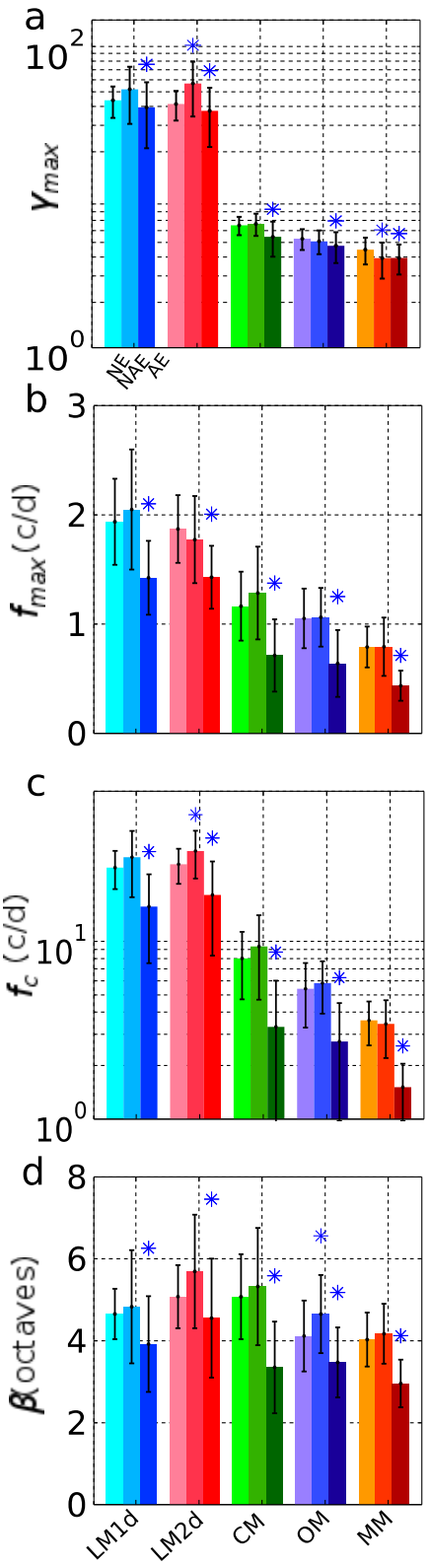
a
b
c
d
Y_{max}
f_{max} (c/d)
f_c (c/d)
β (octaves)
NE
NAE
AE
LM1d
LM2d
CM
OM
MM

Figure 4. Parameter comparison between normal eyes and the NAEs, and between normal eyes and AEs. Each group of three bars, from left to right, are parameter values for normal eyes (normative dataset), NAEs and AEs. For each parameter, bars and error bars represent mean and standard deviation over the 104 normal eyes, 28 NAEs and 28 AEs. a) maximum gain γ_{max}; b) peak frequency f_{max}; c) cutoff frequency f_c; d) bandwidth β. The asterisks indicate that the parameters are significantly different from the normative dataset (two-tail Wilcoxon rank sum test for the NAE and one-tail for the AE, $p < 0.05$), all the other comparisons are not significantly different. Note that the y-axis is on a log-scale in panels a) and c).

The comparison between the parameters of the qCSF model for the first and second-order data of the AE and NAE are shown in a scatter plot, subject-by-subject, in Figure 5. Each parameter of the AE for each subject is plotted against the corresponding parameter of the NAE for the same subject with the first-order conditions on the left and the second-order conditions on the right. From top to bottom, the parameters are the max gain, the peak frequency, the cutoff frequency and the bandwidth. The data are mostly above the identity line for almost all the parameters in all the conditions except that for the max gain parameter in the second-order conditions where the data are approximately equally distributed about the identity line. All the parameters were compared between the AE and the NAE using Wilcoxon Signed Rank one-tail test. Except for the gain in second-order orientation- and motion-modulation and the bandwidth in second-order contrast modulation, all the parameters in all conditions are significantly smaller in the AE than in the NAE ($p<0.05$). Hence compared with the NAE, the AE has significant deficits for first-order processing. For the second-order processing, we found that the AE also has significant deficits, manifested by lower peak frequency and cut off frequency as well as a narrower bandwidth for all three second-order conditions and lower gain for contrast-modulation compared to the NAE. In orientation-modulation and motion-modulation conditions, since the

peak gain (i.e. max gain) is not significantly reduced in the AE compared with the NAE, the deficit is restricted to higher modulation spatial frequencies.

This comparison confirms our observation about the sensitivity function as well as the parameter means, namely that compared to the NAE, the AE is defective in first-order processing at all spatial frequencies and in second-order processing at only high spatial frequencies.

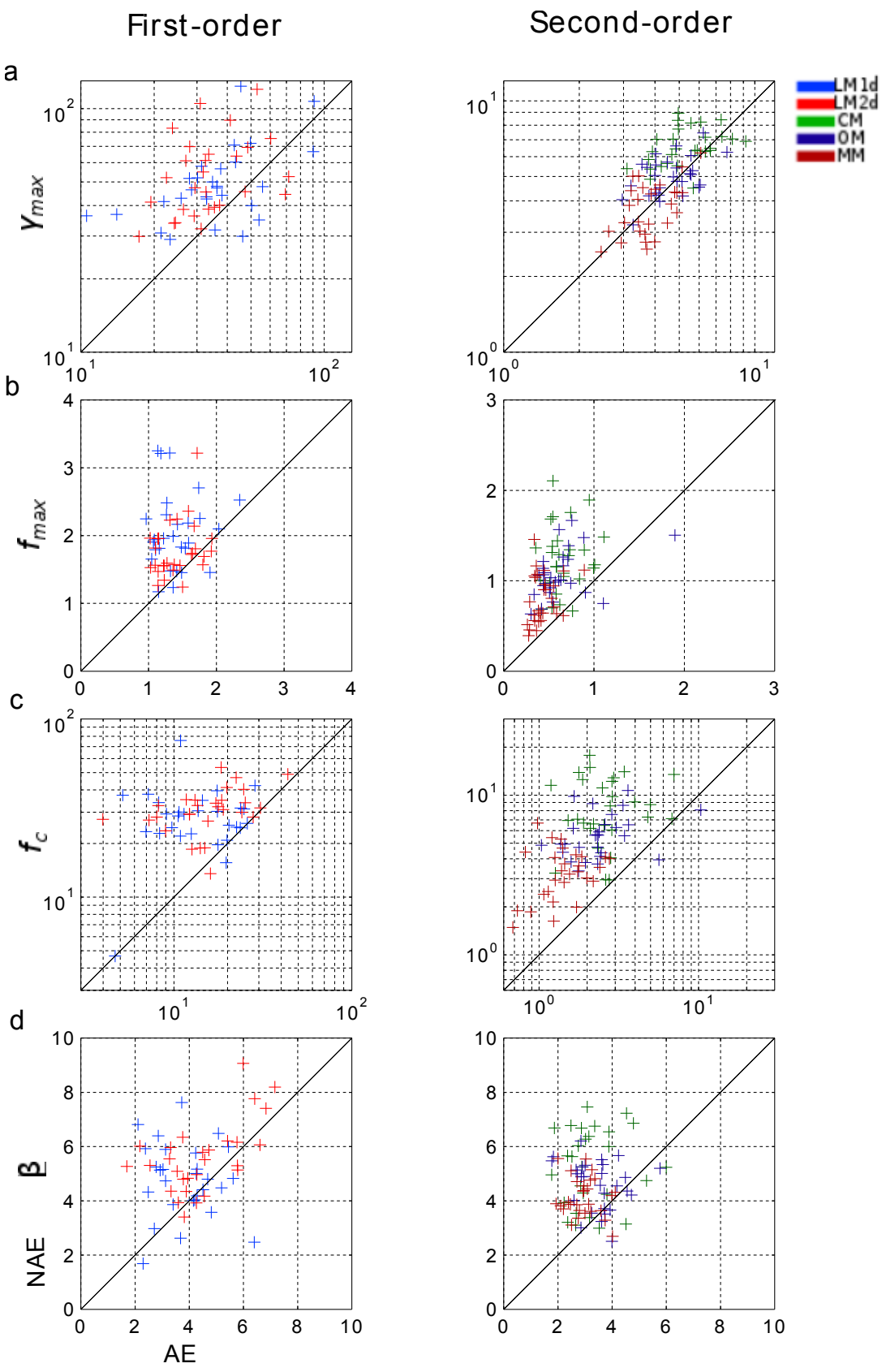
First-order
Second-order
a
b
c
d
Y_{max}
f_{max}
f_c
β
NAE
AE
LM 1d
LM 2d
CM
OM
MM

Figure 5. Individual parameter (qCSF) estimates for the NAE plotted against corresponding values for the AE for both first (left panels) and second order (right panels) conditions. a) maximum gain γ_{max}; b) peak frequency f_{max}; c) cutoff frequency f_c; d) bandwidth β. The color of the symbols refers to the type of stimulus used from the color code of figure 2. Data points above the identity lines indicate that the parameters are larger in the NAE than the AE.

In all the second order conditions except for contrast modulation, the carrier was set to be 10 times its first order threshold to ensure that loss of second order sensitivity was not the result of reduced first-order carrier visibility. This was not done for contrast modulation because we wanted to be able to use the whole contrast range for each spatial frequency, and so we set the mean contrast of the stimulus to 50%. Here we assess the impact of this decision by comparing AE and NAE functions for contrast modulated stimuli that have either a fixed mean contrast of 50% (non-normalized condition- termed CM) or a mean carrier contrast set at 5 times its own detection threshold (normalized condition- termed CMn).

To address the question about the comparison between normalized contrast-modulated second-order stimuli (CMn) and the non-normalized one (CM), firstly the sensitivity functions of each condition are shown in figure 6 separately for the AE and the NAE. From this figure we see that the sensitivity for the CM condition is better than that for the CMn condition only at mid-low spatial frequencies. Indeed, these two conditions don't show any differences at high-spatial frequencies because in this range the first-order contrast thresholds are high, and after normalization, the mean contrast in the CMn condition is close to 50%.

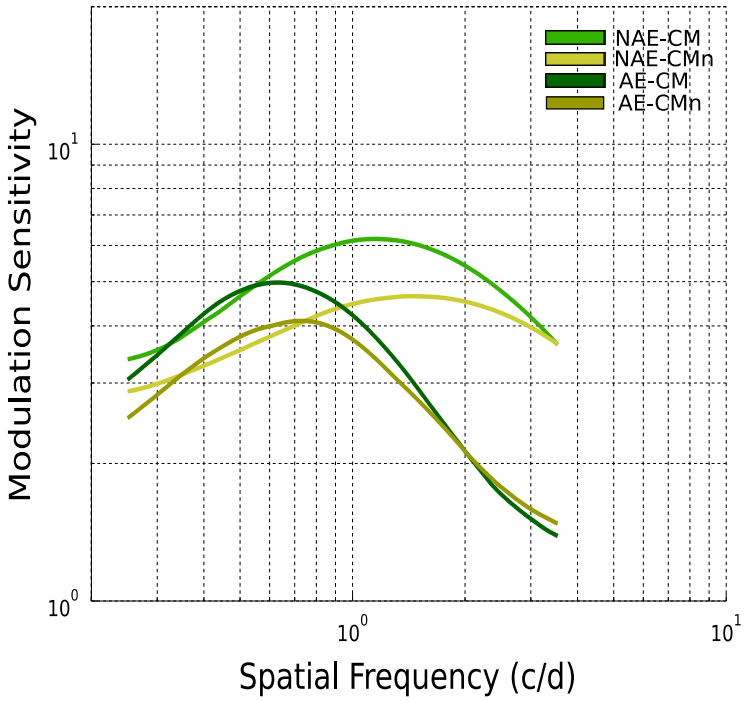

Figure 6. Averaged sensitivity functions comparing AE and NAE for two different contrast-modulated conditions: CM- contrast modulation and CMn- normalized contrast modulation. In the former the mean carrier contrast was fixed at 50% whereas in the latter, the mean contrast was always set to be 5 times its detectability.

In order to further compare the sensitivity functions for the CMn and the CM conditions, figure 7a shows a scatter plot of the sensitivity of CM against CMn over the full spatial frequency range for all the subjects for the NAE and the AE with linear regression. There are more data in the upper part of the quadrant for both eyes, indicating that sensitivity is higher for the CM than for CMn. However, there is no difference in this regard between the AE and the NAE.

In figure 7b the ratio between the sensitivity of CM and CMn for the NAE and the AE is shown over the full spatial frequency range for all the subjects. When the contrast is low, the

ratio for both AE and NAE is relatively high while when the mean contrast is close to 1 (that of the non-normalized condition) the ratio drops to 1. The change of the ratio for both eyes with contrast suggests that the mean contrast of the carrier plays a role in the detection of the contrast modulation. The dashed lines are two regressions of an inverse function with two parameters: the slope and the intercept. Using a bootstrap distribution for each parameter, a Student's t-test revealed these two fitted curves were not significantly different. Thus, there is no significant difference in the way that first-order information inputs into second-order processing in the AE and the NAE. We can conclude two things; first, the influence of using a normalized carrier contrast (i.e. set to a multiple of detection threshold as in the CMn condition) is mostly seen at low mean carrier contrasts corresponding to low-mid modulation frequencies (where sensitivity is best but where there is no difference between AE and NAE) rather than at high modulation frequencies where there is an AE deficit; second, this effect at low mean contrasts is equal for both AE and NAE and would not by itself contribute to additional second order sensitivity deficits. This suggests that the second-order deficits reported here for contrast-defined stimuli are not due to upstream deficits in contrast sensitivity affecting the visibility of the carrier.

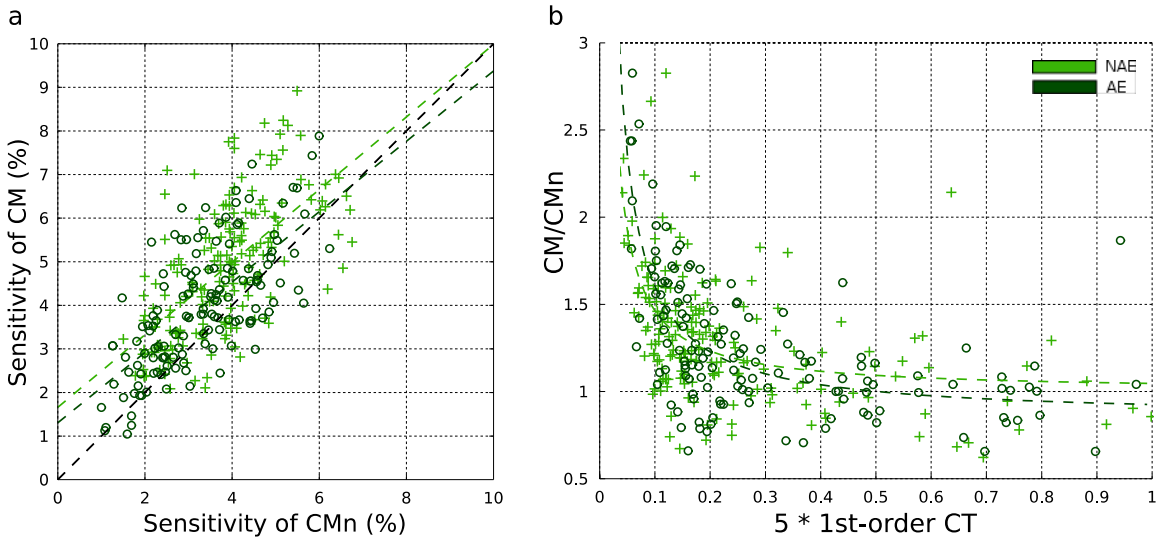

Figure 7. a) Scatter plot of the sensitivity of CM against CMn over the full spatial frequency range for all subjects for the NAEs (crosses) and the AEs (circles). The dashed lines are linear regression lines for each eye respectively; b) the ratio between the sensitivity of CM and CMn over the full spatial frequency range for all the subjects and for the NAEs and the AEs. The dashed lines are regression lines of an inverse function for each eye.

Discussion

In this study we compared both first and second order contrast sensitivity for the amblyopic and fellow non-amblyopic eyes of 28 amblyopes to the non-dominant and dominant eyes of 52 normal observers using an identical psychophysical approach, the qCSF, to address two question, namely;

1. How general is this deficit? For example, are only some types of second order processing affected in amblyopia or are all types of second order processing affected equally?

2.How lateral is this deficit? For example, is this deficit specific to amblyopic eye information or is information from the fixing eye equally affected?

We confirmed the first-order deficit and showed that the second-order deficit is of a general nature affecting the detection of spatial form defined by contrast, orientation and motion. The amblyopic eye exhibits a range of anomalies for these stimuli when compared with that of a normal observer. There is evidence from a case series that while a wide range of second-order functions is affected they may not be equally affected (Simmers et al., 2011). This suggests that the underlying deficit is extensive and possibly not uniform within the cortex because these

different spatial and temporal second-order stimuli optimally drive neurons in different specific regions of ventral and dorsal cortex respectively. Such a conclusion is in line with the available fMRI (Barnes, Hess, Dumoulin, Achtman, & Pike, 2001; Li, Dumoulin, Mansouri, & Hess, 2007) and psychophysical studies that have investigated this issue (Simmers et al., 2005; Simmers et al., 2003; Simmers et al., 2006). Although second-order function can be associated with extra-striate cortex, it is presently unclear the extent of striate (Larsson, Landy, & Heeger, 2006;Hallum, Landy, & Heeger, 2011; Zhou & Baker, 1993, 1994) or indeed pre-striate (Rosenberg, Husson, Mallik, & Issa, 2008; Rosenberg & Issa, 2009) involvement. This uncertainly makes it difficult to go from psychophysical deficit to cortical locus.

An important issue is whether the deficit for the detection of first-order stimuli could be responsible in whole or part for the second order deficit. We set out to use first order stimuli that could serve as carriers for the second order modulation to specifically address this issue. This allowed us to measure the detectability of the carriers so that we could set the carriers at 10 times their detection threshold to ensure that carrier visibility was not the explanation for any observed reduction in second-order sensitivity for the amblyopic eye. We did this for motion and orientation defined. To examine whether carrier visibility played a role in the measured amblyopic deficit for contrast defined form, we compared measurements with a fixed 50% mean contrast (CM) with those for mean contrast set to 5 times their detection threshold (CMn). This comparison shows that the fixed 50% contrast carrier resulted in better modulation sensitivity but only at low modulation spatial frequencies where sensitivity is best but where the different between fixing and normal eyes is least. Additionally, these effects were similar for both fixing and amblyopic eyes. Taken together this strongly suggests that even for the contrast-defined

form stimuli, the visibility of the carrier played little or no role in the measured modulation deficits. This suggests that the deficits reported here are extra-striate in nature.

It has been reported that the fixing eye of amblyopes exhibits a deficit for the detection of second-order stimuli (Giaschi et al., 1992; Ho et al., 2005; Husk et al., 2012; Husk & Hess, 2013; Wong et al., 2001) although the evidence is mainly confined to motion-defined form stimulation (Giaschi et al., 1992; Ho et al., 2005; Husk et al., 2012). We asked how general is this deficit for different types of second-order processing and is it comparable to that exhibited for amblyopic eye stimulation. Our results suggest that there is no general second order deficit for fellow non-amblyopic eye stimulation, our normative database of 104 eyes (Reynaud et al., 2014) provides a firm foundation from which to assert this. However, we did find a significant difference in the qCSF gain parameter between the NAE and the eyes of normal subjects for the motion defined second order stimulus which could indicate a selective motion second-order deficit in the NAE along the lines of that suggested by (Aaen-Stockdale & Hess, 2008). The sparing of the NAE for second order functions (excepting motion-modulation) could be explained by a shift of ocular dominance in regions of the extra-striate (Schroder et al., 2002; Sireteanu et al., 1993)comparable to that previously reported in the striate cortex (Wiesel & Hubel, 1965).

An unexpected finding was that second-order sensitivity at low spatial frequency was better in the AE compared to the NAE. First-order low spatial frequency sensitivity can, in some cases, be better for the amblyopic compared with the fixing eye (Hess and Howell, 1977). This is thought to be due to the added temporal stimulation due to unsteady eye-movements which enhance selectively sensitivity at low spatial frequencies (Robson, 1966). However, since we did not observe such an effect for our first order stimuli, there must be an alternate explanation for the second-order enhancement. One possibility is that, as the spatial frequency is lowered and the

number of cycles reduced, the effect is due more to the reduced cycles than it is to the spatial frequency per se. If this was so then it would suggest anomalous spatial summation for second-order stimuli by the amblyopic eye at low modulation frequencies (<1c/d). Spatial summation for second order stimuli has been found to be normal at 1c/d (E. H. Wong & Levi, 2005) but it is yet to be investigated below 1c/d.

Acknowledgements

This work was supported by National Natural Science Foundation of China grants (NSFC 31300913) to YT, (NSFC 81300796) to L-XF and (NSFC 81261120562) to YZ and a Natural Sciences and Engineering Research Council of Canada grant (NSERC #46528) to RFH.

Manuscript 4: The amblyopic deficit in second-order modulation processing: the role of response nonlinearity for contrast and motion

Yi Gao, Alex S. Baldwin, Yong Tang, Yifeng Zhou, Robert F. Hess

Abstract

Amblyopia is a neural developmental disorder of visual system that influences a wide range of functions. It is caused by a deficient input from one eye during development, resulting in changes to

neural development that permanently impair the use of that eye. Further changes in amblyopia have been found that also affect the processing of input from the non-amblyopic eye. These effects have been established in high-level motion-associated tasks, including second-order motion modulation. Here, we investigate whether the deficit found for motion-modulation compared to contrast-modulation can be attributed to differences in the response nonlinearity. The pedestal masking paradigm was used to measure the shape of the response nonlinearity. Data were fitted with a model that combines divisive gain-control with a decision stage based on signal detection theory. Model-fits revealed that nonlinearities did not differ between the two eyes of amblyopes. However, comparing amblyopic against normal observers reveals a difference in the nonlinearity for motion modulation only. This dissociation between the results found for processing second-order MM and CM indicates, first, they are processed separately; second, in amblyopia, the dorsal and ventral pathways may be affected to different degrees.

Introduction

Amblyopia is a developmental disorder of vision that arises from disrupted visual input to one eye early in life. It is classically defined as a loss of visual acuity in the disrupted eye without an organic ocular disorder. Amblyopia has been reported to affect a wide range of visual functions of the amblyopic eye from low-level contrast sensitivity to higher-level functions such as second-order vision, stereovision and global integration, see recent reviews (Bretas & Soriano, 2016; Hamm et al., 2014; Joly & Franko, 2014; Levi, 2013; Meier & Giaschi, 2017). Interestingly, for higher order visual functions, the deficit is not confined to the amblyopic eye. Studies testing the perception of stimuli shown to the fellow eye of amblyopes have also found deficits compared to normal vision (Meier & Giaschi, 2017).

Many of the deficits found to affect both eyes are related to higher-level motion processing. A global motion deficit in the fellow eye has been reported to approach the strength of the deficit in the amblyopic eye (Aaen-Stockdale & Hess, 2008; Aaen-Stockdale et al., 2007; C. Hou et al., 2008; Kiorpes

et al., 2006; Simmers et al., 2003). The fellow eye deficit exists for different types of global motion including translational, rotational and radial (Simmers et al., 2006a). The deficits for various kinds of global motion patterns in both eyes of amblyopic vision suggest a general deficit in the dorsal pathway of the extra-striate cortex. Deficits affecting both eyes have also been found for second-order motion-modulation detection (Gao et al., 2014). Motion modulation sensitivity was reduced in both the amblyopic and fellow eye compared to normal observers. For contrast- or orientation-modulation only the amblyopic eye showed reduced sensitivity. Fellow eye deficits have also been shown with second-order motion stimuli constructed with modulations of contrast, flicker or texture (Simmers et al., 2011). Motion-defined form perception (sometimes referred to as form-from-motion), which also involves processing second-order motion-modulated boundaries and shapes, has been reported to show fellow eye deficits, especially in children (D. Giaschi et al., 2015; Hayward et al., 2011; J. Wang et al., 2007). The presence of deficits in both eyes has also been reported for a structure-from-motion task (Husk et al., 2012).

According to the parallel processing hypothesis (Goodale & Milner, 1992; Haxby et al., 1991; Van Essen & Gallant, 1994), the extra-striate cortex is organized into two processing streams-the "dorsal" or "action" pathway and the "ventral" or "form" pathway. The dorsal pathway is specialized for processing location and motion of objects while the ventral pathway is specialized for processing form and pattern. The fellow eye deficit found in second-order motion-modulation processing (Gao et al., 2014) is consistent with the results from neurophysiology and imaging studies that the dorsal and ventral pathways of the extra-striate cortex are affected differently. Ocular dominance in the extra-striate cortex of strabismic cats has been shown to be more biased towards the fellow eye in the ventral pathway than the dorsal pathway (Schroder et al., 2002). A deficient (El-Shamayleh et al., 2010; Secen et al., 2011) but more balanced dorsal pathway is consistent with the behavioral finding that motion-related functions are binocularly affected.

In the current study, we investigate the amblyopic deficit for second-order motion-modulation (MM) processing by examining its associated processing nonlinearity. We compare this with the

nonlinearity for second-order contrast-modulation (CM) processing. In our previous study (Gao, Baldwin, & Hess, in preperation), we found different second-order nonlinear response functions for MM and CM processing in normal vision. This suggests a separate mechanism for processing MM compared with other types of second-order modulations (Gao et al., in review), consistent with previous studies which have argued against a cue-invariant mechanism for processing forms and boundaries defined by different types of modulations (Larsson et al., 2010; Larsson et al., 2006; Marcar & Cowey, 1992; Morita et al., 2003). Since MM and CM go through different nonlinearities in normal vision, and the dorsal pathway may be particularly affected by amblyopia (Schroder et al., 2002), we set out to discover whether amblyopia affects the nonlinearities associated with MM and CM. A further question is if so, whether they are affected in the same way.

We employed the pedestal-masking paradigm to study the nonlinearity involved in the detection of MM and CM. This paradigm has been widely used to investigate the nonlinearities in normal vision for both first-order (C. C. Chen & Tyler, 2008; Foley, 1994) and second-order processing (Gao et al., in review; Huang & Chen, 2014; F. A. Kingdom et al., 2003; Landy & Oruc, 2002; Schofield & Georgeson, 1999). It is usually done in a two-interval forced choice task in which observers discriminate between a null interval containing a "pedestal" mask modulation alone, and a test interval containing that pedestal mask with an increment target modulation added to it. Plotting increment threshold against mask level gives the pedestal masking function. If the response to modulation is a nonlinear function of the gain-control format, the pedestal masking function will have a dipper shape. This is typically found by studies employing this paradigm. In the pedestal masking function, there is a facilitative dip, where the increment threshold first decreases at low pedestal mask levels. This reflects the accelerating region of the nonlinear response function. Higher mask levels map onto the inhibitory part of the function, where increment thresholds increase again as the mask level increases (see Figure 1 for an example). This masking effect reflects the saturating region of the response function.

Our model involves a nonlinear response function of the divisive gain-control form (Foley, 1994; N. Graham & Sutter, 2000; Huang & Chen, 2014), and its outputs are considered in the context of signal

detection theory (D. M. Green, Swets, J. A., 1988; Gregory & Cane, 1955). The nonlinear response function is described as

$$f(c)=\frac{c^p}{c^q+z}, \tag{1}$$

where *c* is the modulation depth, *p* and *q* are exponents controlling the shapes of the accelerating and saturating regions of the response function, and z represents general inhibition from divisive gain control process. Under signal detection theory, discriminations of different modulation depths are made against internal noise from various sources in the brain (Faisal et al., 2008). Here we assume additive noise, where samples in each interval are drawn from a Gaussian distribution with zero mean and constant standard deviation σ. According to signal detection theory, the signal-to-noise ratio (d') is

$$d'=\frac{f\left(t+m\right)-f\left(m\right)}{\sigma}, \tag{2}$$

where *m* is the modulation depth of the mask, *t* is the increment target added in the test interval. The percent correct at a threshold level, *d'*=1, is $\Phi\left(\frac{d'}{\sqrt{2}}\right)=76.02\%$.

We measure the increment thresholds at a wide range of pedestal mask levels for MM and for CM. The data are fitted by the nonlinear model to obtain the values of four parameters for each eye of amblyopes in each condition. Features of the pedestal masking functions and the fitted parameters are compared between the amblyopic eye and the fellow eye of the amblyopic observers. The comparison is also made between each eye of the amblyopic observers and normal observers that were tested in a previous study (Gao et al., in preperation). The effects of amblyopia on second-order nonlinearity for MM and CM as well as its implication on normal second-order processing mechanisms are discussed.

Method

Apparatus

The stimuli were generated by a computer running Windows 7 and presented by a Multiscan G220 monitor (32 × 24 cm, refresh rate: 60 Hz, resolution 1024 × 768, mean luminance: 60 cd/m^2). The viewing distance is 86 cm to have a pixel per degree of 48. The experiment and data analysis softwares were written in Matlab (Mathworks) using functions from the Psychophysics Toolbox (Brainard, 1997). The Palamedes toolbox 2 (N. K. Prins, F. A. A. , 2009) was used to fit the psychometric functions.

Participants

All six anisometropic amblyopic observers were graduate students in University of Science and Technology of China at the time of testing (October 2015). Their age ranges from 22 to 25. None of them has been treated with any treatments for amblyopia. All six observers were naïve to the purpose of the current experiment. The clinical information about the six amblyopic observers are shown in Table 1. All procedures were conducted in accordance with the Declaration of Helsinki, and approved by the Ethics Review Board of the Montreal Neurological Institute.

Subject	Gender	Age	Visual Acuity (corrected)		Refractive Error	
			Left eye	Right eye	Left eye	Right eye
WLJ	M	23	0.8	1.0	+2.00DS /+0.50DC*135	-5.75DS
YLG	M	24	1.2	0.4	-0.75DS/-0.50DC*175	+1.00DS/+1.00DC*85
LS	M	23	0.3	1.0	+4.50DS/0.50DC*35	-1.50DS/-0.50DC*30

ShW	M	24	1.0	0.12	Plano	+4.00DS/+1.00DC*85
JS	M	26	0.5	1.0	-1.00DS/+3.50DC*85	-2.00DS/-1.00DC*10
ShL	M	24	0.5	1.0	+2.50DS/0.50DC*90	-0.50DS

Table 1. The clinical details of six amblyopic observers. They are all of anisometropic type.

Stimuli

The two second-order stimuli, CM and MM, are both constructed by multiplying an envelope *G(x,y)*, which is a low-spatial-frequency sinusoidal grating, to a carrier *C(x,y),* which is a high-spatial-frequency sinusoidal grating. The envelope and the carrier are defined as $C(x, y, t) = \sin(2\pi(f_c x + \omega t))$, and $G\left(x,y\right)=\sin\left(2\pi f_e x\right)$, respectively, where f_e and f_c are spatial frequencies of the envelope and the carrier.

The CM stimulus is constructed by modulating the contrast of one moving carrier tilting 45° clockwise by one horizontal envelope. In the null interval, the stimulus containing only the pedestal mask can be described by

$$N\left(x,y\right)=C\left(x,y\right)\left[c+c\times mG\left(x,y\right)\right]\omega\left(x,y\right), \tag{3}$$

where c is the carrier contrast, m is the modulation depth of the pedestal mask, and $\omega(x, y)$ is an raised cosine window with a blur width of 0.5º to soften the edge of the stimulus. In the target interval, the stimulus containing both the pedestal mask and the target is described by

$$T\left(x,y\right)=C\left(x,y\right)\left[c+c\times\left(m+t\right)G\left(x,y\right)\right]\omega\left(x,y\right), \tag{4}$$

where t is the modulation depth of the target grating, the other letters have the same meaning as in Equation 3.

To construct an MM stimulus, we add two CM patterns of which the directions of moving carrier gratings are opposite (45º and -45º) and the phases of the envelopes are also opposite. The MM stimuli in the null interval and the test interval can be described as

$$MM(x,y)=\left\{C_1(x,y)\left[c+c\times mG_1(x,y)\right]+C_2(x,y)\left[c+c\times mG_2(x,y)\right]\right\}\omega(x,y), \quad (5)$$

and

$$MM(x,y)=\left\{C_1(x,y)\left[c+c\times(m+t)G_1(x,y)\right]+C_2(x,y)\left[c+c\times(m+t)G_2(x,y)\right]\right\}\omega(x,y). \quad (6)$$

Figure 1 illustrates the construction of two CM stimuli and a MM stimulus. Among the two CM stimuli shown in Figure 1, only CM1 is actually used in the current experiment. For both CM and MM stimuli, the carriers drift at 2 Hz. The spatial frequency of all carriers is 4 cpd and the spatial frequency of all envelopes is 0.5 cycles per degree. The contrast of carrier is kept constant at 0.48 for the amblyopic eye (AE) of all amblyopic observers. The carrier contrast for the fellow eye (FE) is calculated for each observer in order to keep the ratio of the carrier contrast to the first-order motion direction discrimination threshold same between the AE and the FE. The first-order motion direction discrimination threshold is measured monocularly with the qcsf2d test in our former study (Gao et al., 2014).

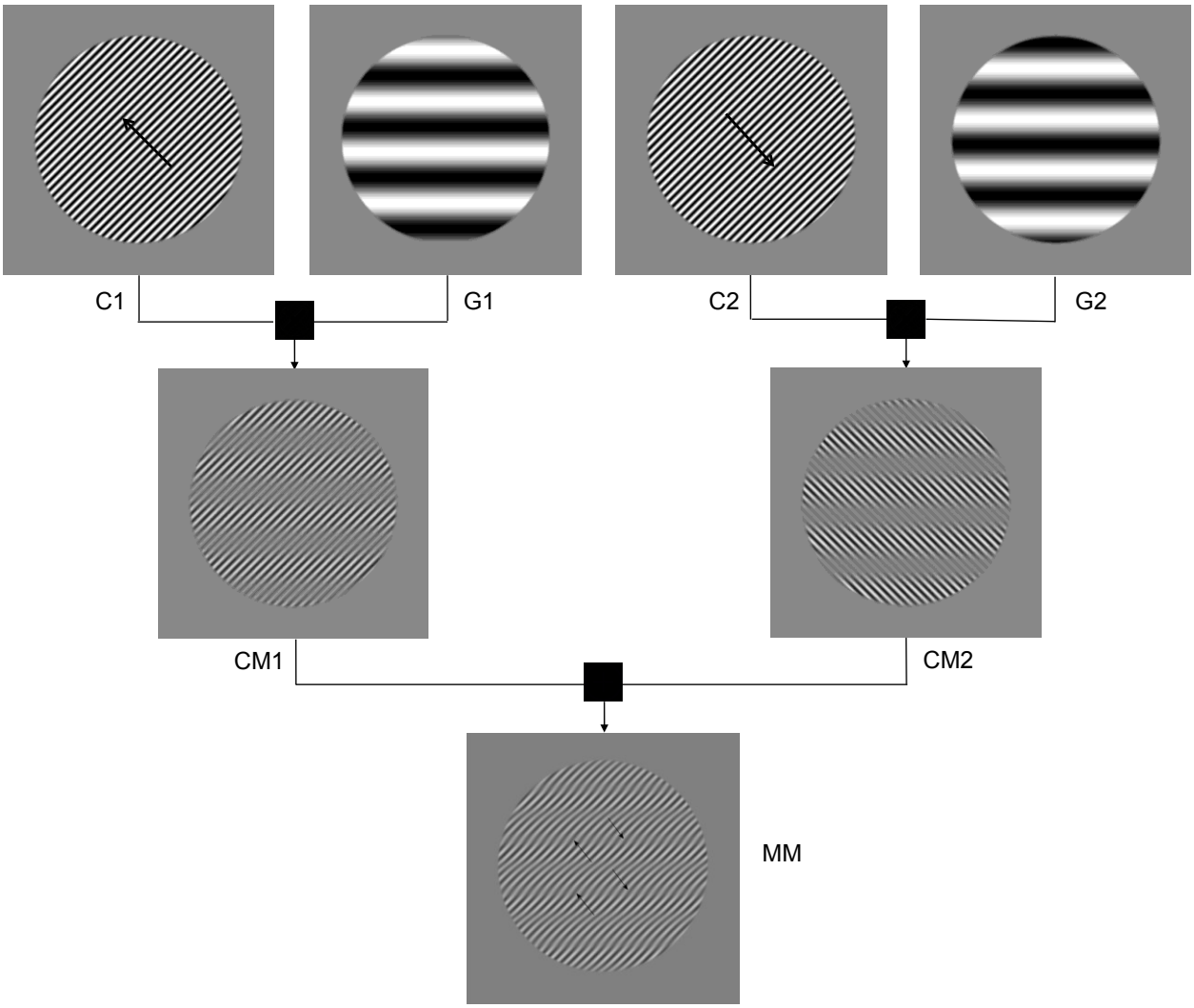

Figure 1. The process of constructing a MM stimulus from adding two CMs with moving carriers of opposite directions (C1 and C2) and envelopes of opposite phases (G1 and G2). CM1 is the CM stimulus that was actually used in the current study. Same as CM2, the CM stimulus is constructed by multiplying a moving carrier grating of high spatial frequency with a static envelope grating of low spatial frequency.

Procedure

We conducted the experiment in blocks of pedestal mask levels with two repetitions for each level. The pedestal levels were adjusted for each observer to give an informative sampling of the masking

function. First, the detection threshold *T* was measured. Then the other seven pedestal mask levels were determined as (*T-12*), (*T-6*), (*T-3*), (*T+3*), (*T+6*) and (*T+12*) *dB*. The unit *dB* is $20\log_{10} c$, where *c* represents the modulation depth. At each pedestal level, a psychometric function was measured with two interleaving staircases and a threshold was obtained by fitting the psychometric function. One staircase was one-up-three-down and the other one was one-up-two-down, both terminated after 60 trials. Therefore, there were 1920 trials in each of the two conditions-CM and MM. The two conditions were measured alternately and the sequence of the two was balanced among observers.

A two-interval forced-choice (2IFC) task was used to measure the increment threshold. The task was to identify which interval is the target interval that contains greater modulation. During each trial, the target and null intervals were presented, each for 500 ms, in a random order with a 400 ms inter-stimulus interval between them. An auditory tone was given at the onset of each interval to reduce temporal uncertainty. The observer responded with a button press on a keypad. Auditory feedback was provided to inform the correctness of each decision. After the auditory feedback, there is an inter-trial-interval of 1000 ms before the onset of next trial.

Results

Pedestal masking functions

The pedestal masking functions for both CM (in blue) and MM (in red) are shown in Figure 2. In each panel the increment thresholds are plotted as dots against pedestal mask level for each of the six observers. The filled dots represent thresholds of the amblyopic eye (AE) and the empty dots represent those of the fellow fixing eye (FE). The increment thresholds were obtained by fitting a Quick psychometric function to the data for each mask level and calculating the stimulus levels corresponding to

76.02% correct. The left-most point in each panel is the detection threshold obtained without a pedestal mask. Both threshold and pedestal mask levels are in dB log units which is calculated as $20 \times log_{10}(m)$.

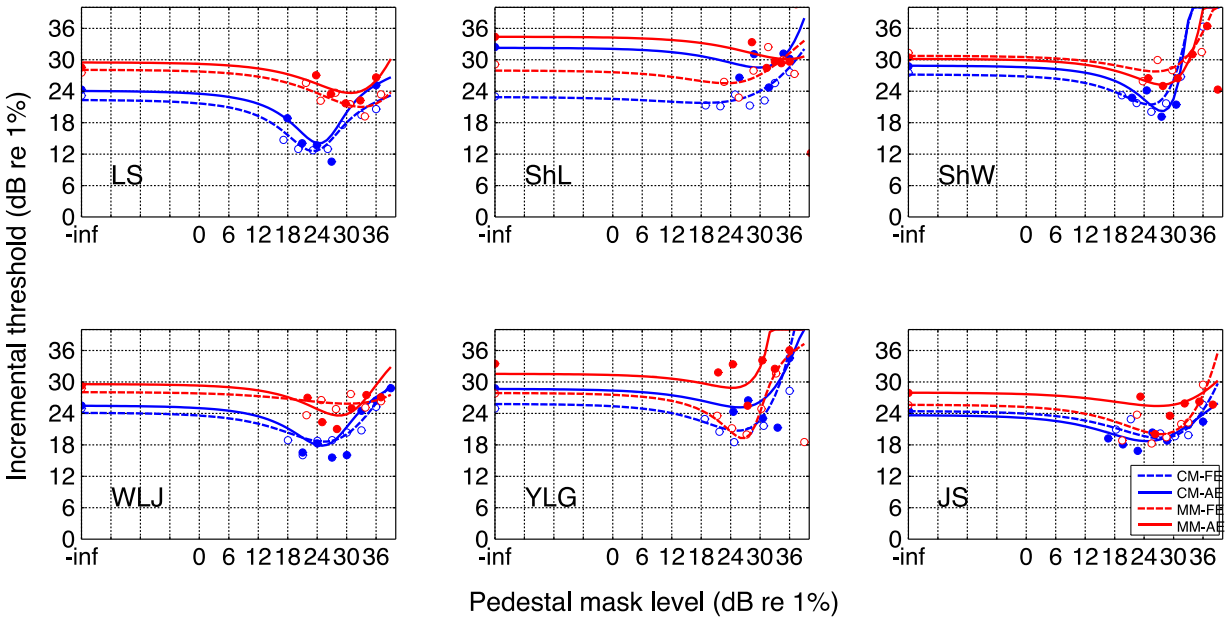

Figure 2. Pedestal masking functions for six amblyopic observers. Dots- blue for CM and red for MM- show increment thresholds obtained by fitting a psychometric function at each pedestal mask level. Curves represent the threshold prediction from fitting our model of nonlinear response function combined with signal detection theory to data as a whole across all mask levels (see *Data analysis* in *Methods* section). Filled dots and solid curves are for the amblyopic eye (AE); Empty dots and dashed curves are for the fellow-fixing eye (FE).

The pedestal masking functions in Figure 2 generally show the typical dipper shape. The greatest facilitation, i.e., smallest increment threshold, occurs around where the mask level is equal to the detection threshold. We calculated the mean dip magnitude for each condition and for the amblyopic eye and the fellow eye respectively (Table 2). The depth of the dip is computed as a difference between the detection threshold and the smallest value among the increment thresholds at the third, the fourth and the fifth mask levels which are (T-3), T and (T+3) dB. T refers to the corresponding detection threshold at

zero mask level. A two-way ANOVA test was conducted to compare the dip depth between eyes and conditions. There is a main effect for conditions ($p = 0.037$), no main effect for eyes ($p = 0.16$) and no interaction ($p = 0.89$). Combined with the values in Table 2, this result indicates that the dip depth is larger for CM than MM in both eyes of amblyopes.

(dB)	FE	AE
CM	6.82 +/- 2.95	9.38 +/- 2.37
MM	5.18 +/- 1.81	7.06 +/- 1.18

Table 2. The depths of dips for the FE and the AE in each of the two conditions-CM and MM are shown as means with standard deviations across six observers.

There are some abnormalities in the shapes of the pedestal masking functions we found. The fellow eye of observer ShL does not show a facilitative dip. Furthermore, at the higher pedestal mask levels, half of the tested eyes do not show greatly increased thresholds compared to the corresponding detection threshold for both CM and MM. This lack of a masking "handle" to the dipper functions is probably due to mask levels not being high enough to show the inhibitory effect. This is consistent with a previous study (Huang & Chen, 2014). Another phenomenon worth noting is that there is a drop in threshold at the highest mask level for MM in three eyes (2 amblyopic eyes and 1 fellow eye). This is probably due to the fact that there is a ceiling effect for the test increment at the highest mask level. As a result, the psychometric function fit is poor and these three increment thresholds are not precisely determined. However, because the raw data for these trials are valid, they still contribute to the maximum likelihood fitting of our model. This will be discussed in the *Model fitting* section.

Model fitting

Our model was fitted using the raw data from each eye. This was done for each observer under each of the two conditions CM and MM. The model was fit using the maximum-likelihood method. The fitting optimized the values of four parameters: the internal noise σ, nonlinear exponents p and q, and the gain-control parameter z. The pedestal masking functions predicted by the fitted parameter values in each condition for each observer are plotted as the solid (amblyopic eye) and dashed (fellow eye) curves in Figure 2, superposed on the increment threshold plot. We calculated the deviance of model fitting which is expressed as

$$D = -2 \times \left(LL_{fit} - LL_{sat}\right), \tag{7}$$

where D denotes deviance, LL_{fit} represents log-likelihood value from fitting the model to the data with maximum likelihood method and LL_{sat} represents log-likelihood from the saturated model. The average values of deviance for each condition and each eye across the six amblyopic observers are reported in Table 3. Although the absolute value of deviance is not very informative in terms of the quality of fitting, it provides good basis for comparing the current model with other models built by peer researchers.

	AE	FE
CM	96.33 +/- 18.55	54.96 +/- 10.37
MM	73.37 +/- 15.20	65.14 +/- 24.21

Table 3. Mean and standard deviation of deviance for model fitting across the six amblyopic observers in each condition and each eye.

The mean values of the four parameters across six observers are shown in Table 4. The internal noise σ and the gain-control parameter z are in dB log units which is calculated as *20 x log10(c)*. To compare the parameters between the amblyopic eye and the fellow eye, as well as those between the two second-order conditions, we performed a two-way ANOVA test for each parameter. For all four parameters, there is no significant main effect or interaction for any parameter. The insignificant

comparison between the amblyopic eyes and the fellow eyes indicates that in terms of second-order nonlinearity the two eyes of amblyopic visual system do not differ from each other.

	AE				FE			
	σ (dB)	p	q	Z (dB)	σ (dB)	p	q	Z (dB)
CM	-5.7 +/ -3.1	2.42 +/- 0.36	2.13 +/- 0.33	61.9 +/- 7.4	-1.6 +/- 2.7	3.12 +/- 0.44	2.80 +/- 0.42	82.0 +/- 11.0
MM	-9.0 +/- 4.8	2.28 +/- 0.51	2.09 +/- 0.47	70 +/- 11	-5.0 +/- 2.2	2.32 +/- 0.21	2.12 +/- 0.21	72.7 +/- 5.1

Table 4. The mean values (across each group of observers) with standard error of four parameters from fitting the best model to the data of CM and MM together, for Experiment 1 and Experiment 2 separately.

The parameter values for each eye and for each condition are also plotted in Figure 3 against the mean values (grey) from eight normal observers in our previous study (Gao et al., in preperation). We compared each parameter of the amblyopic eyes and the fellow eyes to that of the normal eyes (NE) under each condition using a Wilcoxon rank sum test (Table 5). The stars in Figure 3 represent significant differences from the normal eye under the indicated condition. For the nonlinear exponents p and q, in CM there is no significant difference between the normal eye and either the amblyopic eye or the fellow eye. Therefore, the amblyopic deficit in the amblyopic eye for CM does not significantly affect the shape of the nonlinear response function. Whereas in MM, both exponents show significant differences between the amblyopic eye and the normal eye, as well as between the fellow eye and the normal eye. The effect sizes are shown in Table 6. The deficit for MM that was found in both the AE and the FE (Gao et al., 2014) is reflected in smaller exponents. This changes the shape of the nonlinear response function for MM in the amblyopic visual system. For the internal noise, surprisingly we do not find larger values in the amblyopic eye than the fellow eye, or larger values in the two amblyopic eyes than the normal eyes. For the gain control parameter *z*, the amblyopic eye shows a larger value than the normal eye in the CM condition.

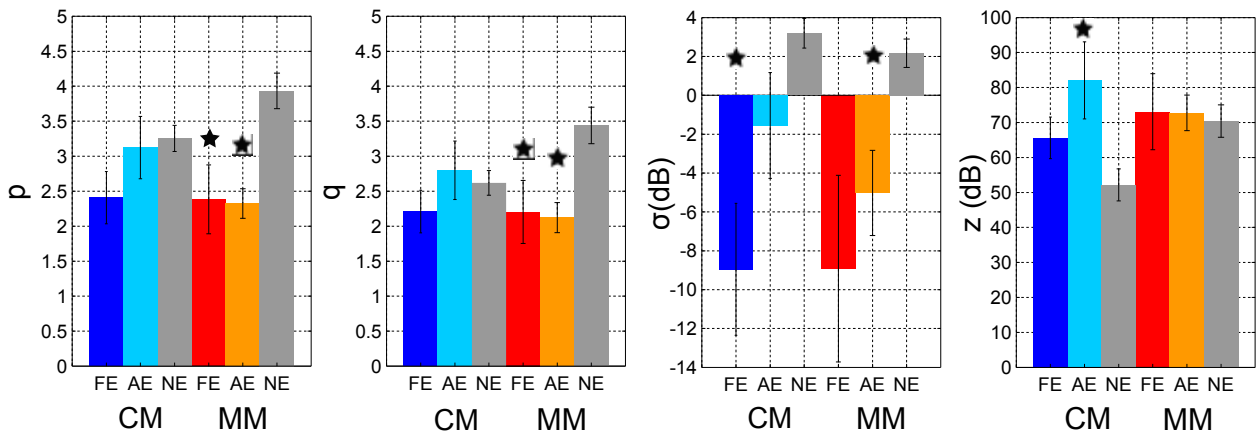

Figure 3. The mean of four fitted parameters from each of the two eyes of the amblyopic observers under two conditions. Darker colors are for the fellow eye (FE) and lighter colors are for the amblyopic eye (AE). Bluish colors represent CM and reddish colors represent MM. The fitted parameters of normal eyes (NE) from our previous study under same conditions (Gao et al., in preperation) are also plotted as grey bars. The stars indicate significant difference in the comparison between one eye of the amblyopic vision and the normal eyes.

Eye	AE				FE			
Param.	σ	p	q	Z	σ	p	q	Z
CM	0.02	0.06	0.28	0.49	0.18	0.75	0.85	0.03
MM	0.14	0.03	0.03	0.57	0.02	<0.01	<0.01	0.34

Table 5. The p values of Wilcoxon rank sum test done between the amblyopic eye (AE) and the normal eyes (NE), as well as between the fellow eye (FE) and the normal eye (NE) for each parameter in each condition. The data of the NE is from our previous study (Gao et al., in review).

Eye	AE				FE			
Param.	σ	p	q	Z	σ	p	q	Z
CM	2.16	1.18	0.67	0.98	1.0	0.16	0.23	1.49
MM	1.43	1.63	1.36	0.13	1.89	2.51	2.0	0.18

Table 6. The effect sizes of comparing each of the four parameters between each eye of the amblyopes with the normal eyes in each condition.

Using the mean parameters from Table 4, we reconstructed the pedestal masking functions for CM (left panel) and MM (right panel) in the AE (solid curve) and the FE (dashed curve) in Figure 4. The pedestal masking functions for the NE for CM and MM are also reconstructed from the data in our previous study and plotted as dashed grey curves in Figure 4. Compared to the NE, both of the AE and the FE show poorer performance at almost all mask levels in both second-order conditions-CM and MM. And consistent with the analysis of parameters, the pedestal masking functions of the AE and the FE are similar in both conditions.

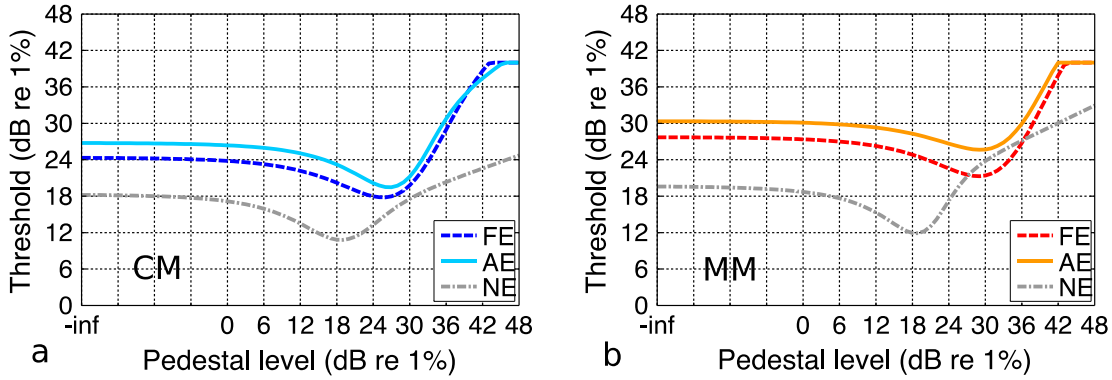

Figure 4. Pedestal masking functions of CM (a) and MM (b) constructed with mean parameters from best model fit in CM and MM, respectively. The grey dashed curve in each panel is the pedestal masking function of normal vision in each condition. Data from our previous study (Gao et al., in preperation) are replotted here as well.

Discussion

This study is the first to present the dipper functions from pedestal masking experiments for second-order contrast- and motion-modulations processing in amblyopic vision. The dipper shape exists not only in the FE but also in the AE of amblyopes. This dipper shape has been found in normal vision for first-order processing (Foley, 1994; Legge & Foley, 1980), as well as for second-order processing, including contrast-modulation (N. Graham & Sutter, 2000; Huang & Chen, 2014; Schofield & Georgeson, 1999), orientation modulation (Gao et al., in review; F. A. Kingdom et al., 2003; Landy & Oruc, 2002) and motion modulation (Gao et al., in preperation). It was also found for first-order contrast discrimination task in amblyopic vision (Bradley & Ohzawa, 1986). A nonlinearity in the form of divisive inhibition (Foley, 1994; Foley & Chen, 1999; Huang & Chen, 2014) describes these functions. This suggests that a divisive inhibitory nonlinearity is involved in amblyopic second-order processing, similar to that of normal vision.

The answers to the two questions proposed in the Introduction session are: first, amblyopia does affect the nonlinearity of second-order modulation processing; second, amblyopia affects CM and MM nonlinearity differently—only the shape of nonlinear transducer function for MM was significantly affected. The change in the shape of the nonlinearity gives smaller p and q values in the nonlinear transducer function for MM in amblyopes. The fact that only MM, not CM, was affected by amblyopia has two implications: first, the mechanisms behind the nonlinearities of MM and CM must be at least partially separate in normal vision; second, the dorsal and ventral pathways may be affected to different degrees in amblyopia.

The first conclusion is consistent with our previous finding of different shapes of second-order nonlinear transducer functions for MM and CM in normal vision (Gao et al., in review). The processing of both MM and CM involves an essential step of detecting the boundaries formed by second-order modulations. A different nonlinear transducer function for MM from CM argues against the classic view of cue-invariant boundary processing (Berkley et al., 1994; Hawley & Keeble, 2006; Leventhal et al.,

1998; Sary et al., 1995; Schofield & Yates, 2005). In the literature, there are some results supporting this idea that motion-defined boundaries are processed by a different mechanism than that used to process other kinds of boundaries. Morita and colleagues found that performance was poorer at detecting boundaries defined by combined motion and luminance variations or motion and color variations compared to single attribute-defined boundaries (Morita et al., 2003). Two fMRI studies (Larsson et al., 2010; Larsson et al., 2006) showed that orientation adaptation to different types of second-order modulation-defined boundaries is elicited in different cortical visual areas with some overlap. For motion-defined boundary, the areas include V3A/B, LO1 (lateral occipital), LO2 and V7; while for contrast-modulation and orientation-modulation, the areas are V1, V2, V3, V3A/B, LO1, hV4 and VO1. One lesion study found that removal of MT affect processing of kinetic boundaries but not luminance-defined boundaries (Marcar & Cowey, 1992).

The second conclusion that the dorsal and ventral pathways of the extra-striate cortex may be affected differently by amblyopia is consistent with two different reports in the literature. First, ocular dominance in extra-striate cortex of strabismic cats is more biased towards the FE in the ventral pathway (Schroder, Fries et al., 2002) resulting in deficits for functions processed along the ventral pathway to be more monocular. Second, the more binocularly affected dorsal pathway (Schroder, Fries et al, 2002) explains why the behavioral findings for motion-related high-level functions are binocularly affected by amblyopia, for example global motion (Aaen-Stockdale & Hess, 2008; Aaen-Stockdale et al., 2007; C. Hou et al., 2008; Kiorpes et al., 2006; Simmers et al., 2003; Simmers et al., 2006a), form-from-motion (D. Giaschi et al., 2015; Hayward et al., 2011; J. Wang et al., 2007) and second-order motion (Gao et al., 2014; Simmers et al., 2011); while deficits for global form (Dallala et al., 2010; Hess et al., 1999; M. R. Joshi et al., 2016; Levi et al., 2007) and second-order orientation (Mansouri et al., 2005) perception have mostly been found to affect only AE function.

Note that the fact that the dorsal pathway may stay more binocular than the ventral pathway does not necessarily mean it is less affected by amblyopia. In fact, the result that the second-order nonlinearity is affected by amblyopia only for MM is consistent with the idea of "dorsal stream vulnerability". It has

been proposed to be a group of problems, including global motion processing, visual-motor action planning, attention etc. that are common across many neural developmental disorders. To name a few: amblyopia, Williams's syndrome, autism and developmental dyslexia (see review (Atkinson, 2017) for more details). For amblyopia, deficits in the dorsal pathway has been reported by fMRI (Secen et al., 2011) and neurophysiological studies (El-Shamayleh et al., 2010) as well.

The next question is: what do these changes in the nonlinearity mean for the underlying neural mechanisms? It is believed that the divisive inhibition model accounts for the physiological results of intracortical inhibition among striate neurons (Allison, Smith, & Bonds, 2001; DeBruyn & Bonds, 1986; N. Graham, Beck, et al., 1992; C. Y. Li & Creutzfeldt, 1984; Morrone et al., 1982; Movshon, Thompson, & Tolhurst, 1978). Therefore, the changes we found in the shape of nonlinear transducer function for processing MM in amblyopic vision could well reflect the changes in the interneuron connectivity of the amblyopic visual system. Explanations involving connectivity changes in the amblyopic brain are appealing, since simple sensitivity reduction of V1 and extra-striate cortex neurons does not explain all the functional deficits that are present (Levi, 2013; A. M. Wong, 2012). Li and colleagues (2011) investigated the effective connectivity of different networks in regions of thalamic, striate and extra-striate cortex in humans with amblyopia. They found that the effective connectivity of these networks driven by the AE was reduced and the reduction was equal between feed-forward and feedback interactions (X. Li, Mullen, Thompson, & Hess, 2011). They did not however find the reduction in connectivity to disproportionately affect the dorsal pathway. Another recent study (Duan, Norcia, Yeatman, & Mezer, 2015) found that the structural properties of some major white matter tracts are affected in strabismic amblyopia. This is an area of active study, and future studies of structural and functional connectivity among different neuron networks will provide meaningful insight for the functional deficits and potential treatments in the amblyopic visual system.

In conclusion, we found the typical dipper shape in second-order pedestal masking functions for both motion-modulation (MM) and contrast-modulation (CM) in amblyopic vision. We confirmed previous finding about the presence of a fellow eye deficit for second-order MM processing. Amblyopia

affects the second-order nonlinearity but in different ways for different types of second-order modulations. The fact that the nonlinearity for only MM is affected, suggests first that MM and CM are processed by at least partially separate mechanisms; second, the dorsal and ventral pathways may be influenced to different degrees in amblyopia. The change in the nonlinearity for MM in both eyes of amblyopes potentially explains binocular deficits in functions like global motion, form-from-motion and second-order motion processing. Changes in the nonlinearity could be explained by a deficit in intracortical interactions.

Acknowledgement

This work was supported by a Canadian Institutes of Health Research Grant (CCI-125686) to RH and a National Natural Science Foundation of China grants (NSFC 31300913) to YT and NSFC 81261120562 to YZ.

Conclusion and discussion

Summary of results

This thesis is the first work that models and compares the second-order nonlinearity involved in three different kinds of second-order modulation including contrast-modulation (CM), orientation-modulation (OM) and motion-modulation (MM) in normal as well as

amblyopic vision. It also reports systematic measurements of the modulation sensitivity function in amblyopia over a large spatial frequency for all three kinds of second-order modulation.

The second-order nonlinearity was investigated with a pedestal masking paradigm. A typical dipper shape was found in the pedestal masking functions for all three modulations for normal vision, as well as for CM and MM for amblyopic vision. All data can be modeled by a linear-nonlinear-linear (LNL) model, which extracts second-order envelope information, followed by a nonlinear transducer function of the form of a divisive gain control and a decision making stage according to signal detection theory. For the second-order nonlinearity, CM and OM are found to share a nonlinearity of highly similar form to the one that was found in first-order processing. While MM processing undergoes a separate nonlinearity of a different form. This result suggests that all second-order modulations are not processed by a common mechanism.

The first amblyopia study found general second-order deficits for CM, OM and MM for amblyopic eye stimulation. This general deficit likely reflects a general abnormality involving a large extent of amblyopic extrastriate cortex. In terms of lateral effect, the fellow eye of amblyopes is also affected but only for MM processing. The different patterns of deficit among various second-order modulations suggest that dorsal and ventral pathways are both likely to be affected but to different degrees. In the second amblyopic study, I investigated whether this difference between MM and CM can be attributed solely to the second-order nonlinearity. The results show that amblyopia affects the second-order nonlinearity only for MM and the two eyes of amblyopes behave similarly in terms of their second-order nonlinearity. These results are consistent with my first three studies in three aspects: first, it implies that MM and CM are processed by separate mechanisms; second, the fellow eye is affected for MM processing; third,

it also suggests that dorsal and ventral pathways are probably affected to different degrees in amblyopia.

Second-order nonlinearity in normal vision

In first two studies, the second-order nonlinearities for CM, OM and MM were studied by the pedestal-masking paradigm and modeled as a nonlinear transducer function as a divisive gain control mechanism. The nonlinear transducer function has three parameters including two exponents that determine the shape of the nonlinearity, and a divisive gain control parameter representing the general divisive inhibition effect from all the mechanisms other than the responsible channels. Compared to CM and first-order contrast processing, the nonlinearity involved in OM has the same exponents, which suggest the same shape for the nonlinearity. While for MM, values of two exponents are significantly different from those for CM and OM, indicating that the nonlinearity is of a different shape for MM.

The difference between the nonlinearity for CM and OM is the larger divisive gain control parameter for OM. This increased divisive gain control parameter could be due to two reasons. First, there is larger divisive inhibition to the output of the second-order channels that are responsible for extracting the modulation in OM. Compared to a CM stimulus, an OM stimulus is likely to elicit more inhibitory input from other channels that have different carrier orientation tuning properties (Dakin & Mareschal, 2000; N. Graham et al., 1993) because it contains one more orientation band in the carrier,. Secondly, cross-orientation suppression between the two orthogonal carriers (Foley, 1994; Morrone et al., 1982) reduces the response of first-stage linear filters, which is equivalent to reducing the carrier contrast. Lower carrier contrast was found to generate a larger divisive gain control parameter in CM (Huang & Chen,

2014). Although it is hard to distinguish these two possible explanations, the same shape of nonlinearity for CM and OM suggests that processing of OM could be done on the basis of two CM stimuli of different carrier orientations. Whether the outputs of two CM processing mechanisms are integrated linearly (Motoyoshi & Nishida, 2004) or chosen according to probability summation (N. Prins, 2008) needs further study to resolve. The difference between the nonlinearities for MM and CM involves a fundamental change in the shape of the nonlinearity and has a potential bearing on this issue. This different nonlinearity is consistent with there being two underlying mechanisms. The MM nonlinearity may reflect a completely separate nonlinear mechanism, which is in a different form from that of CM. The second possibility is that the MM processing mechanism is built up from two CM mechanisms, that have the corresponding carrier velocity tuning, and there is another layer of nonlinearity in the process of integrating the outputs of the two CM mechanisms. There is a way of distinguishing between these two possibilities. If the MM mechanism is built up from CM mechanisms, then there will still be an interaction between the processing of these two stimuli. Therefore, studying the interaction between MM and CM using either adaptation or cross pedestal masking resolves this question.

I also demonstrated, in the second study, that second-order nonlinearity is not affected by carrier contrast. This suggests that the nonlinearity I have been studying is of second-order nature since first-order carrier does not control it.

These two studies are the first ones to systematically model and compare second-order nonlinearities involved in different types of modulations. The different nonlinearities found for MM compared to CM and OM argues against the idea that different types of second-order information are processed by the same mechanism (F. A. Kingdom et al., 2003). It also argues

against a cue-invariant mechanism of boundary processing (Berkley et al., 1994; Filangieri & Li, 2009; Hawley & Keeble, 2006). All the previous studies that support this idea did not compare motion-defined boundaries with static ones. That may be the reason behind the results suggesting a common underlying mechanism. Furthermore, this is consistent with the findings in my first study that the two statically-defined boundaries CM and OM go through the same nonlinearity.

Amblyopia

Second-order deficits

The third study of this thesis was the first to apply qCSF paradigm (Lesmes, Lu, Baek, & Albright, 2010) to the measurement of sensitivities to second-order modulation in amblyopia. It was also the first to systematically compare second-order discrimination sensitivities for CM, OM and MM. A general deficit was found for amblyopic eye stimulation that involved all three types of second-order modulation. This general deficit suggests that amblyopia influences extrastriate cortical function over a large area as it involves functions normally attributed to both the dorsal and ventral pathways. The type of amblyopia, age or gender of the observers did not show any effect on this general second-order deficit. Stimulation of the fellow fixing eye, however, shows a reduced peak sensitivity only for MM. The find that only MM processing is affected by stimulation of either eye may be a consequence of residual binocular function in the dorsal pathway.

Second-order nonlinearity in amblyopia

The results of my fourth study strongly support the conclusions from the aforementioned three studies. The common experimental design allows for the comparison between normal and

amblyopic visual systems. The fourth study was the first to find the dipper shape in the pedestal masking function for second-order processing in amblyopic vision. The increment thresholds for both CM and MM are higher across the whole range of pedestal mask levels in both AE and FE. This helps characterize amblyopic deficit. The result that the AE and FE show the same nonlinearities suggests that these involve binocular, higher-level mechanisms. Second-order processing in amblyopic vision can also be modeled by a LNL model plus a nonlinear transducer function followed by a decision making stage. The nonlinear transducer function also takes the form of divisive normalization. Amblyopia affects the shape of the nonlinearity in only MM and not CM. The only way that the nonlinearity in MM processing is affected while CM is kept intact is if these two kinds of second-order modulation are processed by separate mechanisms. This is a strong conclusion from an amblyopia study that is relevant to normal visual system. This conclusion is also consistent with that of my second study. Since MM and CM are thought to be processed by dorsal and ventral pathway, respectively, the result that only an MM nonlinearity is affected also suggests that dorsal and ventral pathways may be affected by amblyopia to differing degrees. This implication is consistent with that of my third study which found that the fellow fixing eye was affected only for MM. Together with this finding that the MM deficit is binocular, the result suggests that dorsal pathway is affected more but stayed more binocular than the ventral pathway. This deduction is consistent with two results in the literature; first, the dorsal stream vulnerability (Atkinson, 2017) has been shown in many neural developmental disorders including amblyopia; and second, more neurons in the ventral pathway are monocularly driven by the fellow eye than in the dorsal pathway (Schroder et al., 2002).

Fellow eye deficits

An interesting question to consider is why the FE is also affected in unilateral amblyopia. In unilateral amblyopia, only the vision of the amblyopic eye is interrupted in early childhood. It makes sense that there are deficits for amblyopic eye stimulation. However, the fellow fixing eye is also affected for some higher-level, motion-related visual functions. One possible reason is that disrupted visual input from the AE causes abnormalities in the development of binocular vision and deficits in binocular areas such as extra-striate cortex. Subsequently higher-level functions, which are processed in these high-level areas, exhibit binocular deficits. The fact that most FE deficits are motion related suggests that the dorsal pathway remains more binocularly than the ventral pathway. The traditional treatment of patching the FE is unlikely to be the reason even though it disrupts the visual input from this eye temporarily. This is due to (1), the FE deficits still exist for amblyopes who have never received the patching treatment, and (2) the FE deficits are manifested even before the onset of any treatment (Meier & Giaschi, 2017).

The change in nonlinearity suggests that intracortical connectivities in extrastriate cortex are affected by amblyopia. This finding suggests an interesting future research direction looking at functions that depend on intracortical connectivity such as contour integration (Baldwin, Fu, Farivar, & Hess, 2017) and surround suppression (Yazdani, Serrano-Pedraza, Whittaker, Trevelyan, & Read, 2015)

Is the nonlinearity second-order?

With regards to the location of the nonlinearity that was examined in the current thesis, a main concern is that it may be located before the second-stage linear filters, i.e. the nonlinearity is an intermediate or even first-order one instead of a second-order one as I claimed. In the

thesis, I modeled my results in a way that assumed that second-order information was truthfully extracted by the linear filters in the two stages. Thus the modulation level that is the contrast of the envelope was used directly as the input to the second-order nonlinear transducer function. Here in the appendix, I demonstrate that if the gain control nonlinearity is before the second-stage filters, the output or response of the second-stage linear filters will still be linear with regards to the modulation level. In all actuality, regardless of what kind of intermediate nonlinearity is applied, it does not have any influence on the linear shape of the response function of the second-stage filters.

I simulate the whole process of processing a second-order stimulus using the linear-nonlinear-linear (LNL) model. A group of OM stimuli were used to do the simulation of processing. The stimuli have same carriers and their modulation levels range from 15 dB to 40 dB (~5.6% to 100%). This simulation can be generalized to any kind of second-order information.

First, each stimulus at each modulation level is filtered by four Gabor filters. The four filters all have the same spatial frequency as the carriers. Their orientation and phase are the four combinations of two orientations of the two carriers and two phases with half a cycle difference. Each filter is applied by convolving the stimulus matrix with the filter matrix. Then, the output of each filter goes through (1) a half-wave rectification, then (2) a nonlinear transformation as $R_i = \frac{C^p}{C^q + Z}$, where C represents the output of the first linear filters and the three parameters take the values from fitting OM data in Chapter 1 that are 2.4, 2 and ~500. Then (3) values that were originally negative in the output were set back to negative in the responses R_i. After that (4) the four responses of four filters were integrated as such to recover the second-order information:

$M = \sqrt{R_1^2 + R_2^2} - \sqrt{R_3^2 + R_4^2}$ in which R_1 and R_2 are responses of the filters having the same orientation and R_3 and R_4 of the other orientation.

Finally, two second-stage Gabor filters of opposite phases are applied to M also using convolution and combined as the geometric mean to get the final output of the whole LNL model. Geometric sum of the elements in the matrix of the final output is calculated to represent the output level at each modulation level. The outputs at different modulation levels are normalized by the largest value and plotted against the modulation levels that are used to construct the stimuli (Figure 1). Fitting outputs against modulation levels with a 2nd-order polynomial reveals the constant of the 2nd-order term having a value smaller than 0.00001. Because of this finding I fit the results with a linear function instead. The fitted line is plotted in Figure 1 as well. The slope is 0.01 and the intersect is 0.0275.

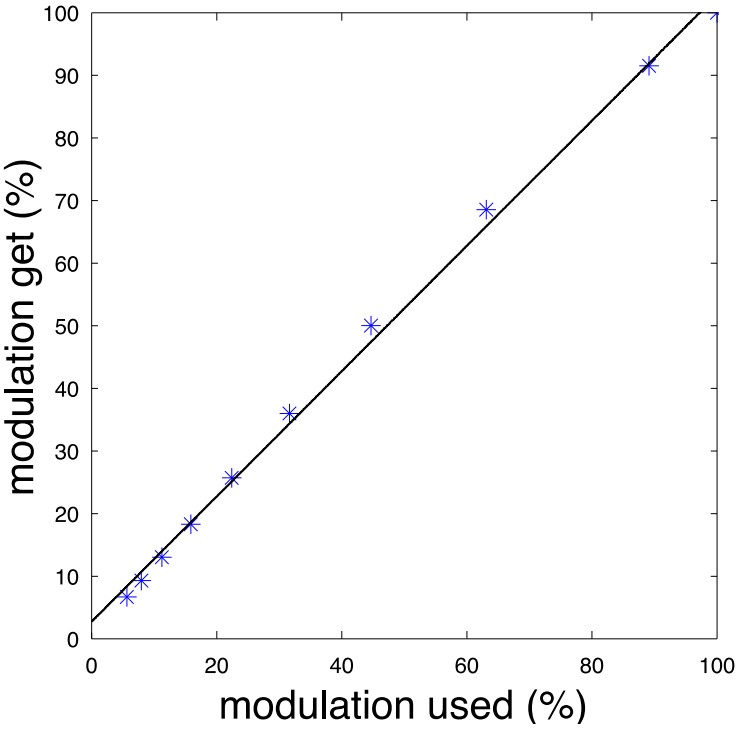

This linear relationship between the final output and the modulation level determines that this mechanism that only with gain control nonlinearity before the second-stage linear filters cannot produce a dipper pedestal masking function. Therefore, a nonlinearity after the second-stage filters is necessary to fit the pedestal masking function data.

Future study

To further understand why the second-order nonlinearity of only MM processing is affected by amblyopia and in both eyes, it is necessary to confirm and establish this finding in a larger amblyopic population. The current paradigm takes six hours to test each subject, which makes it difficult to do on a large number of amblyopes. A good way to reduce the testing time is based on a feature of the pedestal masking function. The dip depth reflects the values of the exponents, i.e. the shape of the nonlinear response function. Obtaining the dip depth, which only requires measuring the detection threshold and one increment threshold at the pedestal level equal to the detection threshold, is enough to characterize the nonlinear response function. This will reduce the testing time to one hour per subject. The hypothesis here is that there will be a dip depth about 3 dB smaller in the amblyopic eye and 5 dB smaller in the fellow eye than that found the normal vision for MM processing.

Conclusion of the conclusion

In summary, the current thesis found an identical second-order nonlinearity for CM and OM which is different from that for MM. Amblyopic second-order nonlinearity was affected binocularly only for MM. These results jointly suggest a separate mechanism for processing MM than other types of second-order modulations. General second-order deficits were found for all

three kinds of modulations in the amblyopic eye suggesting extensive deficits in the extrastriate cortex. Deficits in the fellow eye are only found for MM processing, consistent with the differentially affected second-order nonlinearity in MM. This different deficit pattern for MM suggests that the dorsal and ventral extrastriate pathways are most likely affected to different degrees in amblyopic visual systems.

Reference

Aaen-Stockdale, C., & Hess, R. F. (2008). The amblyopic deficit for global motion is spatial scale invariant. *Vision Res, 48*(19), 1965-1971. doi:10.1016/j.visres.2008.06.012

Aaen-Stockdale, C., Ledgeway, T., & Hess, R. F. (2007). Second-order optic flow deficits in amblyopia. *Invest Ophthalmol Vis Sci, 48*(12), 5532-5538. doi:10.1167/iovs.07-0447

Albrecht, D. G., & Hamilton, D. B. (1982). Striate cortex of monkey and cat: contrast response function. *J Neurophysiol, 48*(1), 217-237.

Albright, T. D. (1992). Form-cue invariant motion processing in primate visual cortex. *Science, 255*(5048), 1141-1143.

Allard, R., & Faubert, J. (2007). Double dissociation between first- and second-order processing. *Vision Res, 47*(9), 1129-1141. doi:10.1016/j.visres.2007.01.010

Allison, J. D., Smith, K. R., & Bonds, A. B. (2001). Temporal-frequency tuning of cross-orientation suppression in the cat striate cortex. *Vis Neurosci, 18*(6), 941-948.

Arsenault, A. S., Wilkinson, F., & Kingdom, F. A. (1999). Modulation frequency and orientation tuning of second-order texture mechanisms. *J Opt Soc Am A Opt Image Sci Vis, 16*(3), 427-435.

Ashida, H., Lingnau, A., Wall, M. B., & Smith, A. T. (2007). FMRI adaptation reveals separate mechanisms for first-order and second-order motion. *J Neurophysiol, 97*(2), 1319-1325. doi:10.1152/jn.00723.2006

Atkinson, J. (2017). The Davida Teller Award Lecture, 2016: Visual Brain Development: A review of "Dorsal Stream Vulnerability"-motion, mathematics, amblyopia, actions, and attention. *J Vis, 17*(3), 26. doi:10.1167/17.3.26

Babenko, V. V., & Ermakov, P. N. (2015). Specificity of brain reactions to second-order visual stimuli. *Vis Neurosci, 32*, E011. doi:10.1017/s0952523815000085

Baker, C. L., Jr. (1999). Central neural mechanisms for detecting second-order motion. *Curr Opin Neurobiol, 9*(4), 461-466. doi:10.1016/s0959-4388(99)80069-5

Baker, C. L., Jr., & Mareschal, I. (2001). Processing of second-order stimuli in the visual cortex. *Prog Brain Res, 134*, 171-191.

Baker, D. H., & Meese, T. S. (2013). Regarding the benefit of zero-dimensional noise. *J Vis, 13*(10). doi:10.1167/13.10.26

Baker, D. H., Meese, T. S., Mansouri, B., & Hess, R. F. (2007). Binocular summation of contrast remains intact in strabismic amblyopia. *Invest Ophthalmol Vis Sci, 48*(11), 5332-5338. doi:10.1167/iovs.07-0194

Baldwin, A. S., Baker, D. H., & Hess, R. F. (2016). What Do Contrast Threshold Equivalent Noise Studies Actually Measure? Noise vs. Nonlinearity in Different Masking Paradigms. *PLoS One, 11*(3), e0150942. doi:10.1371/journal.pone.0150942

Baldwin, A. S., Fu, M., Farivar, R., & Hess, R. F. (2017). The equivalent internal orientation and position noise for contour integration. *Sci Rep, 7*(1), 13048. doi:10.1038/s41598-017-13244-z

Baldwin, A. S., Schmidtmann, G., Kingdom, F. A., & Hess, R. F. (2016). Rejecting probability summation for radial frequency patterns, not so Quick! *Vision Res, 122*, 124-134. doi:10.1016/j.visres.2016.03.003

Barlow, H. B., Kaushal, T. P., Hawken, M., & Parker, A. J. (1987). Human contrast discrimination and the threshold of cortical neurons. *J Opt Soc Am A, 4*(12), 2366-2371.

Barnes, G. R., Hess, R. F., Dumoulin, S. O., Achtman, R. L., & Pike, G. B. (2001). The cortical deficit in humans with strabismic amblyopia. *J Physiol, 533*(Pt 1), 281-297.

Barnes, T., & Mingolla, E. (2013). A neural model of visual figure-ground segregation from kinetic occlusion. *Neural Networks, 37*, 141-164. doi:http://doi.org/10.1016/j.neunet.2012.09.011

Barnes, T., & Mingolla, E. (2013). A neural model of visual figure-ground segregation from kinetic occlusion. *Neural Netw, 37*, 141-164. doi:10.1016/j.neunet.2012.09.011

Bedell, H. D., & Flom, M. C. (1981). Monocular spatial distortion in strabismic amblyopia. *Invest Ophthalmol Vis Sci, 20*(2), 263-268.

Berkley, M. A., Debruyn, B., & Orban, G. (1994). Illusory, motion, and luminance-defined contours interact in the human visual system. *Vision Res, 34*(2), 209-216.

Bonds, A. B. (1989). Role of inhibition in the specification of orientation selectivity of cells in the cat striate cortex. *Vis Neurosci, 2*(1), 41-55.

Bradley, A., & Freeman, R. D. (1981). Contrast sensitivity in anisometropic amblyopia. *Invest Ophthalmol Vis Sci, 21*(3), 467-476.

Bradley, A., & Ohzawa, I. (1986). A comparison of contrast detection and discrimination. *Vision Res, 26*(6), 991-997.

Brainard, D. H. (1997). The Psychophysics Toolbox. *Spat Vis, 10*(4), 433-436.

Bretas, C. C., & Soriano, R. N. (2016). Amblyopia: neural basis and therapeutic approaches. *Arq Bras Oftalmol, 79*(5), 346-351. doi:10.5935/0004-2749.20160099

Burgess, A. E., & Colborne, B. (1988). Visual signal detection. IV. Observer inconsistency. *J Opt Soc Am A, 5*(4), 617-627.

Calvert, J., Manahilov, V., Simpson, W. A., & Parker, D. M. (2005). Human cortical responses to contrast modulations of visual noise. *Vision Res, 45*(17), 2218-2230. doi:10.1016/j.visres.2005.02.012

Campbell, F. W., Cooper, G. F., & Enroth-Cugell, C. (1969). The spatial selectivity of the visual cells of the cat. *J Physiol, 203*(1), 223-235.

Campbell, F. W., & Green, D. G. (1965). Optical and retinal factors affecting visual resolution. *J Physiol, 181*(3), 576-593.

Campbell, F. W., & Robson, J. G. (1968). Application of Fourier analysis to the visibility of gratings. *J Physiol, 197*(3), 551-566.

Carandini, M., Movshon, J. A., & Ferster, D. (1998). Pattern adaptation and cross-orientation interactions in the primary visual cortex. *Neuropharmacology, 37*(4-5), 501-511.
Cavanagh, P., & Mather, G. (1989). Motion: the long and short of it. *Spat Vis, 4*(2-3), 103-129.
Chen, C., Foley, J. M., & Brainard, D. H. (2000a). Detection of chromoluminance patterns on chromoluminance pedestals I: threshold measurements. *Vision Res, 40*(7), 773-788.
Chen, C., Foley, J. M., & Brainard, D. H. (2000b). Detection of chromoluminance patterns on chromoluminance pedestals II: model. *Vision Res, 40*(7), 789-803.
Chen, C. C., & Tyler, C. W. (2008). Excitatory and inhibitory interaction fields of flankers revealed by contrast-masking functions. *J Vis, 8*(4), 10.11-14. doi:10.1167/8.4.10
Chino, Y. M., Smith, E. L., 3rd, Yoshida, K., Cheng, H., & Hamamoto, J. (1994). Binocular interactions in striate cortical neurons of cats reared with discordant visual inputs. *J Neurosci, 14*(8), 5050-5067.
Chubb, C., & Sperling, G. (1988). Drift-balanced random stimuli: a general basis for studying non-Fourier motion perception. *J Opt Soc Am A, 5*(11), 1986-2007.
Clifford, C. W., Mannion, D. J., & McDonald, J. S. (2009). Radial biases in the processing of motion and motion-defined contours by human visual cortex. *J Neurophysiol, 102*(5), 2974-2981. doi:10.1152/jn.00411.2009
Dakin, S. C., & Mareschal, I. (2000). Sensitivity to contrast modulation depends on carrier spatial frequency and orientation. *Vision Res, 40*(3), 311-329.
Dallala, R., Wang, Y. Z., & Hess, R. F. (2010). The global shape detection deficit in strabismic amblyopia: Contribution of local orientation and position. *Vision Res, 50*(16), 1612-1617. doi:10.1016/j.visres.2010.05.023
Dao, D. Y., Lu, Z. L., & Dosher, B. A. (2006). Adaptation to sine-wave gratings selectively reduces the contrast gain of the adapted stimuli. *J Vis, 6*(7), 739-759. doi:10.1167/6.7.6
De Valois, K. K., & Tootell, R. B. (1983). Spatial-frequency-specific inhibition in cat striate cortex cells. *J Physiol, 336*, 359-376.
Dean, A. F. (1981). The relationship between response amplitude and contrast for cat striate cortical neurones. *J Physiol, 318*, 413-427.
DeBruyn, E. J., & Bonds, A. B. (1986). Contrast adaptation in cat visual cortex is not mediated by GABA. *Brain Res, 383*(1-2), 339-342.
Derrington, A. M., Allen, H. A., & Delicato, L. S. (2004). Visual mechanisms of motion analysis and motion perception. *Annu Rev Psychol, 55*, 181-205. doi:10.1146/annurev.psych.55.090902.141903
Duan, Y., Norcia, A. M., Yeatman, J. D., & Mezer, A. (2015). The Structural Properties of Major White Matter Tracts in Strabismic Amblyopia. *Invest Ophthalmol Vis Sci, 56*(9), 5152-5160. doi:10.1167/iovs.15-17097
Durant, S., & Zanker, J. M. (2008). Combining direction and speed for the localisation of visual motion defined contours. *Vision Res, 48*(8), 1053-1060. doi:10.1016/j.visres.2007.12.021
Durant, S., & Zanker, J. M. (2009). Characterizing motion contour detection mechanisms and equivalent mechanisms in the luminance domain. *J Vis, 9*(1), 36.31-16. doi:10.1167/9.1.36
Edwards, M., & Badcock, D. R. (1995). Global motion perception: no interaction between the first- and second-order motion pathways. *Vision Res, 35*(18), 2589-2602.
Eggers, H. M., & Blakemore, C. (1978). Physiological basis of anisometropic amblyopia. *Science, 201*(4352), 264-267.

El-Shamayleh, Y., Kiorpes, L., Kohn, A., & Movshon, J. A. (2010). Visual motion processing by neurons in area MT of macaque monkeys with experimental amblyopia. *J Neurosci, 30*(36), 12198-12209. doi:10.1523/jneurosci.3055-10.2010

Ellemberg, D., Lewis, T. L., Defina, N., Maurer, D., Brent, H. P., Guillemot, J. P., & Lepore, F. (2005). Greater losses in sensitivity to second-order local motion than to first-order local motion after early visual deprivation in humans. *Vision Res, 45*(22), 2877-2884. doi:10.1016/j.visres.2004.11.019

Enroth-Cugell, C., & Robson, J. G. (1966). The contrast sensitivity of retinal ganglion cells of the cat. *J Physiol, 187*(3), 517-552.

F, A. A. K. (2016). Fixed versus variable internal noise in contrast transduction: The significance of Whittle's data. *Vision Res, 128*, 1-5. doi:10.1016/j.visres.2016.09.004

Faisal, A. A., Selen, L. P., & Wolpert, D. M. (2008). Noise in the nervous system. *Nat Rev Neurosci, 9*(4), 292-303. doi:10.1038/nrn2258

Farzin, F., & Norcia, A. M. (2011). Impaired visual decision-making in individuals with amblyopia. *J Vis, 11*(14). doi:10.1167/11.14.6

Filangieri, C., & Li, A. (2009). Three-dimensional shape from second-order orientation flows. *Vision Res, 49*(11), 1465-1471. doi:10.1016/j.visres.2009.03.006

Foley, J. M. (1994). Human luminance pattern-vision mechanisms: masking experiments require a new model. *J Opt Soc Am A Opt Image Sci Vis, 11*(6), 1710-1719.

Foley, J. M., & Chen, C. C. (1999). Pattern detection in the presence of maskers that differ in spatial phase and temporal offset: threshold measurements and a model. *Vision Res, 39*(23), 3855-3872.

Foley, J. M., & Legge, G. E. (1981). Contrast detection and near-threshold discrimination in human vision. *Vision Res, 21*(7), 1041-1053.

Gao, Y., Baldwin, A., & Hess, R. (in preperation). Different nonlinearity in the processing of contrast- vs motion-defined boundaries.

Gao, Y., Baldwin, A., & Hess, R. (in review). Different nonlinearity in the processing of contrast- vs motion-defined boundaries. *Vision Res*.

Gao, Y., Reynaud, A., Tang, Y., Feng, L., Zhou, Y., & Hess, R. F. (2014). The amblyopic deficit for 2nd order processing: Generality and laterality. *Vision Res*. doi:10.1016/j.visres.2014.10.020

Gao, Y., Reynaud, A., Tang, Y., Feng, L., Zhou, Y., & Hess, R. F. (2015). The amblyopic deficit for 2nd order processing: Generality and laterality. *Vision Res, 114*, 111-121. doi:10.1016/j.visres.2014.10.020

Gharat, A., & Baker, C. L., Jr. (2012). Motion-defined contour processing in the early visual cortex. *J Neurophysiol, 108*(5), 1228-1243. doi:10.1152/jn.00840.2011

Gharat, A., & Baker, C. L., Jr. (2017). Nonlinear Y-Like Receptive Fields in the Early Visual Cortex: An Intermediate Stage for Building Cue-Invariant Receptive Fields from Subcortical Y Cells. *J Neurosci, 37*(4), 998-1013. doi:10.1523/jneurosci.2120-16.2017

Giaschi, D., Chapman, C., Meier, K., Narasimhan, S., & Regan, D. (2015). The effect of occlusion therapy on motion perception deficits in amblyopia. *Vision Res, 114*, 122-134. doi:10.1016/j.visres.2015.05.015

Giaschi, D. E., Regan, D., Kraft, S. P., & Hong, X. H. (1992). Defective processing of motion-defined form in the fellow eye of patients with unilateral amblyopia. *Invest Ophthalmol Vis Sci, 33*(8), 2483-2489.

Goodale, M. A., & Milner, A. D. (1992). Separate visual pathways for perception and action. *Trends Neurosci, 15*(1), 20-25.
Graham, N. (1994). Non-linearities in texture segregation. *Ciba Found Symp, 184*, 309-322; discussion 323-338.
Graham, N., Beck, J., & Sutter, A. (1992). Nonlinear processes in spatial-frequency channel models of perceived texture segregation: effects of sign and amount of contrast. *Vision Res, 32*(4), 719-743.
Graham, N., & Sutter, A. (1996). Effect of spatial scale and background luminance on the intensive and spatial nonlinearities in texture segregation. *Vision Res, 36*(10), 1371-1390.
Graham, N., & Sutter, A. (1998). Spatial summation in simple (Fourier) and complex (non-Fourier) texture channels. *Vision Res, 38*(2), 231-257.
Graham, N., & Sutter, A. (2000). Normalization: contrast-gain control in simple (Fourier) and complex (non-Fourier) pathways of pattern vision. *Vision Res, 40*(20), 2737-2761.
Graham, N., Sutter, A., & Venkatesan, C. (1993). Spatial-frequency- and orientation-selectivity of simple and complex channels in region segregation. *Vision Res, 33*(14), 1893-1911.
Graham, N., Sutter, A., Venkatesan, C., & Humaran, M. (1992). Non-linear processes in perceived region segregation: orientation selectivity of complex channels. *Ophthalmic Physiol Opt, 12*(2), 142-146.
Graham, N., & Wolfson, S. S. (2004). Is there opponent-orientation coding in the second-order channels of pattern vision? *Vision Res, 44*(27), 3145-3175. doi:http://dx.doi.org/10.1016/j.visres.2004.07.018
Green, D. M. (1964). Consistency of auditory detection judgments. *Psychol Rev, 71*, 392-407.
Green, D. M., Swets, J. A. (1988). *Signal Detection Theory and Psychophysics*. Los Altos, California: Peninsula Publishing.
Gregory, R. L., & Cane, V. (1955). A statistical information theory of visual thresholds. *Nature, 176*(4496), 1272.
Hallum, L. E., Landy, M. S., & Heeger, D. J. (2011). Human primary visual cortex (V1) is selective for second-order spatial frequency. *J Neurophysiol, 105*(5), 2121-2131. doi:10.1152/jn.01007.2010
Hamm, L. M., Black, J., Dai, S., & Thompson, B. (2014). Global processing in amblyopia: a review. *Front Psychol, 5*, 583. doi:10.3389/fpsyg.2014.00583
Hartline, H. K. (1938). The response of single optic nerve fibers of the vertebrate eye to illumination of the retina. *American Journal of Physiology -- Legacy Content, 121*(2), 400-415.
Hawley, S. J., & Keeble, D. R. (2006). Tilt aftereffect for texture edges is larger than in matched subjective edges, but both are strong adaptors of luminance edges. *J Vis, 6*(1), 37-52. doi:10.1167/6.1.4
Haxby, J. V., Grady, C. L., Horwitz, B., Ungerleider, L. G., Mishkin, M., Carson, R. E., . . . Rapoport, S. I. (1991). Dissociation of object and spatial visual processing pathways in human extrastriate cortex. *Proc Natl Acad Sci U S A, 88*(5), 1621-1625.
Hayward, J., Truong, G., Partanen, M., & Giaschi, D. (2011). Effects of speed, age, and amblyopia on the perception of motion-defined form. *Vision Res, 51*(20), 2216-2223. doi:10.1016/j.visres.2011.08.023
Heeger, D. J. (1992). Half-squaring in responses of cat striate cells. *Vis Neurosci, 9*(5), 427-443.
Heeger, D. J. (1992). Normalization of cell responses in cat striate cortex. *Vis Neurosci, 9*(2), 181-197. doi:10.1017/S0952523800009640

Hess, R. F. (1979). Contrast sensitivity assessment of functional amblyopia in humans. *Trans Ophthalmol Soc U K, 99*(3), 391-397.
Hess, R. F., Campbell, F. W., & Greenhalgh, T. (1978). On the nature of the neural abnormality in human amblyopia; neural aberrations and neural sensitivity loss. *Pflugers Arch, 377*(3), 201-207.
Hess, R. F., & Howell, E. R. (1977). The threshold contrast sensitivity function in strabismic amblyopia: evidence for a two type classification. *Vision Res, 17*(9), 1049-1055.
Hess, R. F., & Ledgeway, T. (2003). The detection of direction-defined and speed-defined spatial contours: one mechanism or two? *Vision Res, 43*(5), 597-606.
Hess, R. F., Mansouri, B., Dakin, S. C., & Allen, H. A. (2006). Integration of local motion is normal in amblyopia. *J Opt Soc Am A Opt Image Sci Vis, 23*(5), 986-992.
Hess, R. F., Wang, Y. Z., Demanins, R., Wilkinson, F., & Wilson, H. R. (1999). A deficit in strabismic amblyopia for global shape detection. *Vision Res, 39*(5), 901-914.
Ho, C. S., Giaschi, D. E., Boden, C., Dougherty, R., Cline, R., & Lyons, C. (2005). Deficient motion perception in the fellow eye of amblyopic children. *Vision Res, 45*(12), 1615-1627. doi:10.1016/j.visres.2004.12.009
Ho, C. S., Paul, P. S., Asirvatham, A., Cavanagh, P., Cline, R., & Giaschi, D. E. (2006). Abnormal spatial selection and tracking in children with amblyopia. *Vision Res, 46*(19), 3274-3283. doi:10.1016/j.visres.2006.03.029
Hou, C., Pettet, M. W., & Norcia, A. M. (2008). Abnormalities of coherent motion processing in strabismic amblyopia: Visual-evoked potential measurements. *J Vis, 8*(4), 2.1-12. doi:10.1167/8.4.2
Hou, F., Huang, C. B., Lesmes, L., Feng, L. X., Tao, L., Zhou, Y. F., & Lu, Z. L. (2010). qCSF in clinical application: efficient characterization and classification of contrast sensitivity functions in amblyopia. *Invest Ophthalmol Vis Sci, 51*(10), 5365-5377. doi:10.1167/iovs.10-5468
Huang, P. C., & Chen, C. C. (2014). A comparison of pedestal effects in first- and second-order patterns. *J Vis, 14*(1). doi:10.1167/14.1.9
Hubel, D. H., & Wiesel, T. N. (1959). Receptive fields of single neurones in the cat's striate cortex. *J Physiol, 148*, 574-591.
Hubel, D. H., & Wiesel, T. N. (1962). Receptive fields, binocular interaction and functional architecture in the cat's visual cortex. *J Physiol, 160*, 106-154.
Hubel, D. H., & Wiesel, T. N. (1965). Binocular interaction in striate cortex of kittens reared with artificial squint. *J Neurophysiol, 28*(6), 1041-1059.
Husk, J. S., Farivar, R., & Hess, R. F. (2012). Amblyopic deficits in processing structure-from-motion. *J Vis, 12*(4). doi:10.1167/12.4.4
Husk, J. S., & Hess, R. F. (2013). Global processing of orientation in amblyopia. *Vision Res, 82*, 22-30. doi:10.1016/j.visres.2013.02.005
Jamar, J. H., & Koenderink, J. J. (1985). Contrast detection and detection of contrast modulation for noise gratings. *Vision Res, 25*(4), 511-521.
Joly, O., & Franko, E. (2014). Neuroimaging of amblyopia and binocular vision: a review. *Front Integr Neurosci, 8*, 62. doi:10.3389/fnint.2014.00062
Joshi, M., Simmers, A., & Jeon, S. (2015). Deficits in integration of global motion and form in noise is associated with the severity and type of amblyopia. *J Vis, 15*(12), 193. doi:10.1167/15.12.193

Joshi, M. R., Simmers, A. J., & Jeon, S. T. (2016). Concurrent Investigation of Global Motion and Form Processing in Amblyopia: An Equivalent Noise Approach. *Invest Ophthalmol Vis Sci, 57*(11), 5015-5022. doi:10.1167/iovs.15-18609
Kastner, S., De Weerd, P., & Ungerleider, L. G. (2000). Texture segregation in the human visual cortex: A functional MRI study. *J Neurophysiol, 83*(4), 2453-2457.
Kingdom, F. A., Baldwin, A. S., & Schmidtmann, G. (2015). Modeling probability and additive summation for detection across multiple mechanisms under the assumptions of signal detection theory. *J Vis, 15*(5), 1. doi:10.1167/15.5.1
Kingdom, F. A., Keeble, D., & Moulden, B. (1995). Sensitivity to orientation modulation in micropattern-based textures. *Vision Res, 35*(1), 79-91.
Kingdom, F. A., Prins, N., & Hayes, A. (2003). Mechanism independence for texture-modulation detection is consistent with a filter-rectify-filter mechanism. *Vis Neurosci, 20*(1), 65-76.
Kingdom, F. A. A., & Prins, N. (2016). Psychophysics : a practical introduction.
Kiorpes, L. (2006). Visual processing in amblyopia: animal studies. *Strabismus, 14*(1), 3-10. doi:10.1080/09273970500536193
Kiorpes, L., Tang, C., & Movshon, J. A. (2006). Sensitivity to visual motion in amblyopic macaque monkeys. *Vis Neurosci, 23*(2), 247-256. doi:10.1017/s0952523806232097
Kontsevich, L. L., & Tyler, C. W. (1999). Nonlinearities of near-threshold contrast transduction. *Vision Res, 39*(10), 1869-1880.
Kovacs, I., Polat, U., Pennefather, P. M., Chandna, A., & Norcia, A. M. (2000). A new test of contour integration deficits in patients with a history of disrupted binocular experience during visual development. *Vision Res, 40*(13), 1775-1783.
Kwan, L., & Regan, D. (1998). Orientation-tuned spatial filters for texture-defined form. *Vision Res, 38*(24), 3849-3855.
Lagreze, W. D., & Sireteanu, R. (1991). Two-dimensional spatial distortions in human strabismic amblyopia. *Vision Res, 31*(7-8), 1271-1288.
Landy, M. S., & Oruc, I. (2002). Properties of second-order spatial frequency channels. *Vision Res, 42*(19), 2311-2329. doi:10.1016/s0042-6989(02)00193-1
Larsson, J., Heeger, D. J., & Landy, M. S. (2010). Orientation selectivity of motion-boundary responses in human visual cortex. *J Neurophysiol, 104*(6), 2940-2950. doi:10.1152/jn.00400.2010
Larsson, J., Landy, M. S., & Heeger, D. J. (2006). Orientation-selective adaptation to first- and second-order patterns in human visual cortex. *J Neurophysiol, 95*(2), 862-881. doi:10.1152/jn.00668.2005
Ledgeway, T., & Hess, R. F. (2006). The spatial frequency and orientation selectivity of the mechanisms that extract motion-defined contours. *Vision Res, 46*(4), 568-578. doi:http://doi.org/10.1016/j.visres.2005.08.010
Ledgeway, T., & Smith, A. T. (1994). Evidence for separate motion-detecting mechanisms for first- and second-order motion in human vision. *Vision Res, 34*(20), 2727-2740.
Legge, G. E. (1979). Spatial frequency masking in human vision: binocular interactions. *J Opt Soc Am, 69*(6), 838-847.
Legge, G. E., & Foley, J. M. (1980). Contrast masking in human vision. *J Opt Soc Am, 70*(12), 1458-1471.
Lesmes, L. A., Lu, Z. L., Baek, J., & Albright, T. D. (2010). Bayesian adaptive estimation of the contrast sensitivity function: the quick CSF method. *J Vis, 10*(3), 17.11-21. doi:10.1167/10.3.17

Leventhal, A. G., Wang, Y., Schmolesky, M. T., & Zhou, Y. (1998). Neural correlates of boundary perception. *Vis Neurosci, 15*(6), 1107-1118.
Levi, D. M. (2013). Linking assumptions in amblyopia. *Vis Neurosci, 30*(5-6), 277-287. doi:10.1017/s0952523813000023
Levi, D. M., & Harwerth, R. S. (1977). Spatio-temporal interactions in anisometropic and strabismic amblyopia. *Invest Ophthalmol Vis Sci, 16*(1), 90-95.
Levi, D. M., & Harwerth, R. S. (1978). Contrast evoked potentials in strabismic and anisometropic amblyopia. *Invest Ophthalmol Vis Sci, 17*(6), 571-575.
Levi, D. M., Harwerth, R. S., & Manny, R. E. (1979). Suprathreshold spatial frequency detection and binocular interaction in strabismic and anisometropic amblyopia. *Invest Ophthalmol Vis Sci, 18*(7), 714-725.
Levi, D. M., Harwerth, R. S., & Smith, E. L. (1980). Binocular interactions in normal and anomalous binocular vision. *Doc Ophthalmol, 49*(2), 303-324.
Levi, D. M., & Tripathy, S. P. (2006). Is the ability to identify deviations in multiple trajectories compromised by amblyopia? *J Vis, 6*(12), 1367-1379. doi:10.1167/6.12.3
Levi, D. M., Yu, C., Kuai, S. G., & Rislove, E. (2007). Global contour processing in amblyopia. *Vision Res, 47*(4), 512-524. doi:10.1016/j.visres.2006.10.014
Lewis, T. L., Ellemberg, D., Maurer, D., Wilkinson, F., Wilson, H. R., Dirks, M., & Brent, H. P. (2002). Sensitivity to global form in glass patterns after early visual deprivation in humans. *Vision Res, 42*(8), 939-948.
Li, C. Y., & Creutzfeldt, O. (1984). The representation of contrast and other stimulus parameters by single neurons in area 17 of the cat. *Pflugers Arch, 401*(3), 304-314.
Li, G., Yao, Z., Wang, Z., Yuan, N., Talebi, V., Tan, J., . . . Baker, C. L., Jr. (2014). Form-cue invariant second-order neuronal responses to contrast modulation in primate area v2. *J Neurosci, 34*(36), 12081-12092. doi:10.1523/jneurosci.0211-14.2014
Li, X., Mullen, K. T., Thompson, B., & Hess, R. F. (2011). Effective connectivity anomalies in human amblyopia. *Neuroimage, 54*(1), 505-516. doi:10.1016/j.neuroimage.2010.07.053
Lowel, S., & Engelmann, R. (2002). Neuroanatomical and neurophysiological consequences of strabismus: changes in the structural and functional organization of the primary visual cortex in cats with alternating fixation and strabismic amblyopia. *Strabismus, 10*(2), 95-105.
Lu, Z. L., & Dosher, B. A. (2008). Characterizing observers using external noise and observer models: assessing internal representations with external noise. *Psychol Rev, 115*(1), 44-82. doi:10.1037/0033-295x.115.1.44
Lu, Z. L., & Sperling, G. (1995). The functional architecture of human visual motion perception. *Vision Res, 35*(19), 2697-2722.
Lu, Z. L., & Sperling, G. (1996). Contrast gain control in first- and second-order motion perception. *J Opt Soc Am A Opt Image Sci Vis, 13*(12), 2305-2318.
Maffei, L., & Fiorentini, A. (1973). The visual cortex as a spatial frequency analyser. *Vision Res, 13*(7), 1255-1267.
Mansouri, B., Allen, H. A., & Hess, R. F. (2005). Detection, discrimination and integration of second-order orientation information in strabismic and anisometropic amblyopia. *Vision Res, 45*(18), 2449-2460. doi:10.1016/j.visres.2005.02.018
Mansouri, B., Allen, H. A., Hess, R. F., Dakin, S. C., & Ehrt, O. (2004). Integration of orientation information in amblyopia. *Vision Res, 44*(25), 2955-2969. doi:10.1016/j.visres.2004.06.017

Mansouri, B., & Hess, R. F. (2006). The global processing deficit in amblyopia involves noise segregation. *Vision Res, 46*(24), 4104-4117. doi:10.1016/j.visres.2006.07.017
Marcar, V. L., & Cowey, A. (1992). The Effect of Removing Superior Temporal Cortical Motion Areas in the Macaque Monkey: II. Motion Discrimination Using Random Dot Displays. *Eur J Neurosci, 4*(12), 1228-1238.
Marcar, V. L., Raiguel, S. E., Xiao, D., & Orban, G. A. (2000). Processing of kinetically defined boundaries in areas V1 and V2 of the macaque monkey. *J Neurophysiol, 84*(6), 2786-2798.
Mareschal, I., & Baker, C. L., Jr. (1998a). A cortical locus for the processing of contrast-defined contours. *Nat Neurosci, 1*(2), 150-154. doi:10.1038/401
Mareschal, I., & Baker, C. L., Jr. (1998b). Temporal and spatial response to second-order stimuli in cat area 18. *J Neurophysiol, 80*(6), 2811-2823.
Mareschal, I., & Baker, C. L., Jr. (1999). Cortical processing of second-order motion. *Vis Neurosci, 16*(3), 527-540.
Meier, K., & Giaschi, D. (2017). Unilateral Amblyopia Affects Two Eyes: Fellow Eye Deficits in Amblyopia. *Invest Ophthalmol Vis Sci, 58*(3), 1779-1800. doi:10.1167/iovs.16-20964
Meier, K., Sum, B., & Giaschi, D. (2015). Global motion perception deficits in children with amblyopia as a function of spatial and temporal stimulus parameters. *J Vis, 15*(12), 653. doi:10.1167/15.12.653
Merigan, W. H. (2000). Cortical area V4 is critical for certain texture discriminations, but this effect is not dependent on attention. *Vis Neurosci, 17*(6), 949-958.
Michelson, A. A. (1927). *Studies in optics*. Chicago, Ill.: The University of Chicago Press.
Morita, H., Morita, M., & Kumada, T. (2003). Integration process of contours defined by different attributes. *Brain Res Cogn Brain Res, 15*(3), 324-327.
Morrone, M. C., Burr, D. C., & Maffei, L. (1982). Functional implications of cross-orientation inhibition of cortical visual cells. I. Neurophysiological evidence. *Proc R Soc Lond B Biol Sci, 216*(1204), 335-354.
Motoyoshi, I., & Kingdom, F. A. (2007). Differential roles of contrast polarity reveal two streams of second-order visual processing. *Vision Res, 47*(15), 2047-2054. doi:10.1016/j.visres.2007.03.015
Motoyoshi, I., & Nishida, S. (2004). Cross-orientation summation in texture segregation. *Vision Res, 44*(22), 2567-2576. doi:10.1016/j.visres.2004.05.024
Movshon, J. A., Thompson, I. D., & Tolhurst, D. J. (1978). Spatial summation in the receptive fields of simple cells in the cat's striate cortex. *J Physiol, 283*, 53-77.
Mysore, S. G., Vogels, R., Raiguel, S. E., & Orban, G. A. (2006). Processing of kinetic boundaries in macaque V4. *J Neurophysiol, 95*(3), 1864-1880. doi:10.1152/jn.00627.2005
Nachmias, J., & Sansbury, R. V. (1974). Letter: Grating contrast: discrimination may be better than detection. *Vision Res, 14*(10), 1039-1042.
Nishida, S., Ledgeway, T., & Edwards, M. (1997). Dual multiple-scale processing for motion in the human visual system. *Vision Res, 37*(19), 2685-2698.
Ohzawa, I., Sclar, G., & Freeman, R. D. (1982). Contrast gain control in the cat visual cortex. *Nature, 298*(5871), 266-268.
Ohzawa, I., Sclar, G., & Freeman, R. D. (1985). Contrast gain control in the cat's visual system. *J Neurophysiol, 54*(3), 651-667.

Olzak, L. A., & Thomas, J. P. (1999). Neural recoding in human pattern vision: model and mechanisms. *Vision Res, 39*(2), 231-256.
Pardhan, S., & Whitaker, A. (2000). Binocular summation in the fovea and peripheral field of anisometropic amblyopes. *Curr Eye Res, 20*(1), 35-44.
Pelli, D. G. (1985). Uncertainty explains many aspects of visual contrast detection and discrimination. *J Opt Soc Am A, 2*(9), 1508-1532.
Popple, A. V., & Levi, D. M. (2008). The attentional blink in amblyopia. *J Vis, 8*(13), 12.11-19. doi:10.1167/8.13.12
Prins, N. (2008). Texture modulation detection by probability summation among orientation-selective and isotropic mechanisms. *Vision Res, 48*(27), 2751-2766. doi:10.1016/j.visres.2008.09.005
Prins, N., & Kingdom, F. A. (2002). Orientation- and frequency-modulated textures at low depths of modulation are processed by off-orientation and off-frequency texture mechanisms. *Vision Res, 42*(6), 705-713.
Prins, N., & Kingdom, F. A. (2003). Detection and discrimination of texture modulations defined by orientation, spatial frequency, and contrast. *J Opt Soc Am A Opt Image Sci Vis, 20*(3), 401-410.
Prins, N., & Kingdom, F. A. (2006). Direct evidence for the existence of energy-based texture mechanisms. *Perception, 35*(8), 1035-1046. doi:10.1068/p5546
Prins, N. K., F. A. A. . (2009). Palamedes: Matlab routines for analyzing psychophysical data. Retrieved from http://www.palamedestoolbox.org/
Quick, R. F., Jr. (1974). A vector-magnitude model of contrast detection. *Kybernetik, 16*(2), 65-67.
Regan, D. (1989). Orientation discrimination for objects defined by relative motion and objects defined by luminance contrast. *Vision Res, 29*(10), 1389-1400.
Reppas, J. B., Niyogi, S., Dale, A. M., Sereno, M. I., & Tootell, R. B. (1997). Representation of motion boundaries in retinotopic human visual cortical areas. *Nature, 388*(6638), 175-179. doi:10.1038/40633
Reynaud, A., & Hess, R. F. (2012). Properties of spatial channels underlying the detection of orientation-modulations. *Experimental Brain Research, 220*(2), 135-145. doi:10.1007/s00221-012-3124-6
Reynaud, A., Tang, Y., Zhou, Y., & Hess, R. F. (2014). A normative framework for the study of second-order sensitivity in vision. *J Vis, 14*(9). doi:10.1167/14.9.3
Ringach, D. L., Hawken, M. J., & Shapley, R. (1997). Dynamics of orientation tuning in macaque primary visual cortex. *Nature, 387*(6630), 281-284. doi:10.1038/387281a0
Rislove, E. M., Hall, E. C., Stavros, K. A., & Kiorpes, L. (2010). Scale-dependent loss of global form perception in strabismic amblyopia. *J Vis, 10*(12), 25. doi:10.1167/10.12.25
Robson, J. G. (1966). Spatial and Temporal Contrast-Sensitivity Functions of the Visual System. *J Opt Soc Am, 56*(8), 1141-1142. doi:10.1364/JOSA.56.001141
Roelfsema, P. R., Konig, P., Engel, A. K., Sireteanu, R., & Singer, W. (1994). Reduced synchronization in the visual cortex of cats with strabismic amblyopia. *Eur J Neurosci, 6*(11), 1645-1655.
Rosenberg, A., Husson, R. T., Mallik, A., & Issa, N. P. (2008). Frequency-doubling in early visual system underlies sensitivity to second-order stimuli. *Journal of Vision, 8*(6), 281a.
Rosenberg, A., Husson, T. R., & Issa, N. P. (2010). Subcortical representation of non-Fourier image features. *J Neurosci, 30*(6), 1985-1993. doi:10.1523/jneurosci.3258-09.2010

Rosenberg, A., & Issa, N. P. (2009). The Y Cell Visual Pathway Implements a Demodulating Nonlinearity. *Neuron, 71*, 348-361.
Rosenberg, A., & Issa, N. P. (2011). The Y cell visual pathway implements a demodulating nonlinearity. *Neuron, 71*(2), 348-361. doi:10.1016/j.neuron.2011.05.044
Sanborn, A. N., & Dayan, P. (2011). Optimal decisions for contrast discrimination. *J Vis, 11*(14). doi:10.1167/11.14.9
Sary, G., Vogels, R., Kovacs, G., & Orban, G. A. (1995). Responses of monkey inferior temporal neurons to luminance-, motion-, and texture-defined gratings. *J Neurophysiol, 73*(4), 1341-1354.
Schofield, A. J., & Georgeson, M. A. (1999). Sensitivity to modulations of luminance and contrast in visual white noise: separate mechanisms with similar behaviour. *Vision Res, 39*(16), 2697-2716.
Schofield, A. J., & Georgeson, M. A. (2000). The temporal properties of first- and second-order vision. *Vision Res, 40*(18), 2475-2487.
Schofield, A. J., & Georgeson, M. A. (2003). Sensitivity to contrast modulation: the spatial frequency dependence of second-order vision. *Vision Res, 43*(3), 243-259. doi:10.1016/s0042-6989(02)00542-4
Schofield, A. J., & Yates, T. A. (2005). Interactions between orientation and contrast modulations suggest limited cross-cue linkage. *Perception, 34*(7), 769-792.
Schroder, J. H., Fries, P., Roelfsema, P. R., Singer, W., & Engel, A. K. (2002). Ocular dominance in extrastriate cortex of strabismic amblyopic cats. *Vision Res, 42*(1), 29-39.
Secen, J., Culham, J., Ho, C., & Giaschi, D. (2011). Neural correlates of the multiple-object tracking deficit in amblyopia. *Vision Res, 51*(23-24), 2517-2527. doi:10.1016/j.visres.2011.10.011
Self, M. W., & Zeki, S. (2005). The integration of colour and motion by the human visual brain. *Cereb Cortex, 15*(8), 1270-1279. doi:10.1093/cercor/bhi010
Sillito, A. M. (1977). Inhibitory processes underlying the directional specificity of simple, complex and hypercomplex cells in the cat's visual cortex. *J Physiol, 271*(3), 699-720.
Sillito, A. M. (1979). Inhibitory mechanisms influencing complex cell orientation selectivity and their modification at high resting discharge levels. *J Physiol, 289*, 33-53.
Simmers, A. J., Ledgeway, T., & Hess, R. F. (2005). The influences of visibility and anomalous integration processes on the perception of global spatial form versus motion in human amblyopia. *Vision Res, 45*(4), 449-460. doi:10.1016/j.visres.2004.08.026
Simmers, A. J., Ledgeway, T., Hess, R. F., & McGraw, P. V. (2003). Deficits to global motion processing in human amblyopia. *Vision Res, 43*(6), 729-738.
Simmers, A. J., Ledgeway, T., Hutchinson, C. V., & Knox, P. J. (2011). Visual deficits in amblyopia constrain normal models of second-order motion processing. *Vision Res, 51*(18), 2008-2020. doi:10.1016/j.visres.2011.07.012
Simmers, A. J., Ledgeway, T., Mansouri, B., Hutchinson, C. V., & Hess, R. F. (2006a). The extent of the dorsal extra-striate deficit in amblyopia. *Vision Research, 46*(16), 2571-2580. doi:10.1016/j.visres.2006.01.009
Simmers, A. J., Ledgeway, T., Mansouri, B., Hutchinson, C. V., & Hess, R. F. (2006b). The extent of the dorsal extra-striate deficit in amblyopia. *Vision Res, 46*(16), 2571-2580. doi:10.1016/j.visres.2006.01.009
Simons, K. (2005). Amblyopia characterization, treatment, and prophylaxis. *Surv Ophthalmol, 50*(2), 123-166. doi:10.1016/j.survophthal.2004.12.005

Sinha, P. (2001). Role of motion integration in contour perception. *Vision Res, 41*(6), 705-710.
Sireteanu, R., Singer, W., Fronius, M., Greuel, J. M., Best, J., Fiorentini, A., . . . Campos, E. (1993). Eye alignment and cortical binocularity in strabismic kittens: a comparison between tenotomy and recession. *Vis Neurosci, 10*(3), 541-549.
Smith, A. T., Greenlee, M. W., Singh, K. D., Kraemer, F. M., & Hennig, J. (1998). The processing of first- and second-order motion in human visual cortex assessed by functional magnetic resonance imaging (fMRI). *J Neurosci, 18*(10), 3816-3830.
Song, Y., & Baker, C. L., Jr. (2007). Neuronal response to texture- and contrast-defined boundaries in early visual cortex. *Vis Neurosci, 24*(1), 65-77. doi:10.1017/s0952523807070113
Stromeyer, C. F., 3rd, & Klein, S. (1974). Spatial frequency channels in human vision as asymmetric (edge) mechanisms. *Vision Res, 14*(12), 1409-1420.
Sutter, A., Beck, J., & Graham, N. (1989). Contrast and spatial variables in texture segregation: testing a simple spatial-frequency channels model. *Percept Psychophys, 46*(4), 312-332.
Sutter, A., & Graham, N. (1995). Investigating simple and complex mechanisms in texture segregation using the speed-accuracy tradeoff method. *Vision Res, 35*(20), 2825-2843.
Sutter, A., Sperling, G., & Chubb, C. (1995). Measuring the spatial frequency selectivity of second-order texture mechanisms. *Vision Res, 35*(7), 915-924.
Tang, Y., Liu, C., Liu, Z., Hu, X., Yu, Y. Q., & Zhou, Y. (2014). Processing deficits of motion of contrast-modulated gratings in anisometropic amblyopia. *PLoS One, 9*(11), e113400. doi:10.1371/journal.pone.0113400
Tripathy, S. P., & Levi, D. M. (2008). On the effective number of tracked trajectories in amblyopic human vision. *J Vis, 8*(4), 8.1-22. doi:10.1167/8.4.8
Tsirlin, I., Colpa, L., Goltz, H. C., & Wong, A. M. (2015). Behavioral Training as New Treatment for Adult Amblyopia: A Meta-Analysis and Systematic Review. *Invest Ophthalmol Vis Sci, 56*(6), 4061-4075. doi:10.1167/iovs.15-16583
Vaina, L. M., Cowey, A., & Kennedy, D. (1999). Perception of first- and second-order motion: separable neurological mechanisms? *Hum Brain Mapp, 7*(1), 67-77.
Van Essen, D. C., & Gallant, J. L. (1994). Neural mechanisms of form and motion processing in the primate visual system. *Neuron, 13*(1), 1-10.
Wang, H. X., Heeger, D. J., & Landy, M. S. (2012). Responses to second-order texture modulations undergo surround suppression. *Vision Res, 62*, 192-200.
Wang, J., Ho, C. S., & Giaschi, D. E. (2007). Deficient motion-defined and texture-defined figure-ground segregation in amblyopic children. *J Pediatr Ophthalmol Strabismus, 44*(6), 363-371.
Westheimer, G. (1960). Modulation thresholds for sinusoidal light distributions on the retina. *J Physiol, 152*, 67-74.
Westrick, Z. M., & Landy, M. S. (2013). Pooling of first-order inputs in second-order vision. *Vision Res, 91*, 108-117. doi:10.1016/j.visres.2013.08.005
Whittle, P. (1986). Increments and decrements: luminance discrimination. *Vision Res, 26*(10), 1677-1691.
Whittle, P. (1992). Brightness, discriminability and the "crispening effect". *Vision Res, 32*(8), 1493-1507.
Wiesel, T. N., & Hubel, D. H. (1963). Effects of visual deprivation on morphology and physiology of cells in the cats lateral geniculate body. *J Neurophysiol, 26*, 978-993.

Wiesel, T. N., & Hubel, D. H. (1965). Comparison of the effects of unilateral and bilateral eye closure on cortical unit responses in kittens. *J. Neurophysiol., 28*, 1029-1040.
Wilson, H. R. (1994). The role of second-order motion signals in coherence and transparency. *Ciba Found Symp, 184*, 227-237; discussion 238-244, 269-271.
Wong, A. M. (2012). New concepts concerning the neural mechanisms of amblyopia and their clinical implications. *Can J Ophthalmol, 47*(5), 399-409. doi:10.1016/j.jcjo.2012.05.002
Wong, E. H., & Levi, D. M. (2005). Second-order spatial summation in amblyopia. *Vision Res, 45*(21), 2799-2809. doi:10.1016/j.visres.2005.05.020
Wong, E. H., Levi, D. M., & McGraw, P. V. (2001). Is second-order spatial loss in amblyopia explained by the loss of first-order spatial input? *Vision Res, 41*(23), 2951-2960.
Yazdani, P., Serrano-Pedraza, I., Whittaker, R. G., Trevelyan, A., & Read, J. C. (2015). Two common psychophysical measures of surround suppression reflect independent neuronal mechanisms. *J Vis, 15*(13), 21. doi:10.1167/15.13.21
Yoonessi, A., & Baker, C. L., Jr. (2011). Contribution of motion parallax to segmentation and depth perception. *J Vis, 11*(9), 13. doi:10.1167/11.9.13
Zhou, Y. X., & Baker, C. L., Jr. (1993). A processing stream in mammalian visual cortex neurons for non-Fourier responses. *Science, 261*(5117), 98-101.
Zhou, Y. X., & Baker, C. L., Jr. (1994). Envelope-responsive neurons in areas 17 and 18 of cat. *J Neurophysiol, 72*(5), 2134-2150.
Zhou, Y. X., & Baker, C. L., Jr. (1996). Spatial properties of envelope-responsive cells in area 17 and 18 neurons of the cat. *J Neurophysiol, 75*(3), 1038-1050.